

“My imperfections and failures are as much a blessing from God as my successes and my talents and I lay them both at his feet.”

Mahatma Gandhi

University of Alberta

**Integrated Multi-band Multi-polarized Microstrip Antenna
Designs**

by

Kashish Jhamb

A thesis submitted to the Faculty of Graduate Studies and Research
in partial fulfillment of the requirements for the degree of

Master of Science

in

Communications

Electrical and Computer Engineering

©Kashish Jhamb

Fall 2011

Edmonton, Alberta

Permission is hereby granted to the University of Alberta Libraries to reproduce single copies of this thesis and to lend or sell such copies for private, scholarly or scientific research purposes only. Where the thesis is converted to, or otherwise made available in digital form, the University of Alberta will advise potential users of the thesis of these terms.

The author reserves all other publication and other rights in association with the copyright in the thesis and, except as herein before provided, neither the thesis nor any substantial portion thereof may be printed or otherwise reproduced in any material form whatsoever without the author's prior written permission.

Dedicated

To my parents

Abstract

Recently, antenna designs with multi-frequency operation and multi-polarization characteristics are in great demand for future wireless systems. In the thesis, several integrated microstrip antenna designs have been proposed for wireless applications. Integrated semi-circular and triangular patch antennas have been designed for various wireless data communication applications exhibiting linear polarization characteristics. In these designs, the patch has been integrated with slots and monopoles for multi-resonance operation. Another multi-band antenna realizing annular ring patch configuration has been designed for similar wireless applications. A technique to independently tune the frequencies of operation has also been introduced. Furthermore, a single layer, multi-band rectangular patch antenna has been proposed for data transmission and localization applications with different polarization requirements. The patch has been integrated with four monopoles to achieve circularly and linearly polarized radiation characteristics. The design procedures of the antennas have been described and their performances have been validated using electromagnetic solvers and measurements.

Acknowledgements

I wish to thank my supervisor Dr. Rambabu Karumudi for his guidance, encouragement and support throughout the entire course of the thesis. I admire his sincerity, dedication and professionalism. I would also like to thank Dr. Adrain Tan for his valuable suggestions throughout this thesis. Early help and guidance from Kevin Chan was also valuable and his contributions are acknowledged. I am thankful for antenna fabrication support from Edward Tiong. I am also grateful to my fellow colleague Lin Li for his continuous support and efforts. Finally, I would like to thank my mother Sneha Jhamb and my father Tilak Raj Jhamb for their endless support and encouragement in all my endeavours.

Contents

1. Introduction	1
2. Design of novel integrated patch antennas for commercial wireless applications	12
2.1 Introduction	13
2.2 Antenna designs	14
2.2.1 Integrated triangular patch antenna design	14
2.2.1.1 Field reflection technique	17
2.2.1.2 Measurement and simulation results	21
2.2.2 Integrated semi-circular patch antenna design	29
2.2.2.1 Measurement and simulation results	33
2.3 Limitations and improvements	39
2.4 Conclusion	39
3. Design of frequency tunable annular ring patch antenna for multi-frequency applications	41
3.1 Introduction	42
3.2 Dual band antenna design	43
3.2.1 Simulation and measurement results of dual band antenna	47
3.3 Frequency tuning technique	52
3.4 Antenna design with multi-band characteristics	63
3.5 Limitations and improvements	67
3.6 Conclusion	68

4. Integrated multi-band multi-polarized microstrip antenna for wireless systems	69
4.1 Introduction	70
4.2 Antenna design V1 and its drawbacks	71
4.2.1 Antenna design V1	72
4.2.2 Drawbacks	73
4.3 Optimized design V2 and its modifications	75
4.3.1 Optimized design V2	75
4.3.2 Modifications	76
4.4 Design methodology	77
4.4.1 GPS frequency	78
4.4.2 3G frequency	79
4.4.3 WLAN frequency	80
4.4.4 Integrated design	83
4.5 Results	84
4.6 Limitations and improvements	92
4.7 Conclusion	93
5. Multi-band multi-polarized antenna designs for future research	94
5.1 Introduction	95
5.2 Design 1	96
5.3 Design 2	97
5.4 Design 3	98
5.5 Conclusion	98

Bibliography	100
---------------------------	------------

List of Figures

Figure 2.1 Structure of the proposed integrated triangular patch antenna design	16
Figure 2.2 Prototype of integrated triangular patch antenna	16
Figure 2.3 Simulated radiation patterns at 1.96 GHz for triangular patch antenna without reflector plane	20
Figure 2.4 Simulated radiation patterns at 2.45 GHz for triangular patch antenna without reflector plane	20
Figure 2.5 Simulated radiation patterns at 3.5 GHz for triangular patch antenna without reflector plane	21
Figure 2.6 Simulated and measured return loss of triangular patch antenna	22
Figure 2.7 Simulated and measured real impedance of triangular patch antenna	22
Figure 2.8 Simulated and measured imaginary impedance of integrated triangular patch	23
Figure 2.9 Current distribution at 1.96 GHz for triangular patch antenna	24
Figure 2.10 Current distribution at 2.45 GHz for triangular patch antenna	25
Figure 2.11 Current distribution at 3.5 GHz for triangular patch antenna	26
Figure 2.12 Simulated and measured radiation patterns at 1.96 GHz for triangular patch antenna	26
Figure 2.13 Simulated and measured radiation patterns at 2.45 GHz for triangular patch antenna	27
Figure 2.14 Simulated and measured radiation patterns at 3.5 GHz for triangular patch antenna	27
Figure 2.15 Measurement setup	28
Figure 2.16 Simulated and measured realizable gain of triangular patch antenna	29
Figure 2.17 Structure of the proposed integrated semi-circular patch antenna design	30

Figure 2.18 Current distribution at 3.5 GHz for semi-circular patch antenna	31
Figure 2.19 Current distribution at 2.45 GHz for semi-circular patch antenna	31
Figure 2.20 Current distribution at 5.5 GHz for semi-circular patch antenna	32
Figure 2.21 Prototype of integrated semi-circular patch antenna	33
Figure 2.22 Simulated and measured return loss of semi-circular patch antenna	34
Figure 2.23 Simulated and measured real impedance of semi-circular patch antenna	35
Figure 2.24 Simulated and measured imaginary impedance of semi-circular patch antenna ...	35
Figure 2.25 Simulated and measured radiation patterns at 2.45 GHz for semi-circular patch antenna	36
Figure 2.26 Simulated and measured radiation patterns at 3.5 GHz for semi-circular patch antenna	37
Figure 2.27 Simulated and measured radiation patterns at 5.5 GHz for semi-circular patch antenna	37
Figure 2.28 Simulated and measured realizable gain of semi-circular patch antenna	38
Figure 3.1 Structure of the proposed dual band annular ring antenna design	46
Figure 3.2 Current distribution at 2.45 GHz for dual band annular ring patch antenna	46
Figure 3.3 Current distribution at 3.5 GHz for dual band annular ring patch antenna	47
Figure 3.4 Prototype of dual band annular ring patch antenna	48
Figure 3.5 Simulated and measured return loss of dual band annular ring patch antenna	49
Figure 3.6 Simulated real impedance of dual band annular ring patch antenna	49
Figure 3.7 Simulated imaginary impedance of dual band annular ring patch antenna	50
Figure 3.8 Simulated realizable gain of dual band annular ring patch antenna	51
Figure 3.9 Simulated radiation patterns at 2.45 GHz for dual band annular ring patch antenna	51

Figure 3.10 Simulated radiation patterns at 2.45 GHz for dual band annular ring patch antenna	52
Figure 3.11 Structure of the proposed single groove and two grooves dual band annular ring antenna design	53
Figure 3.12 Simulated return loss of two grooves dual band annular ring patch antenna	55
Figure 3.13 Measured return loss of two grooves dual band annular ring patch antenna	55
Figure 3.14 Simulated return loss of single groove dual band annular ring patch antenna	56
Figure 3.15 Measured return loss of single groove dual band annular ring patch antenna	56
Figure 3.16 Prototype of single groove dual band annular ring patch antenna	57
Figure 3.17 Prototype of two grooves dual band annular ring patch antenna	57
Figure 3.18 Simulated radiation patterns for single groove dual band annular ring patch antenna	60
Figure 3.19 Simulated radiation patterns for two grooves dual band annular ring patch antenna	61
Figure 3.20 Comparison among theoretical, measured and simulated tuned frequency as a function of groove depth	62
Figure 3.21 Simulated reactance of the two grooves dual band annular ring antenna as a function of groove depth	62
Figure 3.22 Simulated reactance of the single groove dual band annular ring antenna as a function of groove depth	63
Figure 3.23 Simulated and measured return loss of multi-band annular ring patch antenna	65
Figure 3.24 Simulated radiation patterns at 2.45 GHz for multi-band annular ring patch antenna	65
Figure 3.25 Simulated radiation patterns at 3.5 GHz for multi-band annular ring patch antenna.....	66
Figure 3.26 Simulated radiation patterns at 5.5 GHz for multi-band annular ring patch antenna	66

Figure 3.27 Simulated realizable gain of multi-band annular ring patch antenna	67
Figure 4.1 Structure of the proposed integrated microstrip patch antenna design V1	73
Figure 4.2 Prototype of the proposed integrated microstrip patch antenna design V1	74
Figure 4.3 Simulated and measured return loss of antenna design V1	75
Figure 4.4 Structure of the proposed integrated multi-band optimized antenna design V2	78
Figure 4.5 Current distribution at 1.575 GHz for optimised antenna design V2	81
Figure 4.6 Current path at 2.1 GHz for optimized design V2	81
Figure 4.7 Current distribution at 2.1 GHz for optimised antenna design V2	82
Figure 4.8 Current distribution at 2.45 GHz for optimised antenna design V2	82
Figure 4.9 Simulated return loss of optimised antenna design V2	84
Figure 4.10 Simulated real impedance of optimised antenna design V2	85
Figure 4.11 Simulated imaginary impedance of optimised antenna design V2	86
Figure 4.12 Simulated E-plane radiation pattern at 1.575 GHz for optimised design V2	87
Figure 4.13 Simulated H-plane radiation pattern at 1.575 GHz for optimised design V2	87
Figure 4.14 Simulated E-plane radiation pattern at 2.1 GHz for optimised design V2	88
Figure 4.15 Simulated H-plane radiation pattern at 2.1 GHz for optimised design V2	88
Figure 4.16 Simulated E-plane radiation pattern at 2.45 GHz for optimised design V2	89
Figure 4.17 Simulated H-plane radiation pattern at 2.45 GHz for optimised design V2	89
Figure 4.18 Simulated realizable gain of optimised antenna design V2	90
Figure 4.19 Simulated E-plane axial ratio at 1.575 GHz for optimized antenna design V2 as a function of theta	91
Figure 4.20 Simulated H-plane axial ratio at 1.575 GHz for optimized antenna design V2 as a function of theta	91

Figure 4.21 Simulated boresight axial ratio for optimized antenna design V2 as a function of
frequency 92

Glossary

AMPS: Advanced Mobile Phone System

PCS: Personal Communication Service

GSM: Global System for Mobile Communications

DCS: Digital Cellular System

PDC: Personal Digital Cellular

PHS: Personal Handy-phone System

3G: Third Generation

4G: Fourth Generation

WLAN: Wireless Local Area Network

WiMAX: Worldwide Interoperability for Microwave Access

BT: Bluetooth

PDA: Personal Digital Assistant

EM: Electromagnetic

SDARS: Satellite Digital Audio Radio Services

GPS: Global Positioning System

US: United States

CP: Circular Polarization

LP: Linear Polarization

RHCP: Right Hand Circular Polarization

LHCP: Left Hand Circular Polarization

SRT: Sequential Rotation Technique

Chapter 1

Introduction

Immense development in the field of wireless communications has increased the need to design equipments capable of supporting multiple wireless applications with a single portable device. Therefore to satisfy the growing needs of upcoming technologies, one of the desired aspects of the products will be the miniaturized multi-purpose antenna designs for multi-band operations with suitable radiation and polarization characteristics [1-8]. These wireless applications include wireless data transmission, navigational and positional support, satellite radio services and various other applications. Today, wireless technology has become an integral part of the lives of the common people. With the introduction of numerous advancements in the communication industry; the competitiveness in designing multi-purpose antennas has grown manifolds.

1

¹ A version of this chapter had been submitted as MSc. research project proposal ECE 601; **K. Jhamb**, “Miniaturized Multi-band Multi-polarized Microstrip Patch Antennas for Wireless Systems”, April 2010, University of Alberta, Edmonton, Canada.

Nonetheless, many countries have allocated different frequency requirements for same wireless applications that further require incorporation of independent frequency tunability in future antenna designs [9]. For example, the existing first and second generation wireless cellular mobile communication systems operate in the AMPS (824-894 MHz) and PCS (1850-1990 MHz) bands in America, in the GSM (880-960 MHz) and DCS (1710-1880 MHz) bands in Europe, and in the PDC (810-915 MHz) and PHS (1895-1918 MHz) bands in Japan [10]. Therefore, if an antenna incorporates independent frequency tuning, the same design can be implemented to realize an antenna for different countries. Furthermore, the next generation mobile communication systems have also been established in the market. A new spectrum has already been allocated around 2 GHz (IMT 2000) for 3G and 4G communication systems [11]. Thus, the products compatible for multi-wireless applications require different frequency and polarization specifications, which is an impending challenge for the wireless industry.

Among various wireless applications, some of the data communication technologies such as wireless local area network (WLAN), worldwide interoperability for microwave access (WiMAX), personal communication services (PCS) and Bluetooth (BT) are capturing a lot of market interest globally. The WLAN operates in 2.4 GHz band (2400-2484 MHz) and requires linear polarization (LP) [12-14]. WLAN (IEEE 802.11 b/g) enables portable devices like laptops, personal digital assistants (PDA's) or cell phones to have wireless connectivity for various professional and personal applications. Furthermore,

technologies like HomeRF and BT also operate in the same frequency range, thereby making this band useful for various commercial applications. WiMAX operates at 2500/3500/5500 MHz bands and requires linear polarization characteristics [15-16]. It is based on IEEE 802.16 standard, also known as broadband wireless access band and offers similar features as WLAN, but possesses improved connectivity, better range and higher quality of service [15-16]. WiMAX can be as convenient as WLAN and by just turning the user equipment on, it will connect the end user to the nearest WiMAX base station. PCS spectrum has also been categorized under data communication technologies. PCS operates in 1900 MHz band, which is being used for digital mobile phone services [17]. Facilities like call mobility, instant messaging or voice mails can be availed using this band.

In addition to this, other than the stated communication technologies, there are several other satellite based communication services such as satellite digital radio audio communication services (SDARS) and positional support services such as global positioning systems (GPS) that require different polarization characteristics unlike WLAN, WiMAX or PCS [18]. These services are used by millions of users every day, all over the world. The SDARS operates at 2.32 GHz requiring left hand circular polarization (LHCP) and is used for satellite radio services [19]. However, the GPS is compatible with right hand circular polarization (RHCP) and operates in two different bands [20]. The lower band (L2) operates from 1268.75 MHz to 1288.75 MHz, and the upper band (L1) from 1564.4 MHz to 1583.4

MHz. The lower band has been reserved for United States (US) military purposes [21], while the upper band is extensively used for commercial navigational and positioning based products such as GPS systems for vehicular applications, laptops, cell phones, tablets and various other electronic equipments [22-24].

Therefore, in order to get along with the emerging communication technologies, future wireless systems need to support multi-functional services such as voice, video, data transmission, navigational support and entertainment channels, with automatic access and seamless roaming across different operating frequency bands around the globe. Also, wireless equipments that are capable of operating with multi-frequency and multi-polarization requirements need to be miniaturized and inexpensive in order to advance their applicability. For example, a typical wireless system for automobiles needs to support voice (GSM), data transfers (WLAN or WiMAX) and location based services (GPS) along with the audio-radio facility (SDARS). Consequently, the ideal system for the stated automobile applications requires a miniaturized multi-band and multi-polarized antenna that is capable of receiving signals at 900 MHz (voice communication - LP), 2.4 GHz (data transfers - LP), 1.575 GHz (GPS - RHCP) and 2.32 GHz (SDARS - LHCP). These multi-band multi-polarized antennas carry the real potential to create a new market which hands the provision of qualitative multiple services to the user. However to have a good quality of service, signal reliability needs to be maintained that requires appropriate polarization characteristics for the desired applications.

Microstrip antenna configuration is a preferred solution for the stated commercial wireless applications due to its low profile, low volume, low cost, robustness and easy fabrication [25-32]. There are various shapes of the microstrip patch that have been used in the literature, such as rectangular, semi-circular, circular, square, annular ring, triangular etc. All these shapes have been used for distinct requirements and applications [31, 33-40]. Additionally, along with the multi-band operation, radiation requirement at different frequencies also needs to be encountered. For example, in case of wireless applications such as the WLAN and WiMAX the radiation pattern should be sideways in such a way that the connectivity with the base station is always maintained. However, for satellite based applications such as GPS and SDARS, the radiation pattern should be towards zenith so that better signal reception can be achieved through satellites.

As inferred from the published literature, various techniques have been proposed for multi-band antennas. Planar inverted F antennas [2, 41-45], printed monopoles [1, 3, 6, 46-47], folded and printed dipoles [48-49], fractal antenna designs [50-52], multi-layered patch or stacked patches [53-58], aperture coupled resonators [59], slots on the patch [60], using active elements [61-62] and other design configurations of microstrip antenna [63-70] are some of the examples. All the referred designs are limited to single polarization that is either linear or circular, and their configurations can be either multilayered or multi-fed. Also, many of the multi-band referred designs work on a single wide band resonance instead of

multiple resonances and do not possess independent frequency tuning. Hence, controlling polarization of the antenna is not possible.

To achieve both circular and linear polarizations in a frequency tunable microstrip design using single feed and single layer configuration is much more challenging than achieving multi-band resonances with same polarization requirements. There are very few designs available in the published literature that comprehends dual polarizations (linear and circular) in a single layer antenna design. However, these designs are implemented using dual feed, dual substrate or dual patch configurations [71-73]. Multi-feed designs are complex due to multi receiver requirements. Therefore, the design of a single feed, single substrate, microstrip antenna that can resonate at multiple frequencies with multi-polarization is of a great advantage.

In this thesis, a research project is proposed to achieve single feed and single layer multi-polarized antennas with multi-band characteristics. The framework and design strategies to achieve the multi-band and multi-polarized antennas will be presented. The overall research project is divided into two sections. The first section realizes single layer, single probe-fed, multi-band antenna designs with linear polarization characteristics (chapter 2 and chapter 3). Three independent frequency tunable designs will be presented and thoroughly discussed. The second section describes a single layer, single probe-fed, multi-band antenna design with circular and linear polarization characteristics (one RHCP and two

LP; chapter 4). A rectangular microstrip patch is integrated with printed monopoles to achieve the desired characteristics. Nevertheless, in future, more research can be carried out to design single layer multi-band antennas realizing RHCP-LHCP-LP, RHCP-LHCP-RHCP or LHCP-RHCP-LHCP requirements.

The working principles and coherent design procedures for the proposed single feed, single layer multi-band and multi-polarized antennas have been developed. Thorough description of the theoretical and practical aspects of the proposed designs involving different polarization requirements will be stated. Furthermore, design simulations using full wave analysis softwares (CST Microwave studio and Ansoft HFSS) and physical measurements for antenna characteristics such as operating frequencies, gain and radiation patterns have been carried out. Some techniques aimed at realizing the miniaturization of the proposed designs have also been studied. The thesis will be presented in the form of five chapters. Chapter 2 and chapter 3 state the antenna designs for single layer multi-band antennas with linear polarization characteristics, while chapter 4 states a circularly and linearly polarized antenna design for GPS, 3G and WLAN applications. Chapter 5 describes the potential future research that can be carried out in this domain.

For the proposed microstrip antenna configurations such as triangular shape patch, semi-circular patch and annular ring patch, various multi-band antennas have been realized in the literature using slots, truncated corners, shorting pins,

shorting walls etc [33, 35-36, 74-85]. However, the referred designs are either multi-layered or multi-fed and do not achieve desired polarization and radiation requirements with independent frequency tunability. For example, in ref [35,36], shorting pins and walls are used to achieve multi-band or wide-band operations, however, due to size reduction radiation characteristics are not as desired. Even cross polarization levels also got degraded. Therefore, the main goal of this thesis is to design single feed and single layer integrated antennas that achieve multi-resonance operation with desired radiation and polarization requirements with independent frequency tunability. All the design strategies described in this thesis can be used as independent design principles to realize antenna for any wireless applications. All these proposed antennas can be used for commercial applications such as automobiles and laptops for wireless data transmission and navigational support, where antenna can be just mounted on the roof top of the car or behind laptop screens. Furthermore, more research needs to be carried out to realize much miniaturized versions of the antennas using proposed design principle to advance antenna applicability for smart phones, personal digital assistants etc.

In chapter 2 of the thesis, two integrated multiband antenna designs have been presented, incorporating independent frequency tunability. One of the designs is an integrated triangular patch antenna, resonating at PCS (1.96 GHz), WLAN (2.45 GHz) and WiMAX (3.5 GHz) frequencies. The right isosceles triangular patch is integrated with two monopoles, one on the side and one at the bottom of the patch respectively. The monopoles are resonating at 1.96 GHz and 2.45 GHz. However,

the patch resonates at 3.5 GHz. A field reflection technique to enhance the antenna gain and achieve desired radiation characteristics has also been proposed for the triangular patch antenna. This technique has been thoroughly explained in the section 2.2.1.1 of the thesis. The other proposed design in chapter 2 is an integrated multi-band semi-circular patch antenna design for WLAN and WiMAX operations. This design consists of a semi-circular patch resonating at 3.5 GHz integrated with a slot and a monopole. The slot and monopole realize resonances at 5.5 GHz and 2.45 GHz respectively. Simulation and measurement results for both the proposed designs will be demonstrated in section 2.2.1.2 and section 2.2.2.1 of the thesis respectively. An acceptable agreement has been found between simulations and measurements. Furthermore, the research work demonstrated in chapter 2 of the thesis has been accepted for the publication in the journal of IET Microwaves, antennas and propagation [J1].

In chapter 3 of the thesis, a dual-band and a tri-band antenna have been proposed using annular ring patch configuration. Multi-band operation in the proposed annular ring antenna has been achieved by exciting higher order modes of the patch around the dominant mode of annular ring. Since the multi-resonance in the design is due to the higher order modes, independent tunability of the frequencies is not realized. In order to overcome this concern, a novel technique has been proposed to incorporate independent frequency operation in the design. Using this technique, grooves of different depths have been cut on the ring at desired locations to independently tune the frequencies. The proposed antenna resonates

at 2.45 GHz, 3.5 GHz and 5.5 GHz for WLAN and WiMAX applications. Further improvements that can be incorporated into the proposed design will be discussed in section 3.5 of the thesis. The research work demonstrated in chapter 3 of the thesis has also been accepted for the publication in the journal of *IET microwaves, antennas and propagation* [J2].

Finally, a multi-band antenna with dual polarization characteristics is described in chapter 4 of the thesis. The proposed antenna design in chapter 4 comprises of a rectangular patch integrated with four printed monopoles fused along the sides of the patch. This design resonates at 1.575 GHz (GPS) with RHCP, 2.1 GHz (3G) with LP and 2.45 GHz (WLAN) with LP. The antenna possesses return loss better than 10 dB and desired radiation characteristics at all the stated resonant frequencies. The research work demonstrated in chapter 4 of the thesis will be soon submitted for the publication in the *Journal of IEEE transactions on Antennas and Propagation*. Currently, the manuscript is under preparation [J3].

Future works in this domain that can be carried out have been explained in the last chapter (chapter 5) of the thesis. Ideas to achieve the proposed future designs have also been demonstrated.

[J1] **K. Jhamb**, L. Li and K. Rambabu, "Novel Integrated Patch Antennas with Multi-band Characteristics", accepted for publication in the *Journal of IET, Microwaves, Antennas and Propagation*; manuscript ID: MAP-2010-0515.R2, date of acceptance: 23rd May'2011.

[J2] **K. Jhamb**, L. Li and K. Rambabu, “Frequency Adjustable Microstrip Annular Ring Patch Antennas with Multi-band Characteristics”, accepted for publication in the Journal of *IET, Microwaves, Antennas and Propagation*; manuscript ID: MAP-2010-0571.R1, date of acceptance: 8th June’2011.

[J3] **K. Jhamb**, K.K. M Chan, A.E.C. Tan and K. Rambabu, “Integrated Multi-polarized Multi-band Patch Antenna for Vehicular Applications”, to be submitted in the Journal of IEEE Transactions on Antennas and propagation, current status: Manuscript under preparation.

Chapter 2

Design of novel integrated patch antennas for commercial wireless applications

Abstract

In this chapter, two integrated multi-band microstrip patch antennas have been proposed for the next generation wireless systems. The first design is based on the microstrip triangular patch configuration that comprises of a right isosceles triangular patch integrated with a pair of monopoles. The patch resonates at 3.5 GHz (WiMAX) and the monopoles realize resonances at 2.45 GHz (WLAN) and 1.96 GHz (PCS) respectively. Furthermore, to enhance the antenna gain and to achieve the desired radiation characteristics, a field reflection technique has been introduced. As a part of this technique, a reflector metal sheet has been placed below the patch. However, the detailed analysis of this technique has been thoroughly explained in section 2.2.1.1 of this chapter.

2

² A version of this chapter has been accepted for publication in the Journal of IET Microwaves, Antennas and Propagation. Manuscript ID: MAP-2010-0515.R2. Date of acceptance: 23rd May'2011. **K. Jhamb**, L. Li and K. Rambabu, "Novel Integrated Patch Antennas with Multi-band Characteristics".

Similarly, the second proposed antenna design is also based on the microstrip patch configuration. It consists of a semi-circular patch integrated with a slot and a monopole. The patch resonates at 3.5 GHz, while the slot and the monopole are resonating at 5.5 GHz (WiMAX) and 2.45 GHz respectively. Both the designs are realized on a 1.58 mm thick FR4 substrate (dielectric constant = 4.4) and possess return loss better than 10 dB with desired radiation characteristics at the specified resonant frequencies. Prototypes of the proposed designs have been fabricated and their radiation characteristics have been measured. A close agreement has been found between simulations (CST microwave studio and Ansoft HFSS) and measurements.

2.1 Introduction

Among various shapes of the microstrip patch antenna; the triangular and semi-circular configurations are preferred due to their miniaturized configuration and their suitability for wireless applications [35, 74]. As inferred from the published literature, there are various multi-band microstrip patch designs with triangular and semi-circular shape configurations using slots [33, 75-76], notches [77], truncated corners [78, 79], active elements [80], shorting pins and walls [81-82], shorting strips [83], excitation of higher order modes by the patch [84], shorting planes [35], different feeding techniques [36, 85] or achieving single wideband resonance instead of multiple resonances [86]. However, in this chapter, two novel designs have been proposed for the commercial wireless applications. These

designs realize return loss better than 10 dB and possess desired radiation characteristics at the stated resonant frequencies. The proposed designs are novel in terms of integration with monopoles and slot. In addition to this, simplicity, flexibility and frequency tunability in the designs have also been maintained.

The first proposed design is a right isosceles triangular patch antenna integrated with a pair of monopoles. This design realizes resonances at 1.96 GHz, 2.45 GHz and 3.5 GHz respectively, thus making the design capable of multi-band operation (PCS, WLAN, and WiMAX). A field reflection technique to achieve the desired directive radiation characteristics has also been introduced. Similarly, the second antenna design is also based on the microstrip patch configuration and consists of a semi-circular patch integrated with a slot and a monopole. The patch resonates at 3.5 GHz, while the slot and the monopole resonate at 5.5 GHz and 2.45 GHz respectively. The prototypes for both the designs have been fabricated.

2.2 Antenna designs

2.2.1 Integrated triangular patch antenna design

The proposed antenna design comprises of a right isosceles triangular patch integrated with a pair of monopoles as shown in Fig. 2.1. The patch resonates at 3.5 GHz for WiMAX operations while the monopoles resonate at 2.45 GHz and 1.96 GHz for WLAN and PCS communication services respectively. The monopole fused along the base (bottom) of the isosceles triangular patch

resonates at WLAN frequency (2.45 GHz), while the other monopole fused along the height (side) of the triangular patch is responsible for the PCS (1.96 GHz) operations (refer Fig. 2.1). The design principle of the patch has been introduced in [84]. However, the monopoles are quarter wavelength long including the fringe field depth. As shown in the Fig. 2.1, a part of the printed monopoles acts as a microstrip feed line while the other part acts as a radiating strip. The patch has been fed through a single coaxial feed while the monopoles fused along the patch are fed through the currents from the patch. Furthermore, the width and location of the monopoles have been optimized using electromagnetic (EM) solvers in such a way that maximum current flows into the monopole, thus achieving better impedance match at 2.45 GHz and 1.96 GHz.

The monopoles have been bent in order to achieve miniaturization in the design (refer Fig. 2.1). The novelty in this design is the integration of the patch with two monopoles, making it capable of multi-band operation and at the same time simplicity in the design has also been maintained. The proposed design is a probe-fed design and is realized on a 1.58 mm thick glassy epoxy substrate with a dielectric constant of 4.4. The structural view and dimensions of the proposed design have also been shown in Fig. 2.1. Prototype of the design has been fabricated and is shown in Fig. 2.2. A close agreement has been found between simulations and measurements.

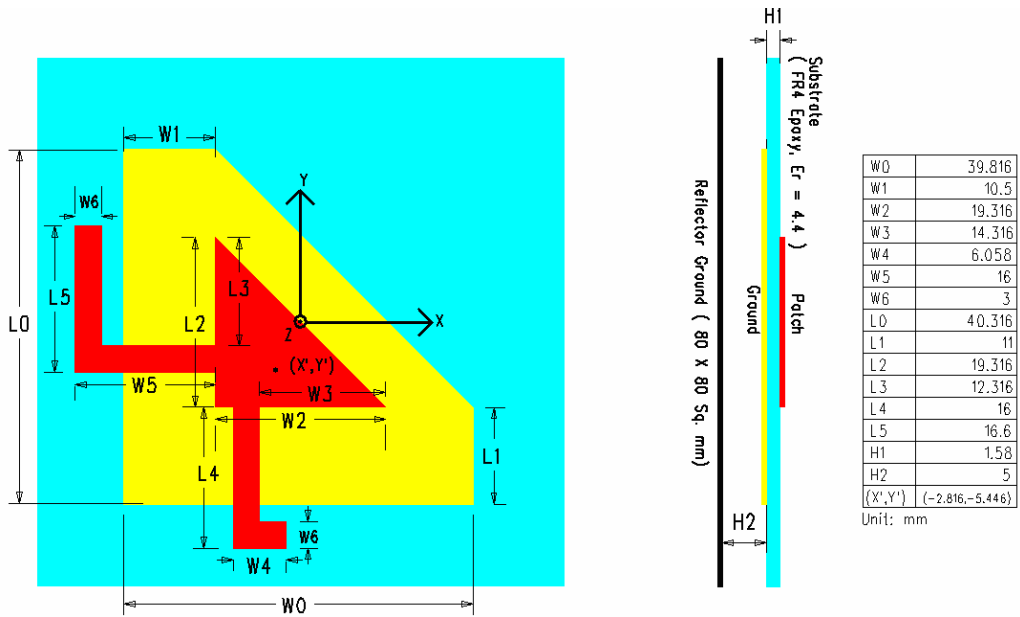


Figure 2.1 – Proposed integrated triangular patch antenna design. This figure represents the top (left) and side view (centre) of the antenna design. All the dimensions of the antenna have been shown in the table (right).

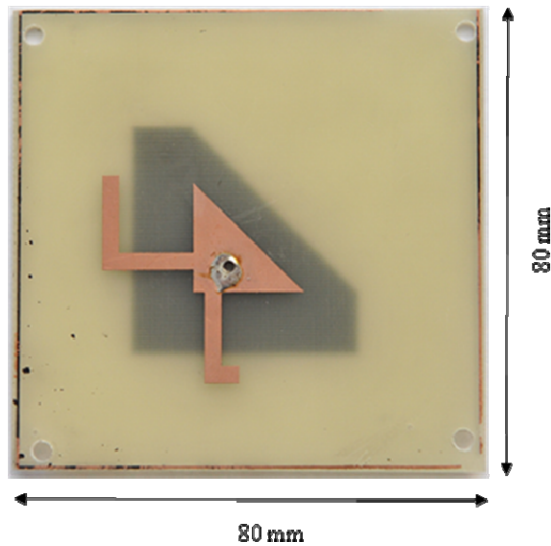


Figure 2.2 – Prototype of the proposed triangular patch antenna. This antenna has been fabricated on a 1.58 mm thick FR4 substrate with a dielectric constant of 4.4. Photo etching technique has been used for fabrication of this antenna.

2.2.1.1 Field reflection technique

The major drawback of the proposed design was that the boresight radiation from the patch and the monopoles was not in the same direction. The radiation beam from the patch was focussed towards zenith. However, the beam, due to the monopoles, got tilted towards the backward direction (below the patch). The stated reason for the beam tilt is due to the existence of dielectric substrate below the radiating strip of the printed monopoles. The radiation characteristics of the proposed antenna without realizing pattern synthesis technique have been shown in Fig. 2.3, Fig. 2.4 and Fig. 2.5. Fig. 2.5 shows the radiation from the patch with a realizable gain of 5 dBi. While Fig. 2.3 and Fig. 2.4 show radiation from the monopoles and possess realizable gain of 3.4 dBi and 3.5 dBi at 1.96 GHz and 2.45 GHz respectively. It can be easily noticed from Fig. 2.3 and Fig. 2.4 that the radiation peak is beneath the patch that makes the antenna impractical for the stated applications and hence justifies the need of a reflector for the proposed design. It can be seen from these figures that the peak radiation from the antenna at 2.45 GHz and 3.5 GHz is below the patch which is undesirable for the stated applications.

Hence, in order to overcome this radiation problem, a reflector metal sheet has been added below the actual ground plane of the patch to accomplish high gain as well as desired radiation characteristics. The location of the reflector plane has been optimized at 5 mm below the ground plane of the patch. The basic concept of this technique is to choose location of the reflector plane in such a way that the

reflected signal from this sheet adds in a phase with the radiated signal from the patch and improves the gain of the proposed antenna as well as the radiation peak is focussed in the desired direction. A parametric study on the location of the reflector plane has been carried out using EM solvers (CST Microwave Studio and Ansoft HFSS) and it has been found that the minimum dimension of the reflector plane is 80 X 80 mm². However, in practice, the mounting platform can be used as the reflector plane to achieve stated radiation and gain characteristics. The detailed parametric analysis that was carried out using CST microwave studio has been shown in the table 2.1. Antenna structure was simulated with different sizes of reflector plane at different locations below the patch to find the optimum case with desired radiation characteristics for stated commercial applications (the optimum case has been highlighted in the table 2.1 shown below). For the stated wireless applications (PCS, WLAN and WiMAX), the radiation characteristics should be in such a way that the connectivity with the base station antennas is ubiquitously maintained. Using this technique, the desired radiation characteristics and gain profile have been attained.

<u>Reflector plane size (sq. mm)</u>	<u>Location of reflector below the patch (mm)</u>	<u>Beam direction</u>	<u>Gain (dBi)</u>	<u>Return loss (dB)</u>
Original design without reflector	N/A	Backward direction	3.5/3.4/5 at 1.96/2.45/3.5 GHz	-13/-22/-13 at 1.96/2.45/3.5 GHz
40 X 40	3 mm	Backward direction	N/A	N/A
40 X 40	5mm	Backward direction	N/A	N/A

40 X 40	7 mm	Backward direction	N/A	N/A
40 X 40	9 mm	Backward direction	N/A	N/A
60 X 60	3 mm	Backward direction	N/A	N/A
60 X 60	5 mm	Backward direction	N/A	N/A
60 X 60	7 mm	Both sided	4.5/5.5/6 at 1.96/2.45/3.5 GHz	-11/-11/-21 at 1.96/2.45/3.5 GHz
60 X 60	9 mm	Both sided	4.58/6/6.58 at 1.96/2.45/3.5 GHz	-11/-11.3/-18 at 1.96/2.45/3.5 GHz
80 X 80	3 mm	Towards zenith	3.62/7.5/7.6 at 1.96/2.45/3.5 GHz	-18/-7/-21 at 1.96/2.45/3.5 GHz
80 X 80	5 mm	Towards zenith	6/8.1/7.2 at 1.96/2.45/3.5 GHz	-13/-13/-21 at 1.96/2.45/3.5 GHz
80 X 80	7 mm	Towards zenith	6.88/7.5/6.96 at 1.96/2.45/3.5 GHz	-13/-13.1/-18 at 1.96/2.45/3.5 GHz
80 X 80	9 mm	Towards zenith	6.6/8/6.83 at 1.96/2.45/3.5 GHz	-14/-14/-15 at 1.96/2.45/3.5 GHz

Table 2.1 – This table shows the parametric analysis carried out using CST Microwave Studio towards the size and location optimization of reflector plane below the patch. The highlighted case in the table has been realized for the proposed integrated triangular patch design. Note: Slight variations in the resonant frequencies were also noticed while optimising dimensions of the reflector sheet (that have not been shown here). These variations in resonant frequencies were further optimized to original frequencies by changing corresponding dimensions in the antenna.

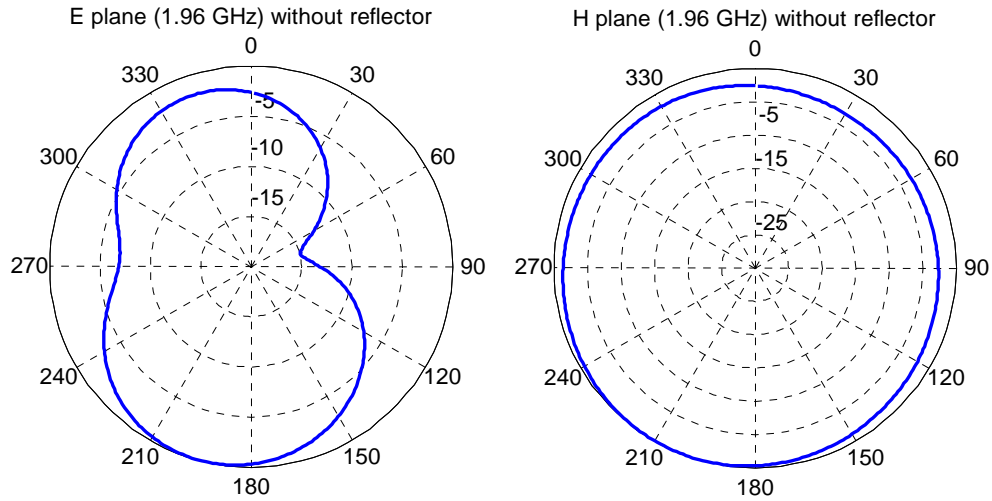


Figure 2.3 – Simulated (solid line) radiation patterns without reflector plane at 1.96 GHz. This figure shows both E-plane (X-Z plane) and H-plane (Y-Z plane) normalized patterns at PCS frequency of operation.

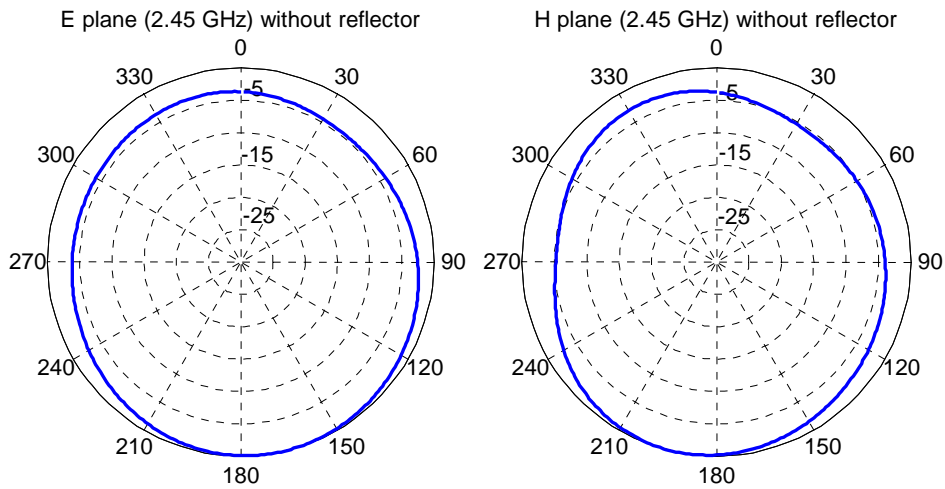


Figure 2.4 – Simulated (solid line) radiation patterns without reflector plane at 2.45 GHz. This figure shows both E-plane (X-Z plane) and H-plane (Y-Z plane) normalized patterns at WLAN frequency of operation.

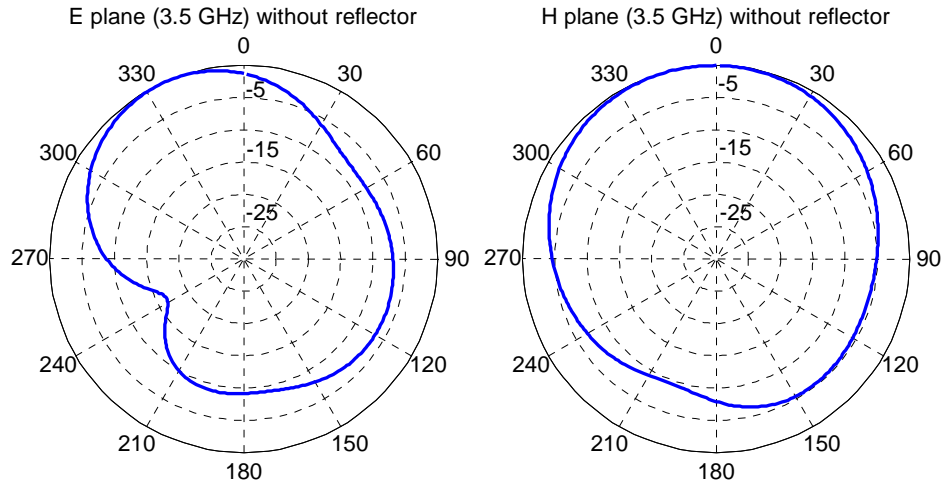


Figure 2.5 – Simulated (solid line) radiation patterns without reflector plane at 3.5 GHz. This figure shows both E-plane (X-Z plane) and H-plane (Y-Z plane) normalized patterns at WiMAX frequency of operation.

2.2.1.2 Measurement and simulation results

The antenna operation has been verified using two EM solvers - CST Microwave Studio and Ansoft HFSS, and the experimental measurements. The simulated and measured return loss has been shown in Fig. 2.6. The simulated (CST) return loss at 1.96 GHz, 2.45 GHz and 3.5 GHz are -23.46 dB, -16.55 dB and -14.12 dB respectively. While the measured return loss are around -12.97 dB, -10.87 dB and -8.6 dB respectively at the specified resonant frequencies. The percentage error between the simulation and measurements with regard to shift in the resonant frequency is around 1.9 %, 1.45 % and 2 % at 1.96 GHz, 2.45 GHz and 3.5 GHz respectively. The real and imaginary impedances of the antenna have also been shown in Fig. 2.7 and Fig. 2.8 respectively. The simulated and measured impedances plots illustrate an acceptable impedance match at the resonant

frequencies i.e. the real part of the impedance is close to 50 ohms while the imaginary value is as low as 0 ohms.

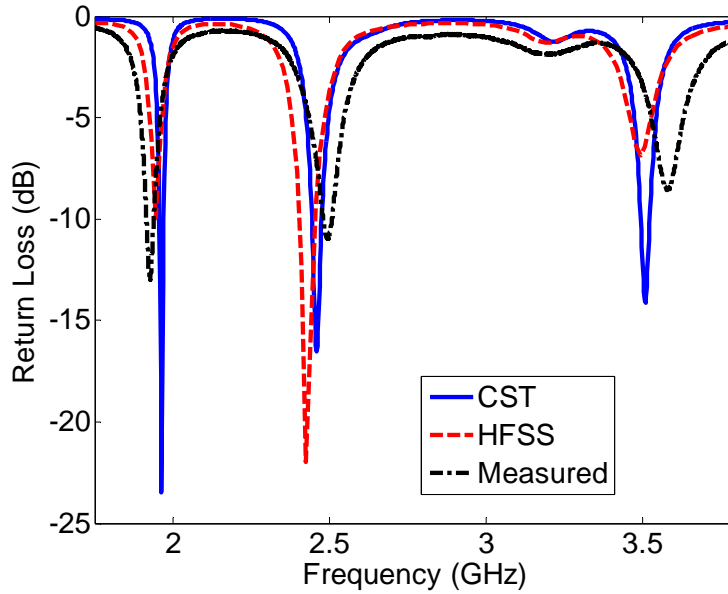


Figure 2.6 – Return loss vs. frequency. This figure shows the comparison of return loss characteristics for the proposed antenna design between two EM solvers (CST microwave studio and Ansoft HFSS) and measurements.

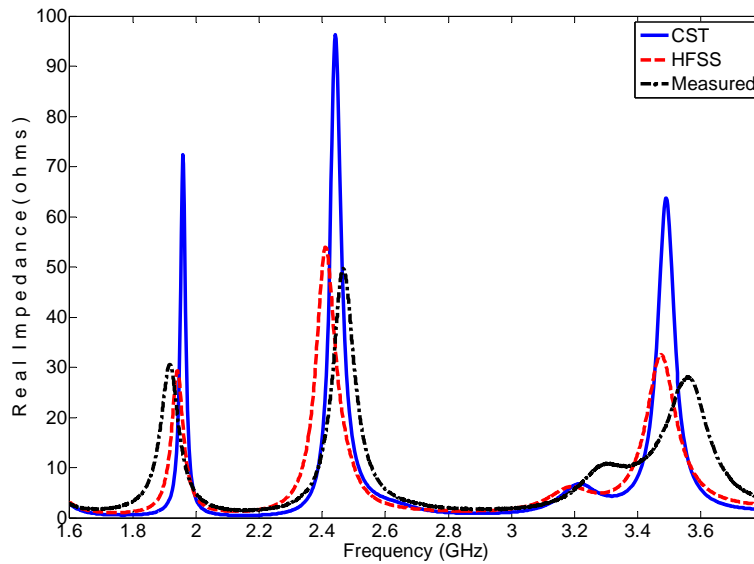


Figure 2.7 – Simulated and measured real impedance vs. frequency. This figure represents the variation of real impedance versus the frequency.

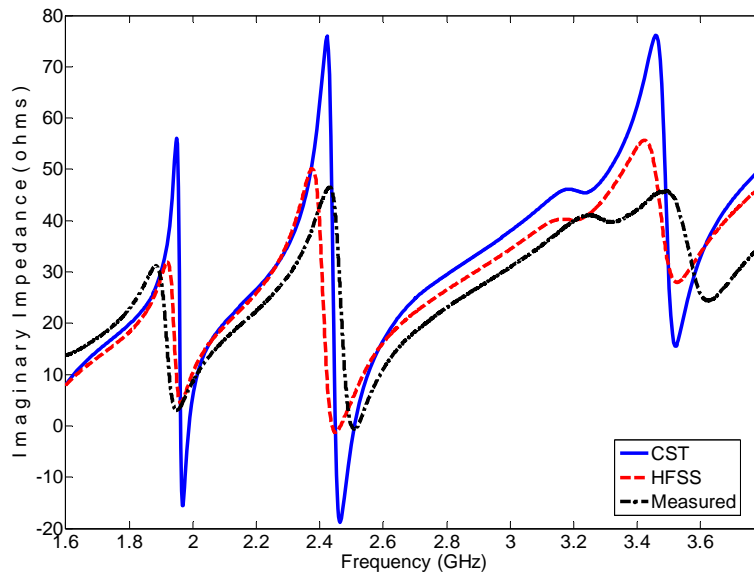


Figure 2.8 – Simulated and measured imaginary impedance vs. frequency. This figure represents the variation of imaginary impedance versus frequency. It can be noticed that the imaginary impedance is close to 0 ohms at 1.96 GHz, 2.45 GHz and 3.5 GHz as desired.

Furthermore, the current distribution patterns (CST) at 1.96 GHz, 2.45 GHz and 3.5 GHz have also been shown in Fig 2.9, Fig. 2.10 and Fig. 2.11 respectively. These patterns clearly demonstrate the independent functionality of the design with regard to resonant frequency operation. Nevertheless, a similar design procedure can be followed to realize an antenna design for different commercial applications.

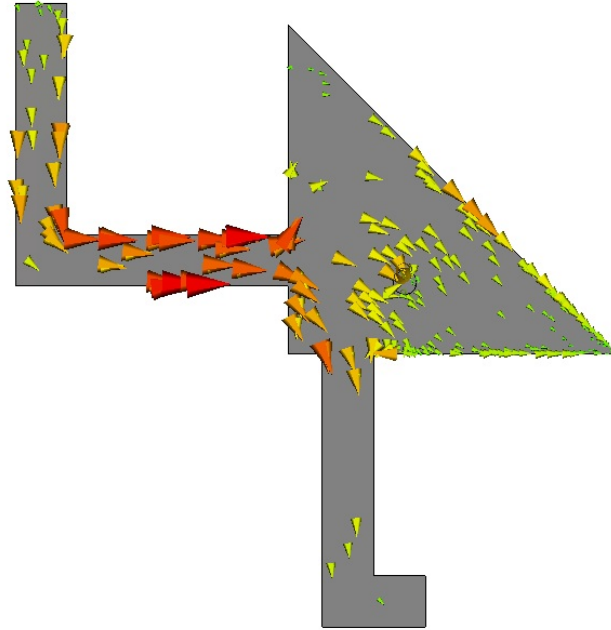


Fig 2.9 – Surface current distribution at 1.96 GHz. This figure noticeably shows that the strong surface currents exist on the monopole fused along the height (side) of the triangular patch that realizes resonance at PCS frequency.

The simulated and measured radiation patterns of the antenna at PCS, WLAN and WiMAX frequencies have also been shown in Fig. 2.12, Fig. 2.13 and Fig. 2.14 respectively. The measured radiation patterns are very similar to the simulated patterns; thus making this design suitable for the stated applications. All the patterns shown below are the normalized patterns. The simulated beamwidths in E-plane (X-Z plane) and H-plane (Y-Z plane) at the specified resonant frequencies are typically around 77° and 80° respectively. However, in terms of comparison between the simulated and the measured patterns, the typical error in the E-plane and H-plane beamwidths is about 4.9 % and 13.3 % respectively. Due to the lack of availability of anechoic chamber, all the measurements have been

carried out in the free space environment using power meter as the receiver and network analyzer as the source. However, the agreement found between simulated and measured patterns is still very close to each other. The measurement setup that has been used to assess radiation characteristics and gain of the antenna has been shown in Fig. 2.15. During free space measurements, a turn table has been used to capture the signal at different angles in the far field (c.f. Fig. 2.15). Furthermore, peaking has been carried out to measure the boresight gain in the far field.

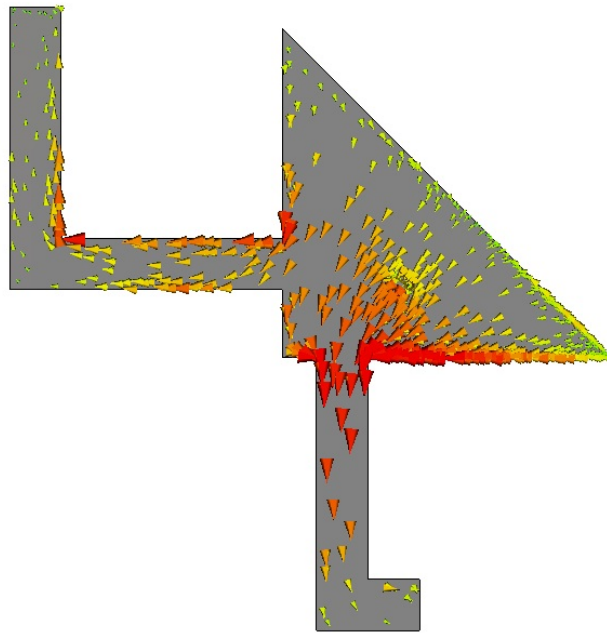


Fig 2.10 – Surface current distribution at 2.45 GHz. This figure noticeably shows that the strong surface currents exist on the monopole fused along the base (bottom) height of the triangular patch that realizes resonance at WLAN frequency.

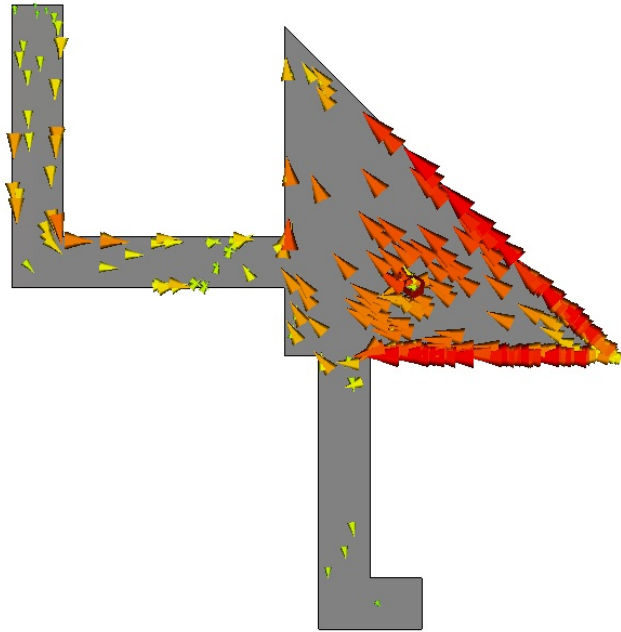


Fig 2.11 – Surface current distribution at 3.5 GHz. This figure noticeably shows that the strong surface currents exist on the right isosceles triangular patch that resonates at WiMAX frequency of operation.

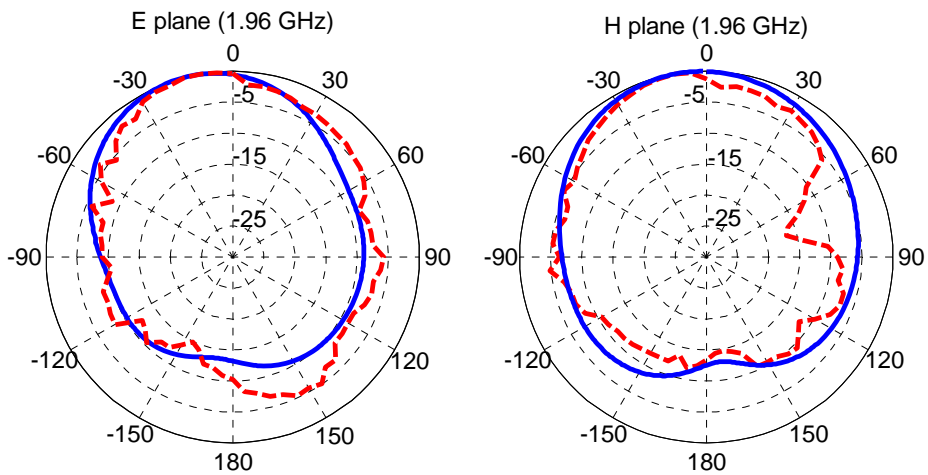


Figure 2.12 – Simulated (solid line) and Measured (dash line) radiation patterns at 1.96 GHz. This figure shows both E-plane (X-Z plane) and H-plane (Y-Z plane) normalized patterns at PCS frequency of operation.

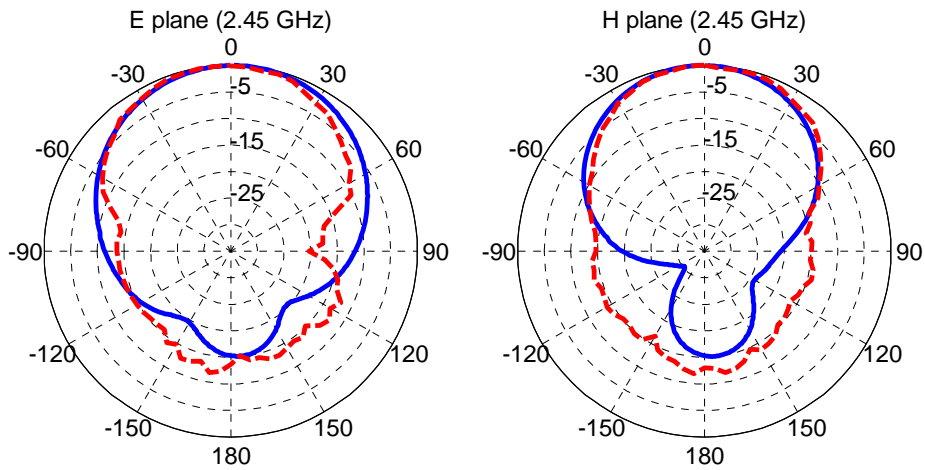


Figure 2.13 – Simulated (solid line) and Measured (dash line) radiation patterns at 2.45 GHz. This figure shows both E-plane (X-Z plane) and H-plane (Y-Z plane) normalized patterns at WLAN frequency of operation.

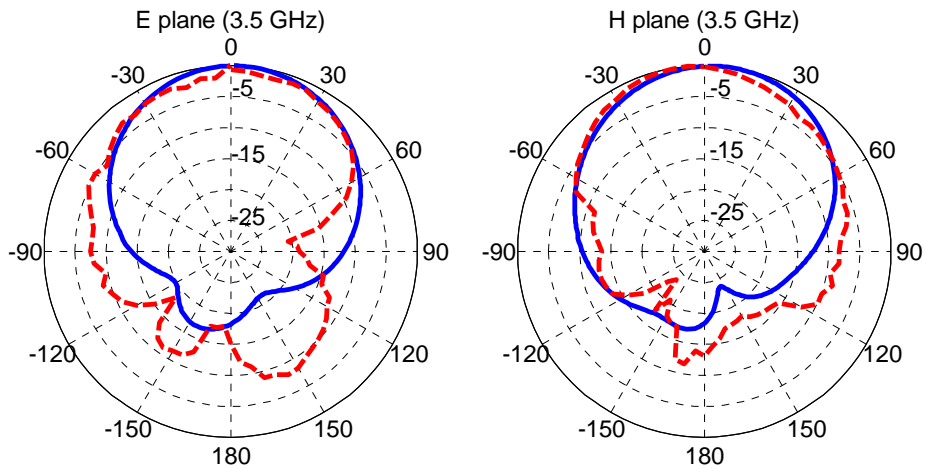


Figure 2.14 - Simulated (solid line) and Measured (dash line) radiation patterns at 3.5 GHz. This figure shows both E-plane (X-Z plane) and H-plane (Y-Z plane) normalized patterns at WiMAX frequency of operation.

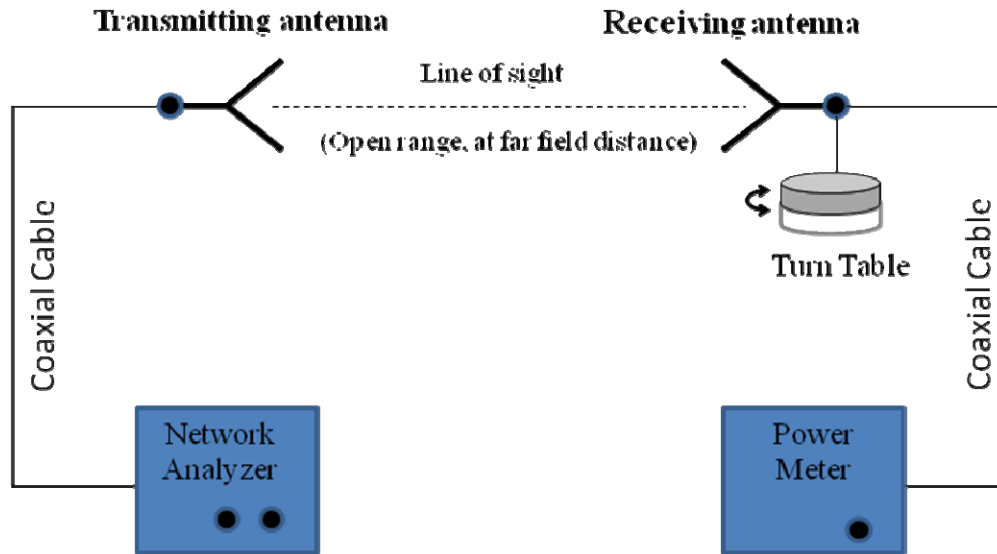


Fig 2.15 - Measurement setup. This figure shows the measurement setup that has been used to carry out the measurements. All the measurements have been done in the open range at far field distance.

The simulated and measured realizable gain has also been shown in Fig. 2.16. The simulated (CST) realizable gain at all the resonant frequencies is better than 5 dBi, which explains the role of the reflector ground plane below the patch to achieve directive radiation characteristics. The simulated realizable gain (CST) at 1.96 GHz, 2.45 GHz and 3.5 GHz is 5.8 dBi, 7.9 dBi and 7.5 dBi respectively. The measured gain at the resonant frequencies is around 1.3 dBi, 6.28 dBi and 7.95 dBi respectively. Also, it is found that the measured impedance bandwidth is smaller than the simulated impedance bandwidth. However, to improve the bandwidth of the antenna, broadband monopole configurations can be integrated at different resonant frequencies [87-88].

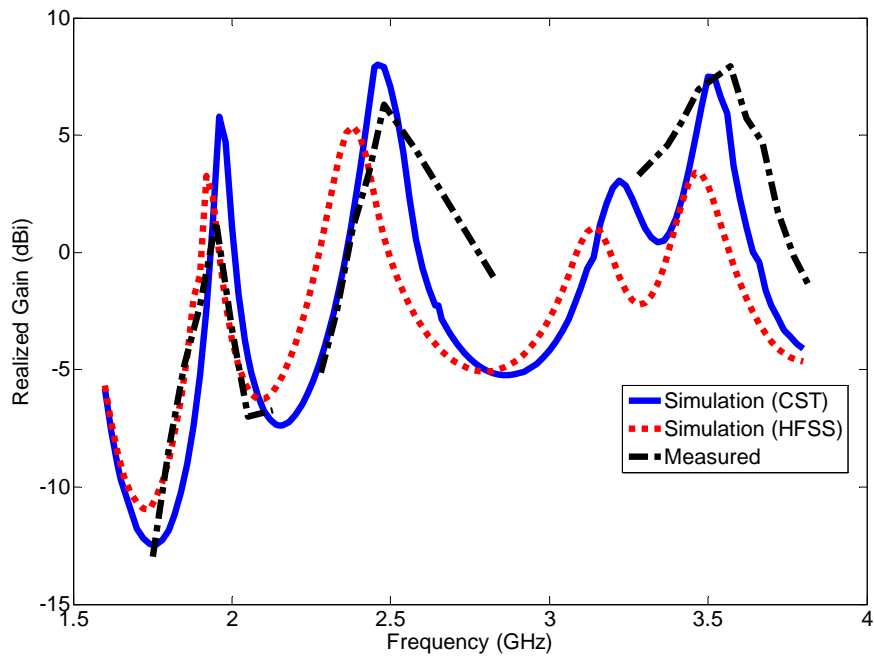


Figure 2.16 – Simulated and measured realized gain vs. frequency. This figure shows antenna gain profile as a function of frequency. Note: Measured realized gain data has been shown only at desired frequencies due to the limitation of measurement facilities.

2.2.2 Integrated semi-circular patch antenna design

The second proposed antenna design is also a single probe-fed design that comprises of a semi-circular patch integrated with a slot and a monopole. The patch resonates at 3.5 GHz (WiMAX), while the slot and the monopole resonate at 5.5 GHz (WiMAX) and 2.45 GHz (WLAN) respectively. The design and structural view of the proposed design is shown in Fig. 2.17.

The design principle of the semi-circular patch can be followed using this empirical equation:

$$D \approx \lambda_g, \tag{1}$$

Where, D is the diameter of the patch and $\lambda_g = \frac{c}{f_0 \sqrt{\epsilon_{reff}}}$

Where, c is the speed of the light, f_0 is the frequency of the operation and ϵ_{reff} is the effective dielectric constant [26].

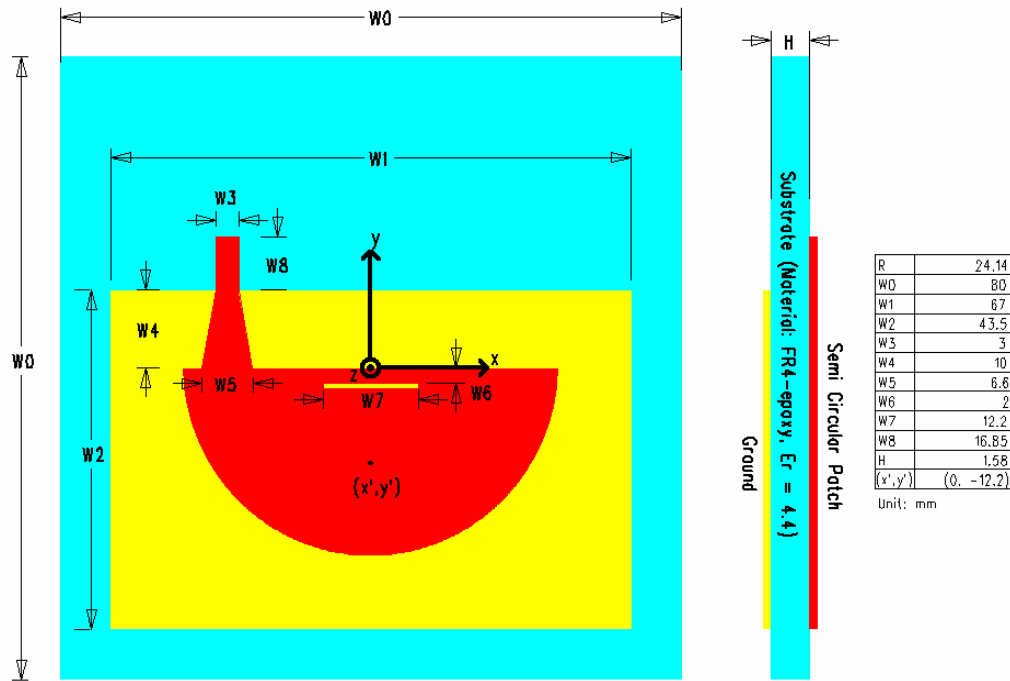


Figure 2.17 – Integrated semi-circular patch antenna design. This figure represents the top (left) and side view (centre) of the antenna design. All the dimensions of the antenna have been shown in the table (right).

The stated empirical equation is derived based on detailed parametric study and current distribution analysis of the patch. The current distribution at 3.5 GHz is shown in Fig. 2.18. Two half wavelength variations can be easily observed from the current pattern shown in Fig. 2.18, which supports the stated mathematical

interpretation in equation (1). Furthermore, the current distribution at the other two resonant frequencies (2.45 GHz and 5.5 GHz) has also been shown in Fig. 2.19 and Fig. 2.20. The current distribution patterns shown below at specified frequencies support the concept of independent frequency operation in the proposed integrated semi-circular patch antenna design.

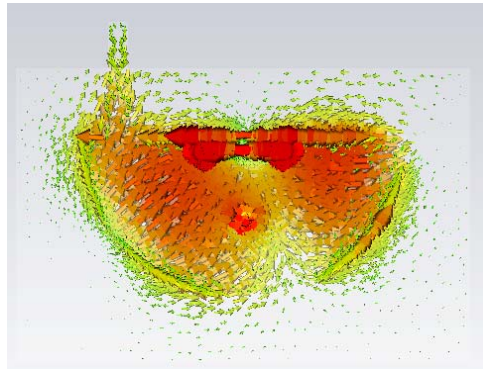


Fig 2.18 – Surface current distribution at 3.5 GHz. This figure noticeably shows that the strong surface currents exist on the semi-circular patch that realizes resonance at WiMAX frequency (3.5 GHz).

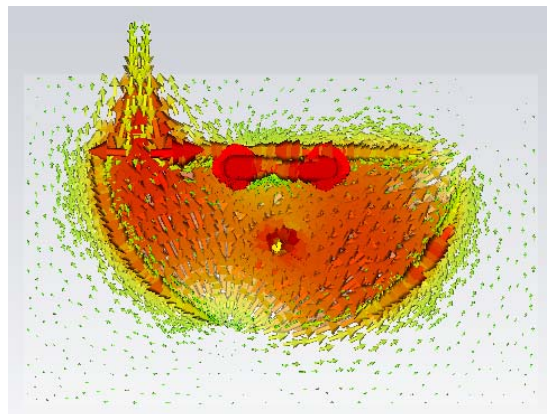


Fig 2.19 – Surface current distribution at 2.45 GHz. This figure noticeably shows that the strong surface currents exist on the monopole that realizes resonance at WLAN frequency of operation.

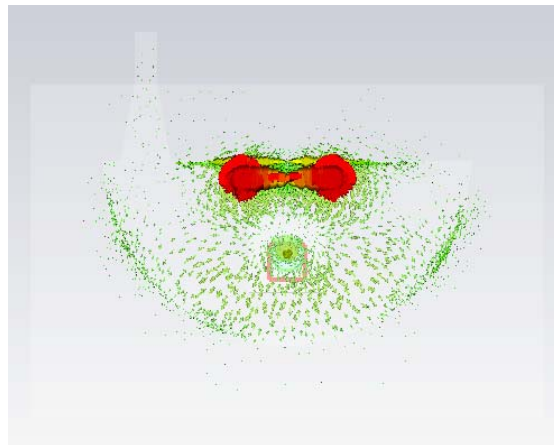


Fig 2.20 – Surface current distribution at 5.5 GHz. This figure noticeably shows that the strong surface currents exist on the slot that realizes resonance at WiMAX (5.5 GHz) frequency.

The monopole integrated into the antenna design is a quarter wavelength monopole including fringing field depth. As shown in Fig. 2.17, tapers have been added to the monopole to enhance the flow of current into it. The taper width however has been optimized in accordance with the return loss characteristics at 2.45 GHz using EM solvers. A part of the monopole acts as a feeding microstrip line (with ground plane) and the other part as the radiating strip (without ground plane).

Also, as stated earlier, to realize resonance at 5.5 GHz, a slot has been cut on the patch at the location where the surface currents are maximum at 5.5 GHz. The dimension of the slot has been calculated based on the analysis that slot acts as

an $\lambda/2$ electric dipole in the far field including the effect of effective dielectric constant [26]. So the length of the slot can be approximated as

$$l \approx \lambda_g / 2 \quad (2)$$

where l is the length of the slot. However, the width of the slot is optimized for the impedance matching at 5.5 GHz. The dimension of the proposed design has been shown in Fig. 2.17. This design is also realized on a 1.58 mm thick FR4 substrate ($\epsilon_r = 4.4$). Prototype of the proposed design has been fabricated and is shown in Fig 2.21.

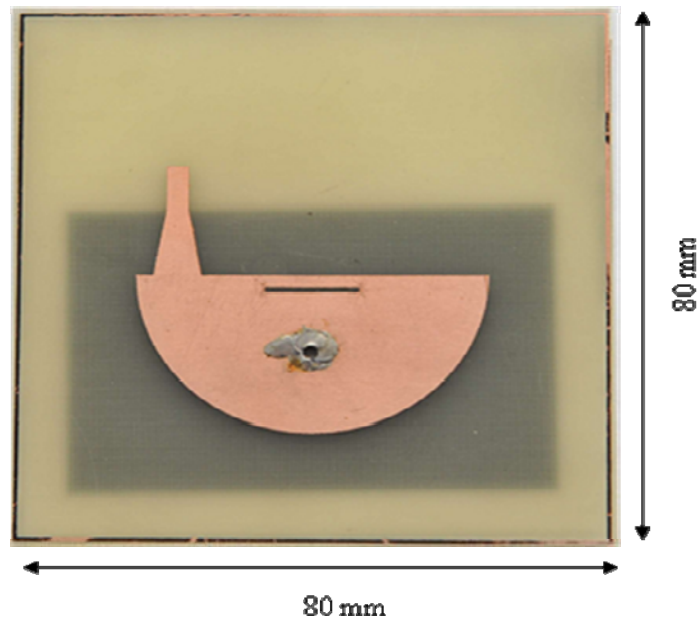


Figure 2.21 – Prototype of the proposed semi-circular patch antenna. This antenna has been fabricated on a 1.58 mm thick FR4 substrate with a dielectric constant of 4.4. Photo etching technique has been used for fabrication of this antenna.

2.2.2.1 Measurement and simulation results

Two EM solvers (CST Microwave Studio and Ansoft HFSS) have been used for the verification of the antenna characteristics. An agreeable match has been found between simulated and measurement results. The simulated and measured return loss has been shown in Fig. 2.22. The simulated return loss at 2.45 GHz, 3.5 GHz and 5.5 GHz is 19.8 dB, 12.1 dB and 10.91 dB, while the measured return loss at the specified resonant frequencies are 23.2 dB, 9.8 dB and 15.8 dB respectively. The typical error in terms of the shift in the resonant frequency between the simulation and the measurements is around 7.9 %, 6.8 % and 1.8% at 2.45 GHz, 3.5 GHz and 5.5 GHz respectively. The simulated and measured impedances (real and imaginary) of the antenna have also been shown in Fig. 2.23 and Fig. 2.24 respectively.

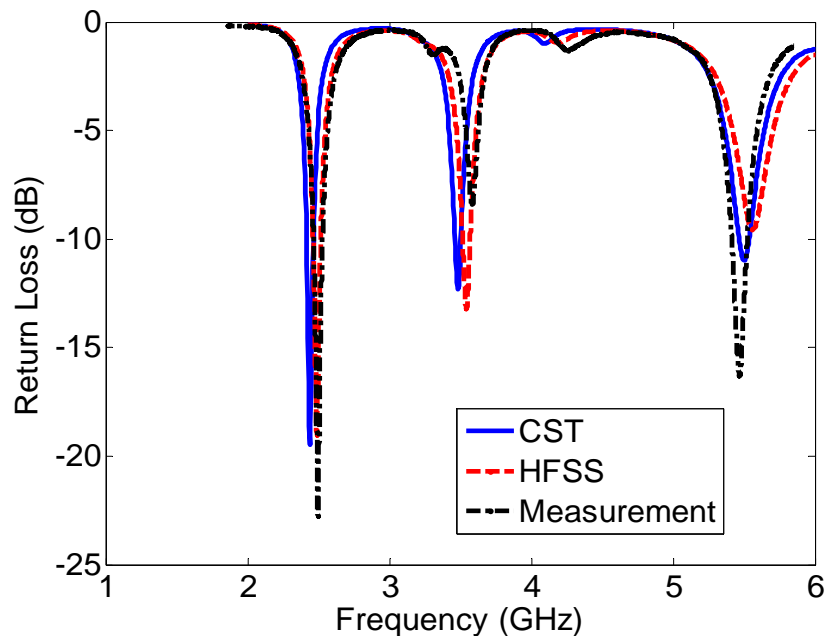


Figure 2.22 – Return loss vs. Frequency. This figure shows the comparison of return loss characteristics for the proposed antenna design among two EM solvers (CST microwave studio and Ansoft HFSS) and measurements.

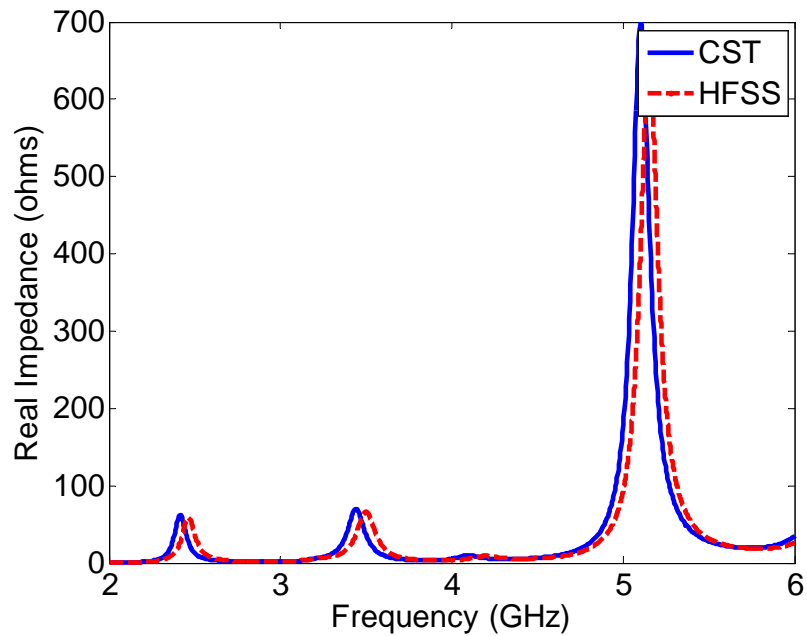


Figure 2.23 – Simulated and measured real impedance vs. frequency. This figure represents the variation of real impedance versus frequency. It can be noticed that the real impedance is close to 50 ohms at 2.45 GHz, 3.5 GHz and 5.5 GHz as desired.

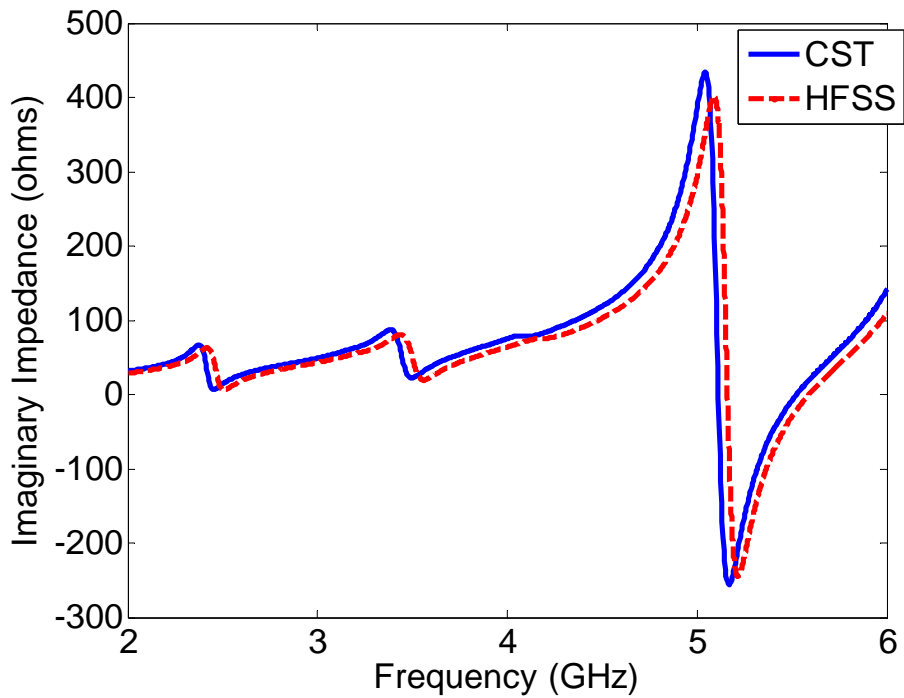


Figure 2.24 – Simulated and measured imaginary impedance vs. frequency. This figure represents the variation of imaginary impedance versus frequency. It can be noticed that

the imaginary impedance is close to 0 ohms at 2.45 GHz, 3.5 GHz and 5.5 GHz as desired.

Furthermore, the simulated and measured radiation patterns of the antenna at WLAN (2.45 GHz) and WiMAX (3.5/5.5 GHz) frequencies have been shown in Fig. 2.25, Fig. 2.26 and Fig. 2.27 respectively. The typical simulated beamwidth in E-plane (Y-Z plane) and H-plane (X-Z plane) at specified resonant frequencies is around 127° and 72° respectively. The percentage difference between the simulated and measured beamwidth is around 8.5 % and 21 % for the E-plane and H-plane respectively.

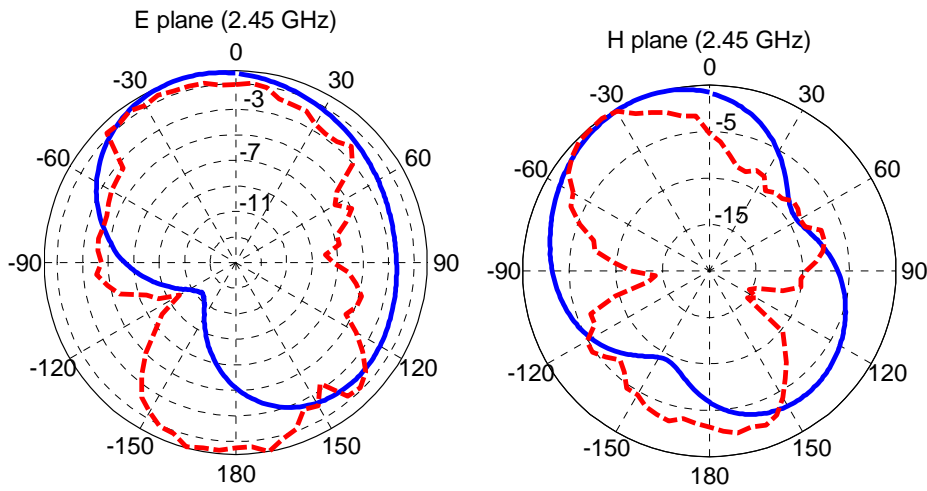


Figure 2.25– Simulated (solid line) and Measured (dash line) radiation patterns at 2.45 GHz. This figure shows both E-plane (X-Z plane) and H-plane (Y-Z plane) normalized patterns at WLAN frequency of operation.

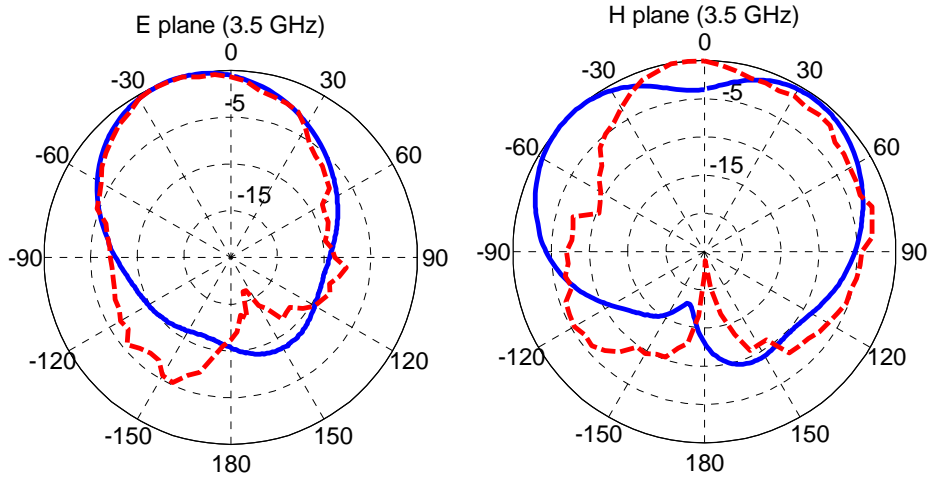


Figure 2.26– Simulated (solid line) and Measured (dash line) radiation patterns at 3.5 GHz. This figure shows both E-plane (X-Z plane) and H-plane (Y-Z plane) normalized patterns at WiMAX (lower band) frequency of operation.

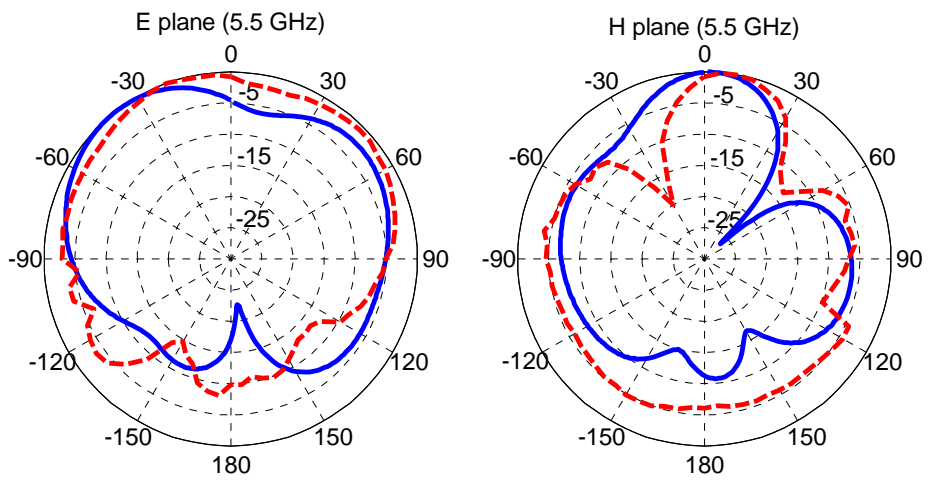


Figure 2.27– Simulated (solid line) and Measured (dash line) radiation pattern at 5.5 GHz. This figure shows both E-plane (X-Z plane) and H-plane (Y-Z plane) normalized patterns at WiMAX (Upper band) frequency of operation.

The simulated and measured realizable gain has also been shown in Fig.2.28. The simulated realizable gain at 2.45 GHz and 3.5 GHz and 5.5 GHz is 1.2 dBi, 1.5

dBi and 1.8 dBi, while the measured gain at the resonant frequencies is around 1.7 dBi, 2 dBi and 3.9 dBi respectively. It can be noticed that at 5.5 GHz, the reported measured gain (3.9 dBi) is quite higher than the simulated gain (1.8 dBi). The anticipated reason for this could be due to the free space measurement setup (ref. Fig. 2.12) that might give rise to multiple reflections. Nevertheless, the stated comparisons between the simulation and the measurements support the design operation and its usability for the specified applications.

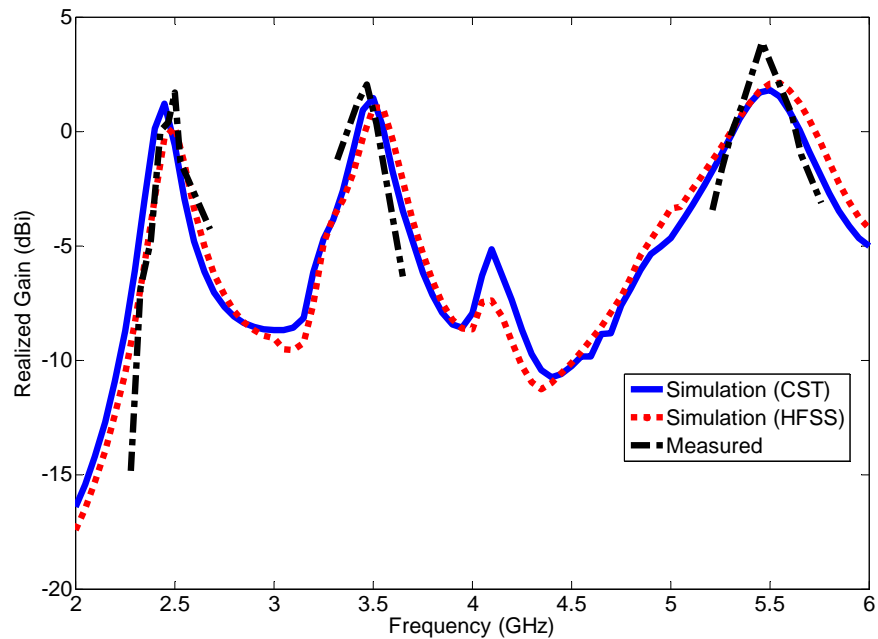


Figure 2.28– Simulated and measured realized gain vs. frequency. This figure shows antenna gain profile as a function of frequency. Note: Measured realized gain data has been shown only at desired frequencies due to the limitation of measurement facilities.

2.3 Limitations and Improvements

Both the designs have been thoroughly explained in the above stated sections of the chapter. One of the major drawbacks that both these designs have is the limited bandwidth. However, in the future works, more research can be carried out to increase the antenna bandwidth. Different countries provide the same wireless services using different sub channels of the allocated wireless bands [9]. Hence, increased bandwidth will support the usability and applicability of the proposed antenna designs in more countries. Some of the ideas that can be implemented for the proposed designs to improve the bandwidth are using broadband configurations of monopoles [87-88], realizing shorting walls and strips [81-83], using modified ground planes [89] or by changing the substrate properties like thickness and permittivity [26]. Furthermore, other improvements that can be entertained towards the betterment of the proposed antenna designs depend on additional miniaturization of the designs to advance applicability and incorporation of more frequency bands in the same design.

2.4 Conclusion

Two multi-band probe-fed microstrip patch antenna designs have been proposed. Both the designs are realized on a 1.58 mm thick FR4 substrate with a dielectric constant of 4.4. The first design comprises of a right isosceles triangular patch integrated with a pair of monopoles. The patch resonates at 3.5 GHz (WiMAX frequency); however, the monopoles realize resonance at 2.45 GHz (WLAN

frequency) and 1.96 GHz (PCS frequency) respectively. Additionally, to achieve better radiation characteristics and higher gain, a reflector ground plane has been placed below the patch. The second proposed design consists of a semi-circular patch integrated with a slot and a monopole. The patch resonates at 3.5 GHz; however, the slot and monopole resonate at 5.5 GHz and 2.45 GHz respectively. For the analysis of the proposed designs, two EM solvers are used – CST Microwave Studio and Ansoft HFSS. A reasonable agreement has been found between simulation and experimental results.

Chapter 3

Design of frequency tunable annular ring patch antenna for multi- frequency applications

Abstract

In this chapter, a frequency tunable dual-band microstrip annular ring patch antenna design has been proposed for wireless local area network (2.45 GHz) and WiMAX (3.5 GHz) applications. The proposed antenna achieves realizable gain over 5dBi and return loss better than 10 dB for the stated applications. The antenna design consists of an annular ring patch loaded with a slot or gap. The loaded ring patch excites higher order modes around the dominant mode (TM_{11}) of the annular ring thus making this design capable of dual-band operation. This design is realized on a 1.57 mm thick PTFE (Poly Tetra Fluoro Ethylene) substrate using a co-axial probe feed. A novel technique for independent frequency tuning has also been introduced by cutting grooves on the periphery of the ring at the desired locations.

3

³ A version of this chapter has been accepted for publication in the Journal of IET Microwaves, Antennas and Propagation. Manuscript ID: MAP-2010-0571.R1. Date of acceptance: 8th June'2011. **K. Jhamb**, L. Li and K. Rambabu, "Frequency Adjustable Microstrip Annular Ring Patch Antenna with Multi-band Characteristics".

Furthermore, the design capability for multi-band operation (2.45 GHz/3.5 GHz/5.5 GHz) has been explained in the later section of the chapter. Two EM solvers (CST Microwave Studio and Ansoft HFSS) and measurements have been used to verify the operation of the proposed annular ring antenna. An acceptable agreement has been found between the simulated and the measured results.

3.1 Introduction

Among various shapes of microstrip patch antennas, ring antennas are one of the types preferred for wireless equipments due to their compatibility with small portable units [90-92]. Bandwidth, input impedance and radiation pattern characteristics for ring antennas have been studied in [93]. As inferred from the published literature [94-98], microstrip ring antennas are generally loaded with stubs, notches and slots to improve polarization purity or to improve impedance match at the dominant mode of operation. However, in this paper, an antenna design has been proposed for the dual-band operation by loading the ring with a gap that excites higher order modes of the patch for multi-band operation. The proposed design realizes resonance at 2.45 GHz and 3.5 GHz for WLAN and WiMAX applications respectively. The design principle for this technique has been discussed in [95]. The proposed design realizes gain better than 5 dBi, return loss better than 10 dB and the desired radiation characteristics at 2.45 GHz and 3.5 GHz.

Generally, for this design, the freedom to independently tune the resonant frequencies is not possible due to the excitation of higher order modes of the patch. In this chapter, a novel technique to independently tune the resonant frequencies has been introduced by cutting grooves of different depths at the desired locations on the ring. The detailed description of this technique has been explained in the later part of the chapter. Furthermore, analytical analysis for the frequency tuning technique has also been described by deriving empirical equations. The capability of the design for multiband operation has also been shown. A prototype for the proposed design has been fabricated. The antenna design has been verified using two EM solvers – Microwave CST Studio and Ansoft HFSS, and measured results. A close agreement has been found between the simulation and the measurements.

3.2 Dual band antenna design

Emerging trends in the field of wireless communication systems and the zeal to develop the devices with integrated services have turned out in a need to achieve products that are capable of receiving and transmitting wireless signals at the appropriate frequency bands. Introducing WLAN and WiMAX applications into a single mobile device is a growing trend in commercial applications. It makes end user capable of operating all wireless services with a single device. So the desired scenario will be a miniaturized antenna that supports multiple frequency operation with the appropriate polarizations, and the suitable radiation characteristics that maximize the signal connectivity.

The structure of the proposed dual-band annular ring antenna comprises of an annular ring patch loaded with a gap as shown in Fig. 3.1. The concept of loading to excite higher order modes of the patch and the design procedure have been introduced in [95] and have been utilized for the proposed design. The effect of loading on the radiation characteristics of the antenna has also been studied in [95]. For the proposed dual-band design, the loaded structure has been optimized to resonate at 2.45 GHz and 3.5 GHz respectively. This single coaxial probe-fed design is realized on a 1.57 mm thick PTFE substrate (dielectric constant = 2.5). Furthermore, the structural view and dimensions of the design have been shown in Fig. 3.1.

The cavity model of the ring can be obtained by replacing its peripheries with magnetic walls; and since there is no magnetic field component along the direction of signal propagation, the modes are designated as TM_{mn} modes [95]. The dominant mode of operation for the annular ring is TM_{11} mode [95-96]. The dual band characteristic for this structure has been achieved due to the slot or loading, which excites higher order modes of the patch around the dominant mode of the annular ring. The proposed antenna achieves design applicability for WLAN (2.45 GHz) and WiMAX (3.5 GHz) applications. First resonant frequency (f_1) that is WLAN frequency is due to the dominant mode of the annular ring. While the second resonant frequency (f_2), for WiMAX, is due to the gap that excites higher order mode of the patch.

The resonant wavelength of the dominant mode is approximately equal to the average circumferential length of the ring resonator, which is equal to $2\pi(R_{avg})$. It can be calculated using $R_{avg}=(R_1+R_2)/2$, where R_1 and R_2 are the outer and inner radii of the annular ring respectively as shown in Fig. 3.1.

However, in terms of empirical equations, it can be interpreted as:

$$\lambda_g \approx 2\pi(R_{avg}) \quad (1)$$

Where, λ_g represents resonant wavelength for the dominant mode. Therefore, resonant frequency for the dominant mode (f_1) can be calculated as

$$f_1 \approx c / 2\pi R_{avg} \sqrt{\epsilon_{reff}} \quad (2)$$

Where, ϵ_{reff} is the effective dielectric constant of the substrate.

The current distribution at 2.45 GHz and 3.5 GHz has been plotted in Fig. 3.2 and Fig. 3.3 respectively using CST microwave studio. At WLAN frequency (ref. Fig. 3.2), the ring structure possesses two half wavelength variations as current patterns, one on the upper half and the other on the lower half of the structure respectively. However, at WiMAX frequency, it can be found that the ring possesses three-half wavelength variations in current, as three 120 degree sectors on the circular ring, as shown in Fig. 3.3.

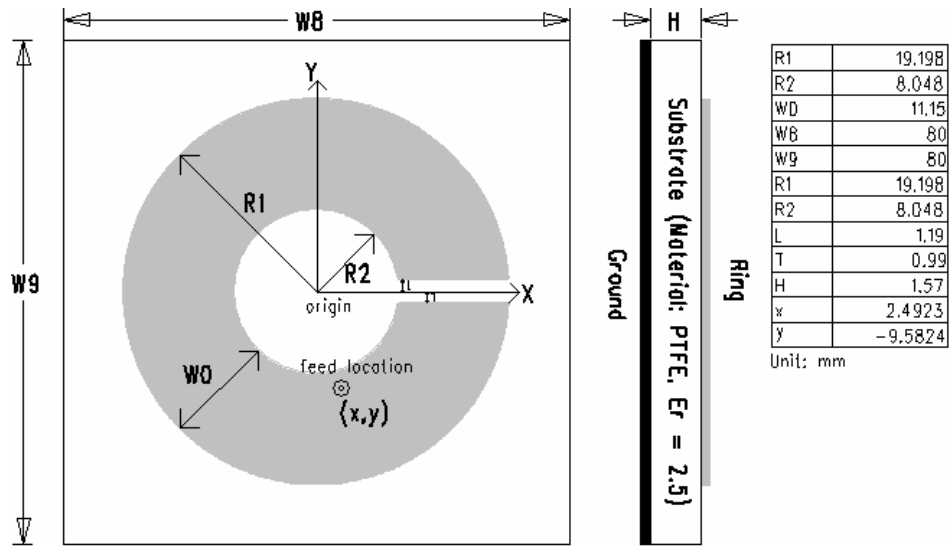


Figure 3.1 – Design of dual band antenna. This figure represents the top (left) and side view (centre) of the dual band antenna design. All the dimensions of the antenna have been shown in the table (right).

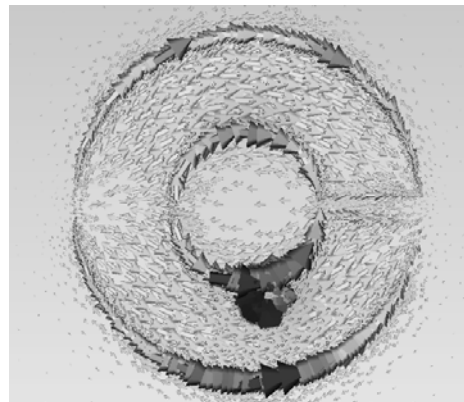


Figure 3.2 – Current distribution at 2.45 GHz. The proposed dual band antenna realizes two half wavelength variations in current distribution pattern at WLAN frequency of operation.

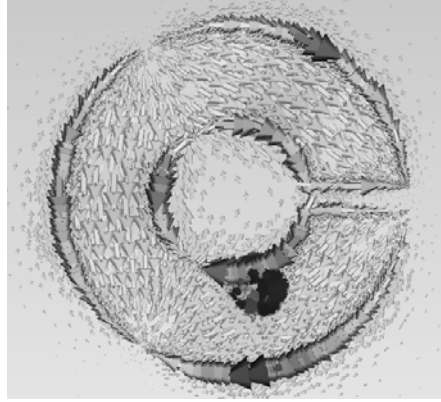


Figure 3.3 – Current distribution at 3.5 GHz. The proposed dual band antenna realizes three half wavelength variations in current distribution pattern at WiMAX frequency of operation.

3.2.1. Simulation and measurement results of dual-band antenna

For the simulation of the proposed design, two EM solvers – CST Microwave Studio and Ansoft HFSS have been used. In terms of comparison, a close agreement has been found between two solvers with regard to the antenna parameters like return loss, realizable gain and input impedance. A prototype of the proposed dual band antenna has been fabricated and is shown in Fig. 3.4. The fabrication has been carried out using photo etching process and all the measurements have been done in the free space environment using network analyzer.

For the proposed design, the ring and slot dimensions are optimized in such a way to make this structure suitable for the stated wireless applications. The simulated and measured return loss vs. frequency has been shown in Fig.3.5. The simulated

return loss at 2.45 GHz and 3.5 GHz is 19.5 dB and 11.4 dB respectively. However, the measured return loss at these frequencies is 19 dB and 11.2 dB respectively. Furthermore, the simulated real and imaginary impedances of the antenna have also been shown in Fig. 3.6 and Fig. 3.7 respectively. The proposed design possesses an acceptable impedance match at the desired resonant frequencies, thus supporting the usability of the design for commercial applications.

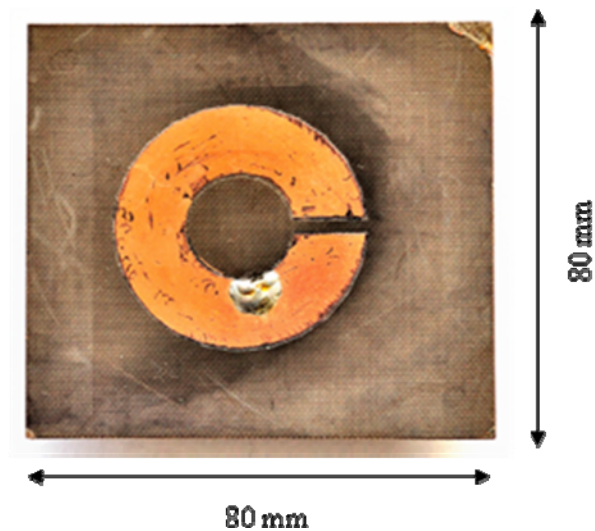


Figure 3.4 – Prototype of the proposed semi-circular patch antenna. This antenna has been fabricated on a 1.57 mm thick PTFE substrate with a dielectric constant of 2.5. Photo etching technique has been used for fabrication of this antenna.

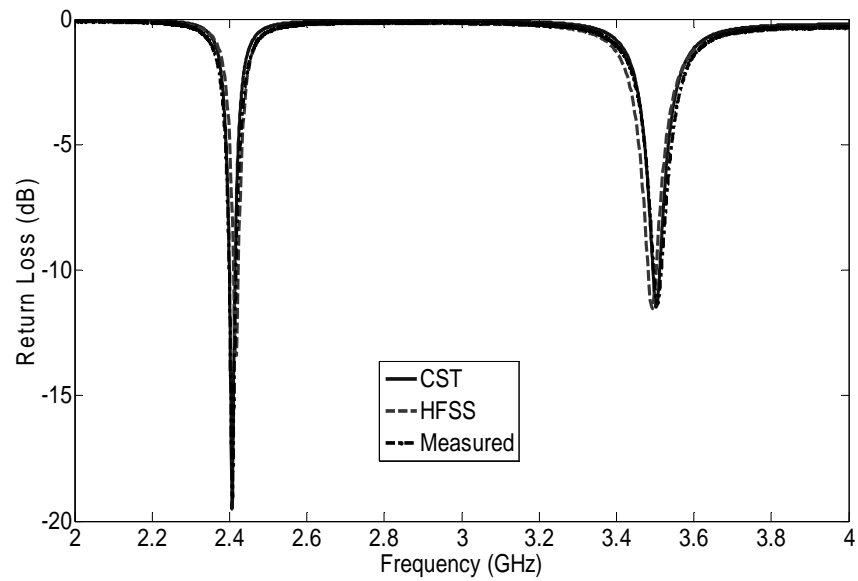


Figure 3.5 – Return loss vs. frequency. This figure shows the comparison of return loss characteristics for the proposed antenna design among two EM solvers (CST microwave studio and Ansoft HFSS) and measurements.

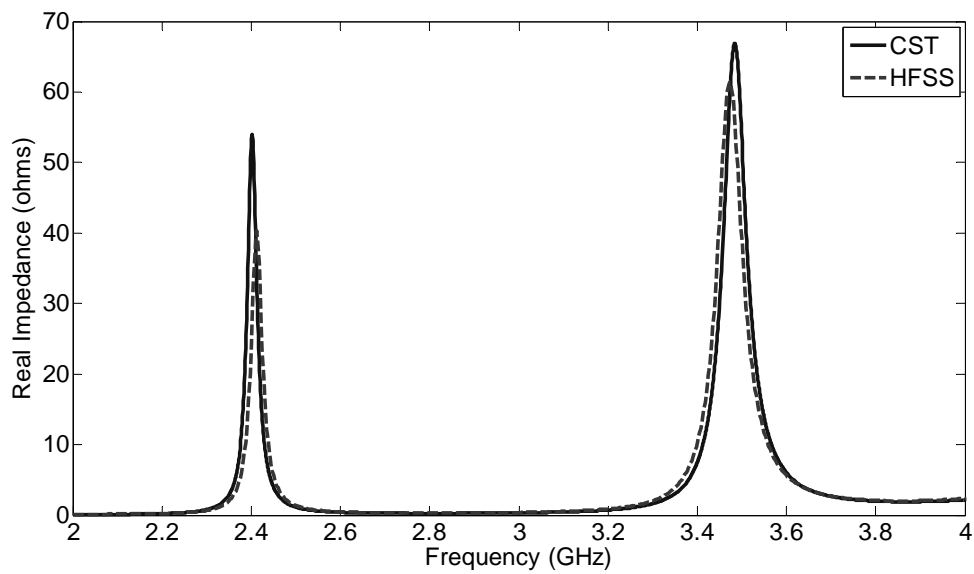


Figure 3.6 – Simulated real impedance vs. frequency. This figure represents the variation of real impedance versus frequency. It can be noticed that the real impedance is close to 50 ohms at 2.45 GHz and 3.5 GHz as desired.

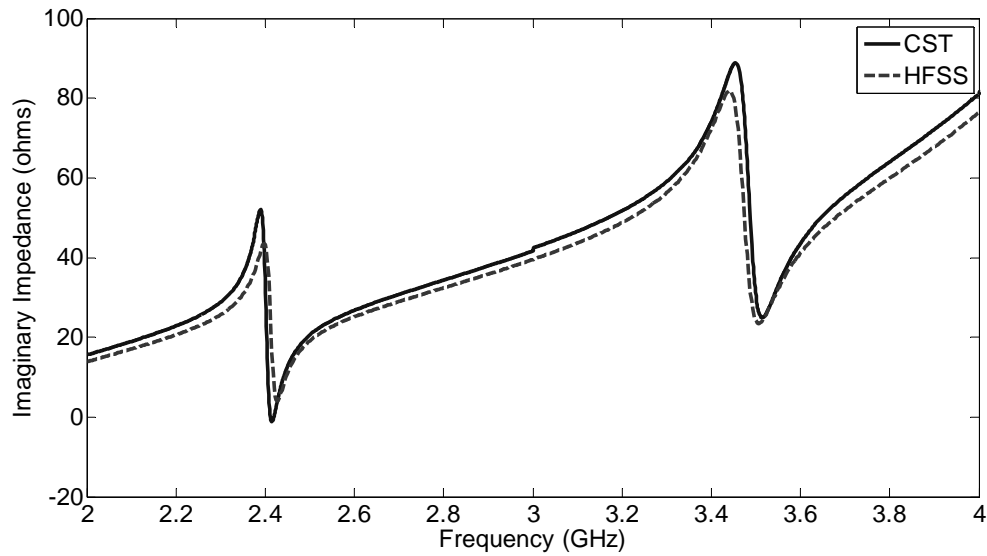


Figure 3.7 – Simulated imaginary impedance vs. frequency. This figure represents the variation of imaginary impedance versus frequency. It can be noticed that the imaginary impedance is close to 0 ohms at 2.45 GHz and 3.5 GHz as desired.

The simulated realizable gain vs. frequency has also been shown in Fig. 3.8 that supports the suitability of the antenna for the proposed applications. The realizable gain is better than 5 dBi at both the WLAN and WiMAX frequency band. At 2.45 GHz and 3.5 GHz, the simulated realizable gain is 7.3 dBi and 7 dBi respectively. Nevertheless, the radiation characteristics of the antenna are also one of the important parameters of the design, considering the design suitability for the commercial applications. HFSS simulated radiation patterns at 2.45 GHz and 3.5 GHz have been shown in Fig. 3.9 and Fig. 3.10 respectively. The typical E-plane/H-plane beamwidth at 2.45 GHz and 3.5 GHz is around $100^{\circ}/88^{\circ}$ and $74^{\circ}/100^{\circ}$ respectively. All the plotted radiation patterns have been normalized.

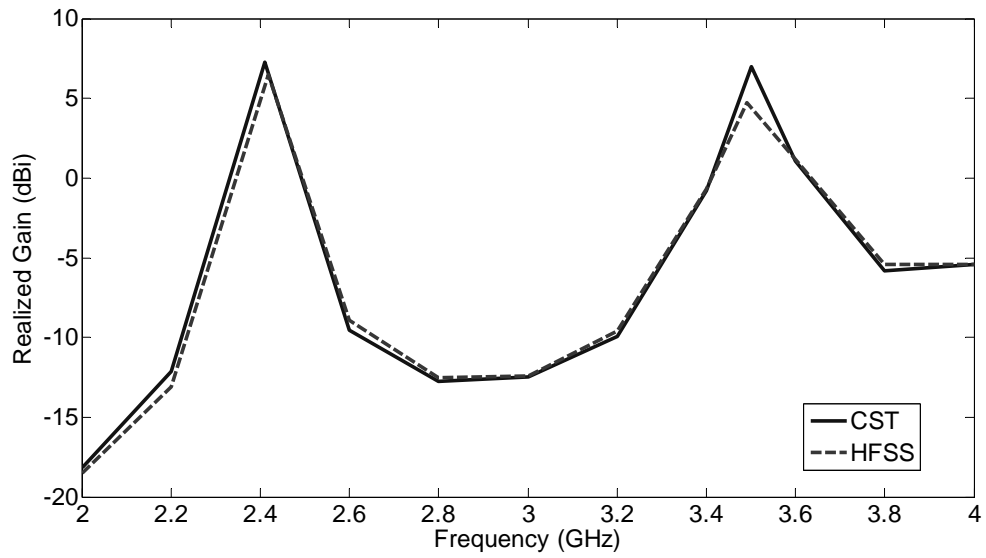


Figure 3.8 – Simulated realizable gain vs. frequency. This figure shows antenna gain profile as a function of frequency.

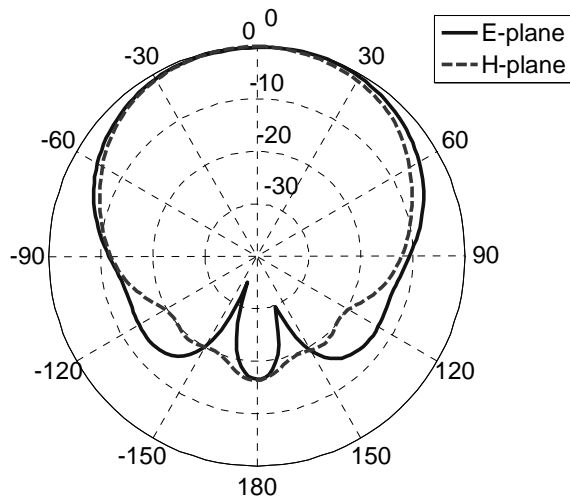


Figure 3.9 – Simulated radiation patterns at 2.45 GHz. This figure shows both E-plane (X-Z plane) and H-plane (Y-Z plane) normalized patterns at WLAN frequency of operation.

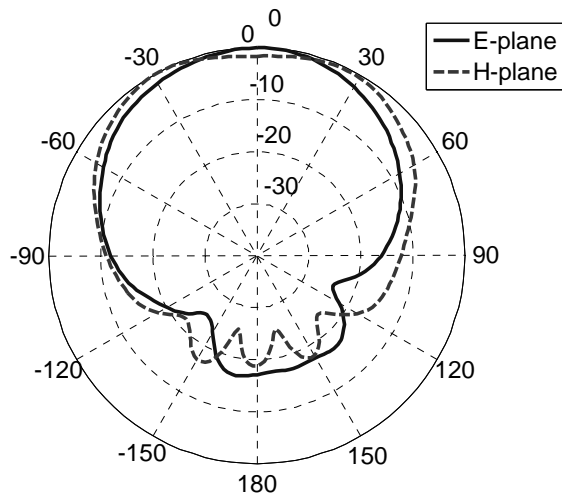


Figure 3.10 – Simulated radiation pattern at 3.5 GHz. This figure shows both E-plane (X-Z plane) and H-plane (Y-Z plane) normalized patterns at WiMAX frequency of operation.

3.3. Frequency tuning technique

Although the above design is resonating at 2.45 GHz (WLAN) and 3.5 GHz (WiMAX) frequencies; the resonant frequencies are not independently tunable. The dual band operation is due to the excitement of higher order modes, therefore, tuning the resonant frequencies independently is challenging. At the same time, incorporation of independent frequency tunability without any distortion in radiation characteristics is further more difficult. Hence, in this chapter, we propose a novel technique to independently tune the resonant frequencies of the proposed antenna by cutting grooves at different locations on the periphery of the ring as shown in Fig. 3.11.

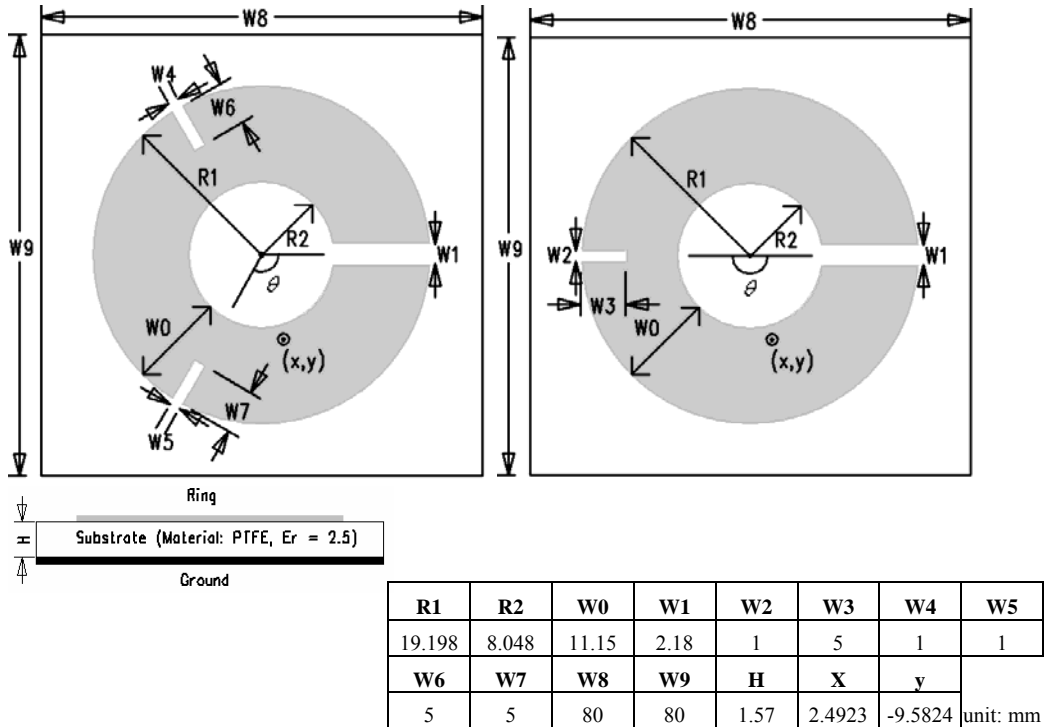


Figure 3.11 – Antenna design with single groove and two grooves. This figure represents the top (left) and side view (centre) of the dual band antenna design. All the dimensions of the antenna have been shown in the table (right).

Furthermore, the location of the grooves on the periphery of the antenna should be selected in such a way that the current distribution of the other mode is not disturbed. For example, to tune the resonant frequency of the WiMAX application, a single groove has been cut on the periphery of the antenna at the location where WLAN excitation has zero currents (c.f. Fig 3.2). Therefore, this groove will not have any effect on WLAN operating frequency. Same principle can be applied to tune the WLAN frequency operation. As explained above, at 2.45 GHz, the ring possess two half wavelength variations while at 3.5 GHz, it possess three half wavelength variations like three 120 degree sectors in the circle

(c.f. Fig. 3.3). Therefore, based on the ring structure and current distributions at 2.45 GHz and 3.5 GHz, an empirical equation (3) has been derived to find the location of the groove. For the notation of θ , refer to Fig. 3.11.

$$\theta = \frac{k\pi}{3}$$

(3)

Where k defines the number of half wavelength variations of current at that resonant frequency on the surface of the ring, for example the value of k is 2 and 3 for 2.45 GHz and 3.5 GHz respectively.

By using this technique, the same antenna can be used for the stated wireless applications in different countries. The variations of WLAN and WiMAX standards in different countries have been reported in [9]. To tune the WLAN frequency without affecting the WiMAX frequency, two grooves have been cut as shown in Fig. 3.11. The effect of groove depth on the operating frequency can be easily analysed by the simulated and measured return loss shown in Fig. 3.12 and Fig. 3.13 respectively. Similarly, a single groove has been cut to achieve independent tuning characteristics at 3.5 GHz as shown in Fig. 3.11. The simulated and measured return loss vs. frequency for the single groove design has also been shown in Fig. 3.14 and Fig. 3.15 respectively. It can be easily investigated from these plots that as the groove depth increases, the currents on the surface of patch travels longer electrical path. Hence, it reduces the operating frequency further down. Prototypes of the antenna, for single groove and two

grooves design have also been fabricated and measurements have been done for different depths of the groove. The prototypes for the single groove and two groove designs have been shown in Fig. 3.16 and Fig. 3.17 respectively.

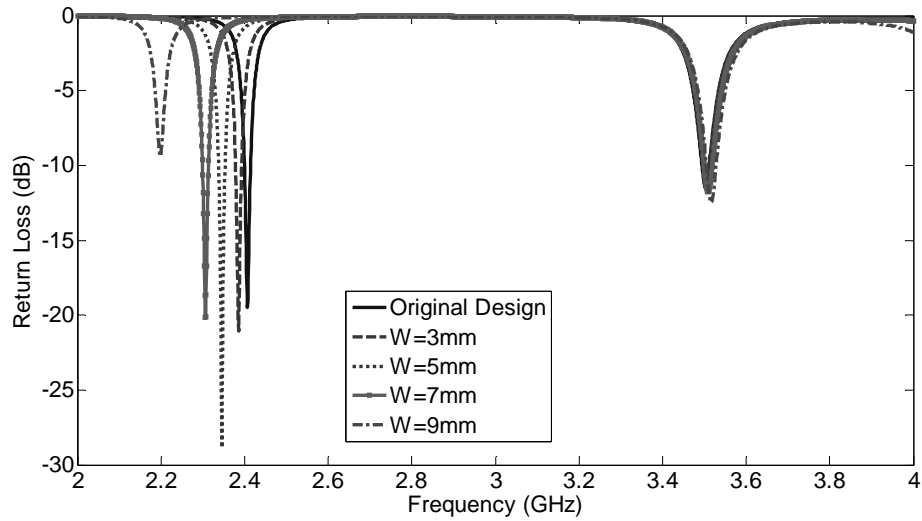


Figure 3.12 – Simulated (CST) return loss vs. frequency for two groove design. This figure shows the return loss characteristics for the proposed antenna design with different depths of the groove.

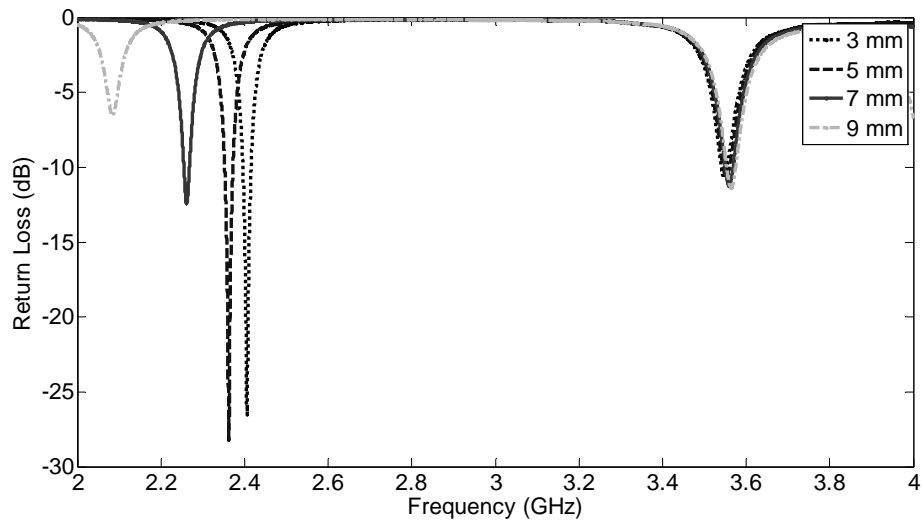


Figure 3.13 – Measured return loss vs. frequency for two groove design. This figure shows the measured return loss characteristics for the proposed antenna design with different depths of the groove.

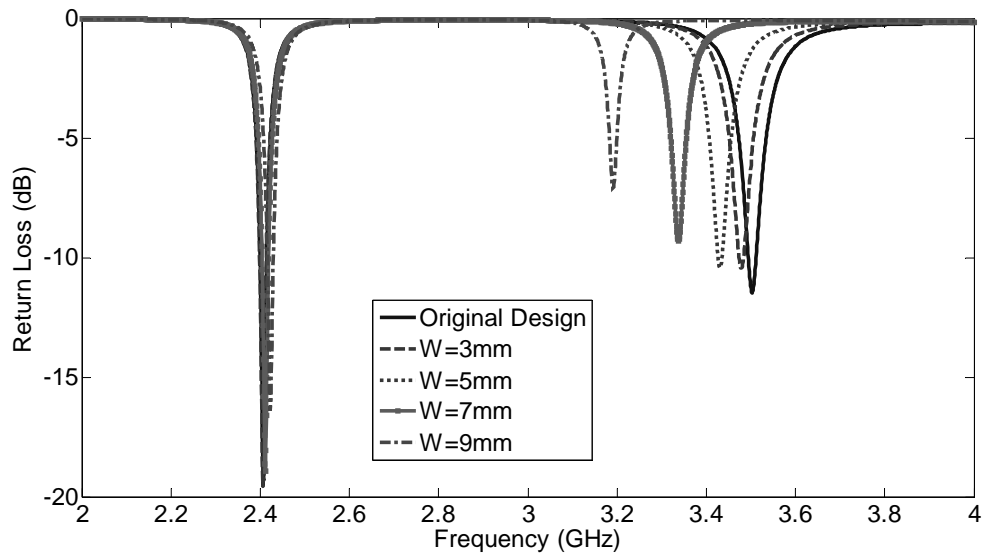


Figure 3.14 – Simulated (CST) return loss vs. frequency for single groove design. This figure shows the return loss characteristics for the proposed antenna design with different depths of the groove.

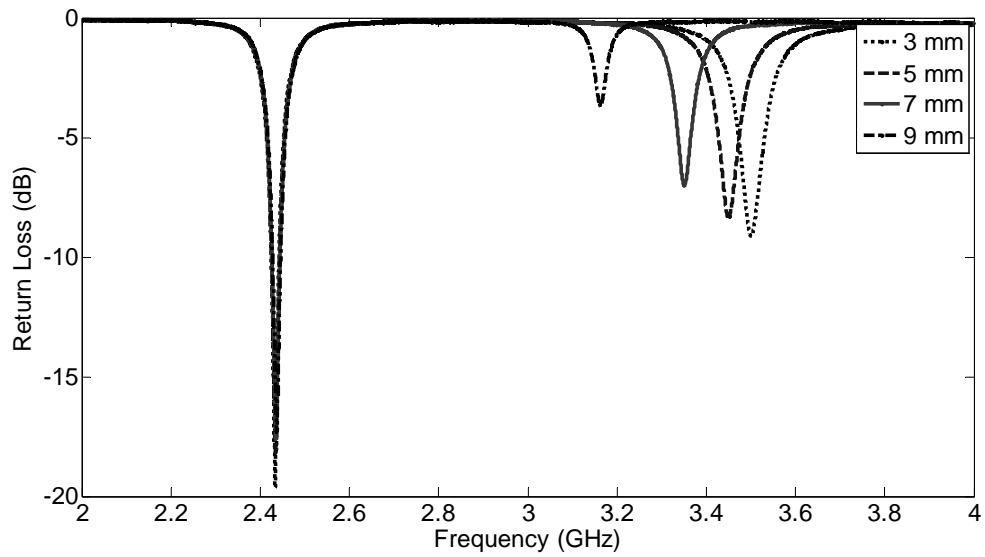


Figure 3.15 – Measured return loss vs. frequency for two groove design. This figure shows the measured return loss characteristics for the proposed antenna design with different depths of the groove.

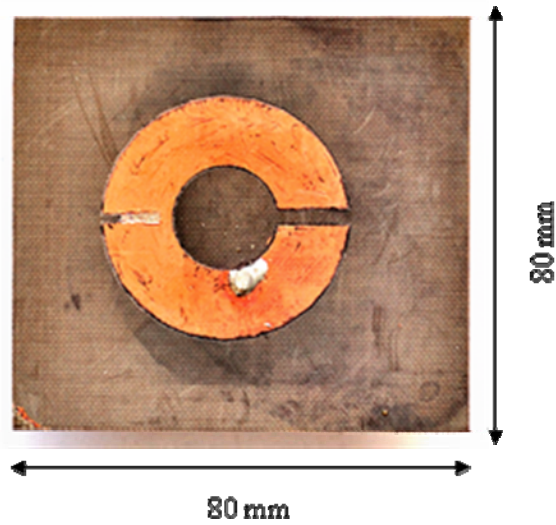


Figure 3.16 – Prototype of the proposed single groove antenna design. This antenna has been fabricated on a 1.57 mm thick PTFE substrate with a dielectric constant of 2.5. Photo etching technique has been used for fabrication of this antenna.

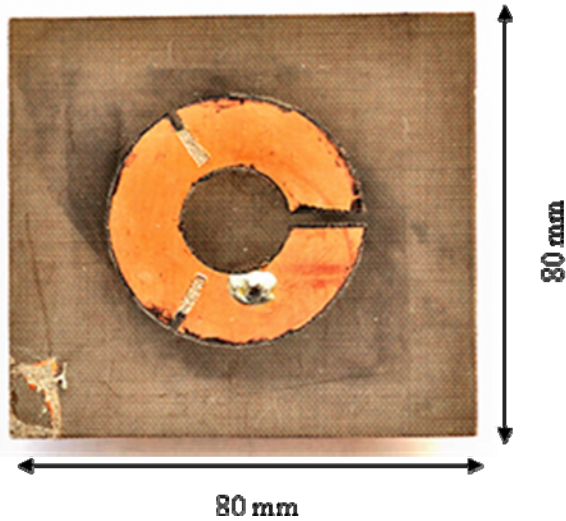


Figure 3.17 – Prototype of the proposed two groove antenna design. This antenna has been fabricated on a 1.57 mm thick PTFE substrate with a dielectric constant of 2.5. Photo etching technique has been used for fabrication of this antenna.

A theoretical analysis for the frequency tuning technique has also been presented in this section by deriving the empirical equations shown below. In this analysis,

we have assumed uniform current distribution along the groove towards the inner periphery. An empirical equation, based on a parametric study, has been presented below to calculate the tuned resonant frequency that depends on the depth and width of the groove.

$$f_{tuned} = f_0 \frac{l_{original}}{l_{new}} \quad (4)$$

$$\text{Where, } l_{new} = l_{original} + \frac{(2d + W) \cdot n \cdot d}{(R_1 - R_2) \cdot \sqrt{\epsilon_{reff}}} \quad (5)$$

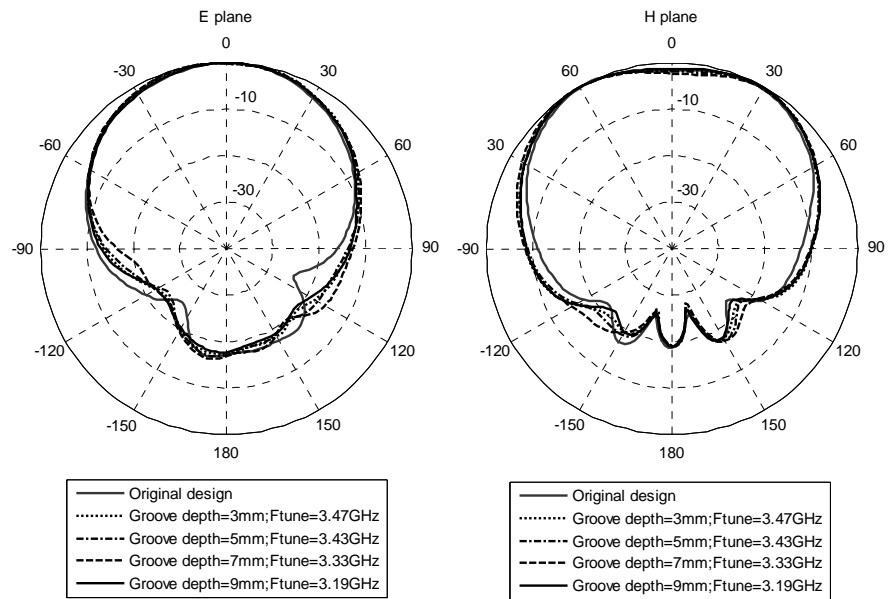
$$\text{Where, } l_{original} = k \frac{\lambda_g}{2} \quad (6)$$

In these equations, f_{tuned} is the tuned resonant frequency, f_0 is the original operating frequency, l_{new} is the electrical path travelled by surface currents after cutting the groove, $l_{original}$ is the total electrical length at f_0 without any groove, d is the depth of the groove, W is the width of the groove, n is the number of grooves ($n = 1$ at 3.5 GHz and $n = 2$ at 2.45 GHz), R_1 and R_2 are the outer and inner radii of the ring respectively and λ_g is the resonant guided wavelength in the dielectric. Here, k represents the number of half wavelength variations of the surface current along the ring at f_0 . In equation (6), the value of k is 2 and 3 at 2.45 GHz and 3.5 GHz respectively (ref. Fig 3.2 and Fig. 3.3).

Since, l_{new} determines the modified electrical length; the depth of the groove can be adjusted for the desired shift in the operating frequency. However, in our

analysis, we have shown the performance of the antenna for four different groove depths i.e. 3 mm, 5 mm, 7 mm and 9 mm. Furthermore, the simulated E plane and H plane radiation patterns for both single and two groove designs, with different groove depths, have been shown in Fig. 3.18 and Fig. 3.19 respectively. All these patterns have been plotted in comparison with the original design (without any grooves). It can be easily found from these plots that even after cutting the grooves; the radiation characteristics are not changed. Nevertheless, a table stating typical E plane and H plane beamwidths at each shifted resonant frequency have also been shown in Fig. 3.18 and 3.19 respectively.

In order to verify the stated empirical equation, a plot has been shown in Fig. 3.20 to compare the theoretically calculated f_{tuned} and simulated f_{tuned} (Microwave CST studio) with respect to groove depth. It can be found from this plot that as n and d increases, the error also increases. The anticipated reason for this error is the non-uniformity in the current distribution along the groove. The typical percentage error between the theory and simulated data is around 6.7%, verifying the validity of the stated empirical equation.



Freq (GHz)	HPBW (degrees)	
	E-plane	H-plane
3.5	74	100
3.47	74	108
3.43	78	108
3.33	80	108
3.19	78	114

Figure 3.18 – Radiation patterns and HPBW for a single groove design. E plane and H plane patterns are shown at each tuned frequency in comparison to original design without groove.

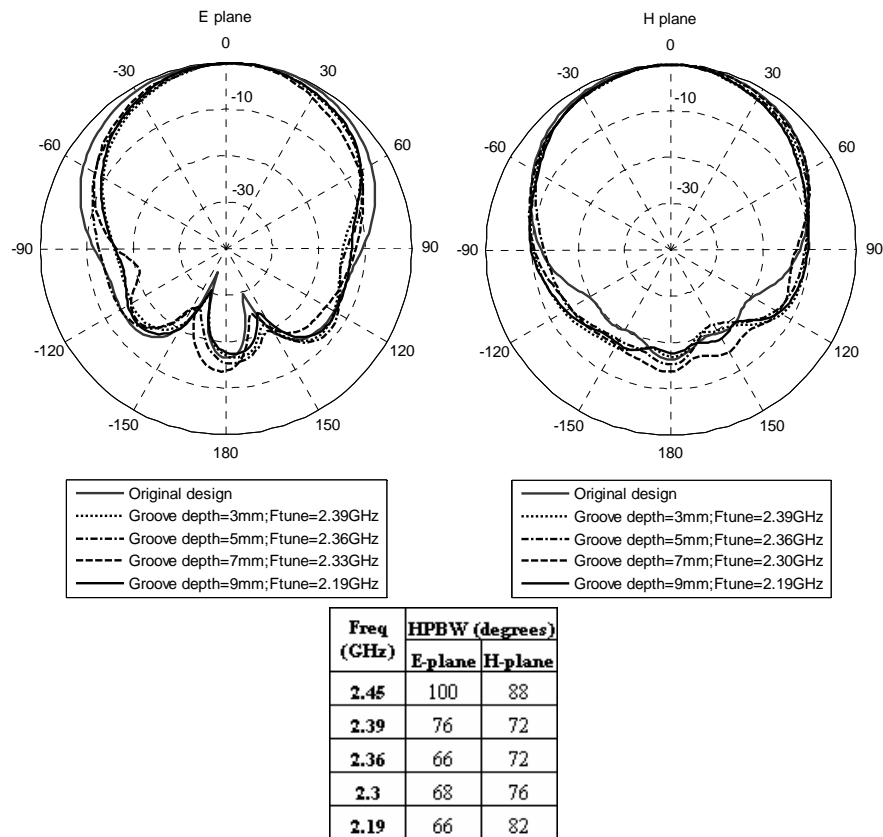


Figure 3.19 – Radiation patterns and HPBW for a two groove design. E plane and H plane patterns are shown at each tuned frequency in comparison to original design without groove.

Furthermore, for the better understanding and justification of the proposed frequency tuning technique, circuit theory analysis has also been introduced and explained below. Based on the circuit analysis, the depth and width of the groove that has been cut on the ring can be analyzed as series inductance and capacitance introduced in the circuit respectively. Since for the proposed design, a groove has been cut on the patch to independently tune the frequency of operation, the reactance of the patch should become more inductive as the groove depth increases at the tuning frequency. However, there should not be a major change in

reactance at the other frequency of operation. Fig 3.21 and Fig. 3.22 shows the simulated reactance plots for the single groove and two groove design respectively.

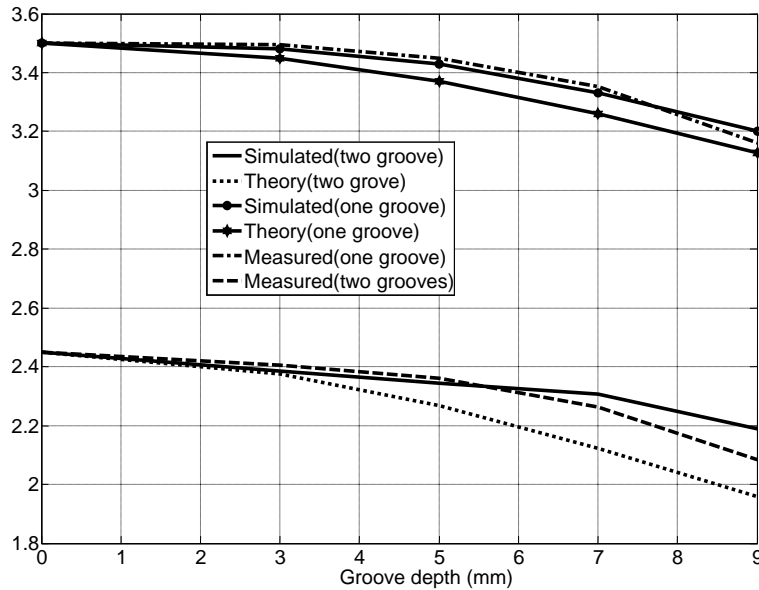


Figure 3.20 – Measured, simulated, and theoretically calculated tuned frequency vs. groove depth. A comparison has been shown among the simulated, measured and theoretical data to justify the validation of derived empirical equations.

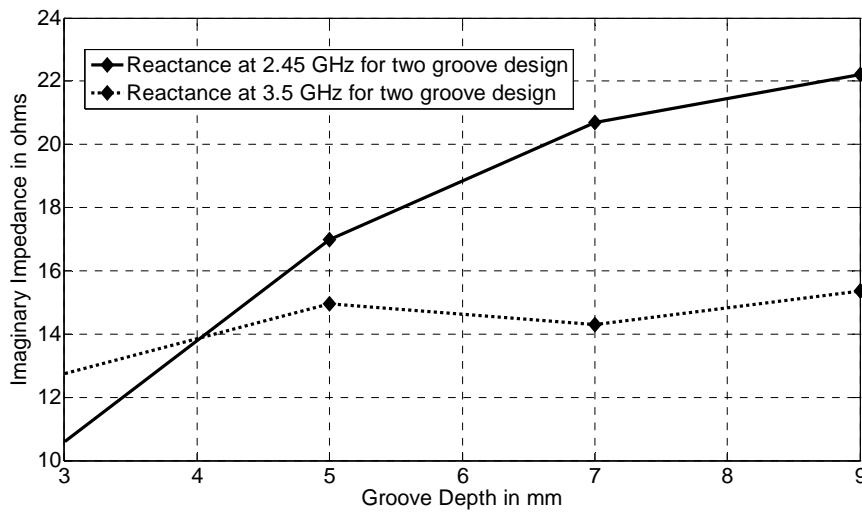


Figure 3.21 - Reactance (ohms) vs. Groove depth (mm) at 2.45 GHz and 3.5 GHz for two groove design. It can be seen from the figure that as the groove depth increases from 3

mm to 9 mm; reactance gets more inductive at 2.45 GHz (from 10.5 ohms to 22 ohms). However, reactance at 3.5 GHz remains almost the same (within 13-15 ohms).

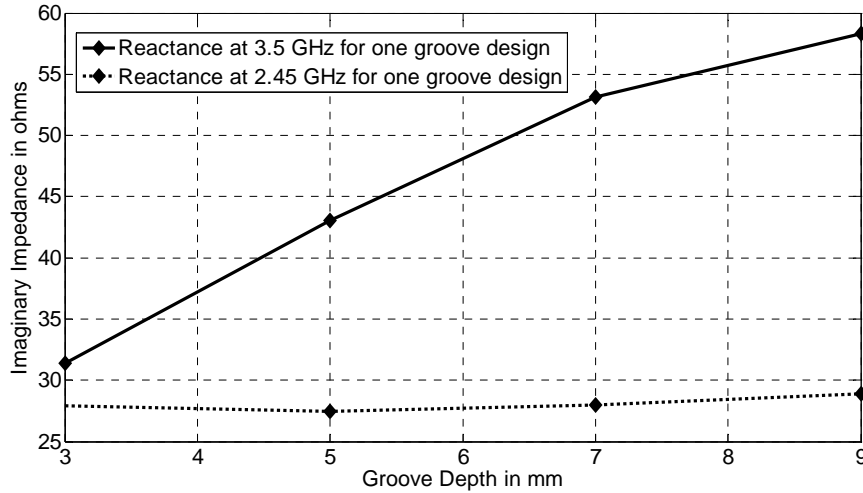


Figure 3.22 - Reactance (ohms) vs. Groove depth (mm) at 2.45 GHz and 3.5 GHz for single groove design. It can be seen from the figure that as the groove depth increases from 3 mm to 9 mm; the reactance gets more inductive at 3.5 GHz (from 31 ohms to 58 ohms). However, reactance at 2.45 GHz is almost the same (within 27.7 to 28.9 ohms).

It has been clearly demonstrated through Fig. 3.21 and Fig. 3.22 that based on the groove location; the change in reactance will affect only that frequency that needs to be tuned while the other frequency remains constant. Furthermore, this analysis justifies the applicability of the frequency tuning technique for the proposed antenna design.

3.4 Antenna design with multi-band characteristics

The capability of the proposed design to be used as a multi-band antenna (tri band) has been described in this section of the chapter. By optimizing the ring

dimensions and the gap, this multi-band antenna resonates at 2.45 GHz, 3.5 GHz and 5.5 GHz respectively. This probe-fed design is also realized on a 1.57 mm thick PTFE substrate and the structure looks same as that shown in Fig. 3.1, with the dimensions $R_1=19.2$ mm, $R_2=8.0$ mm and gap =2.38 mm. The simulated return loss vs. frequency for the multiband design has been shown in Fig. 3.23, which shows return loss better than 10 dB for the above wireless applications. The resonance at 4.5 GHz is the second harmonic of the WLAN frequency that cannot be actually used for any application because of the undesired radiation characteristics. The simulated (CST) return loss at 2.45 GHz, 3.5 GHz and 5.5 GHz are 19.2 dB, 11.1 dB and 10.6 dB respectively. Furthermore, the E plane and H plane radiation patterns at the stated resonant frequencies have been shown in Fig. 3.24, Fig. 3.25 and Fig. 3.26 respectively. The typical E plane and H plane beamwidths at the specified resonant frequencies are around 87 degree and 94 degree respectively. The realizable gain vs. frequency has also been shown in Fig. 3.27. It can be observed that at all the three resonant frequencies, the realizable gain is better than 5 dBi. All these simulated results have been verified using two commercially available EM solvers.

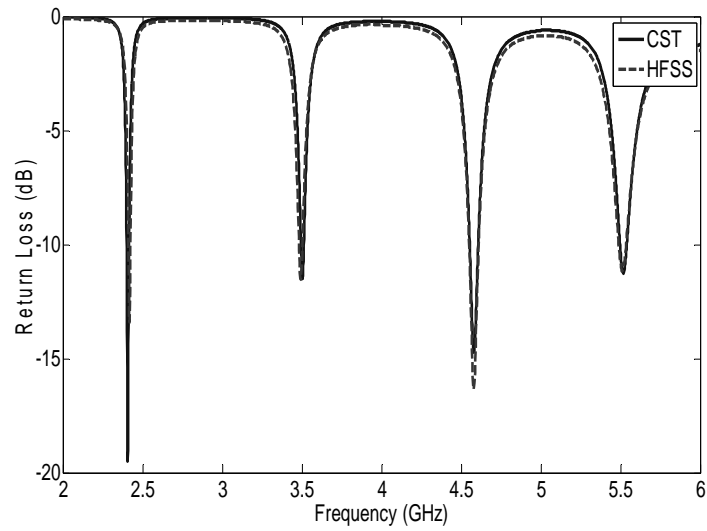


Figure 3.23 – Return loss vs. frequency for the multi-band design. This figure shows the comparison of return loss characteristics for the proposed antenna design among two EM solvers (CST microwave studio and Ansoft HFSS designer) and measurements.

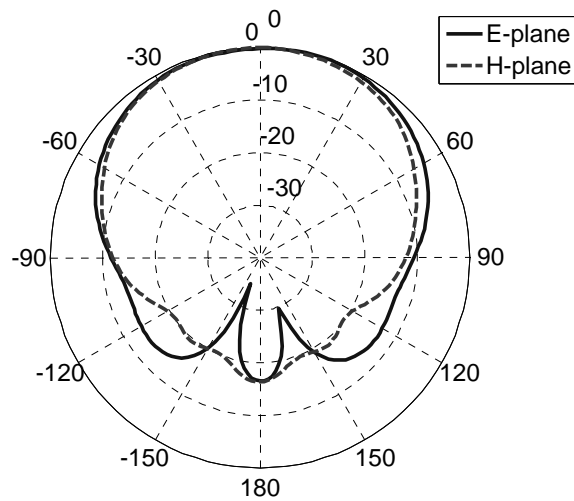


Figure 3.24 – Simulated radiation pattern at 2.45 GHz. This figure shows both E-plane (X-Z plane) and H-plane (Y-Z plane) normalized patterns at WLAN frequency of operation.

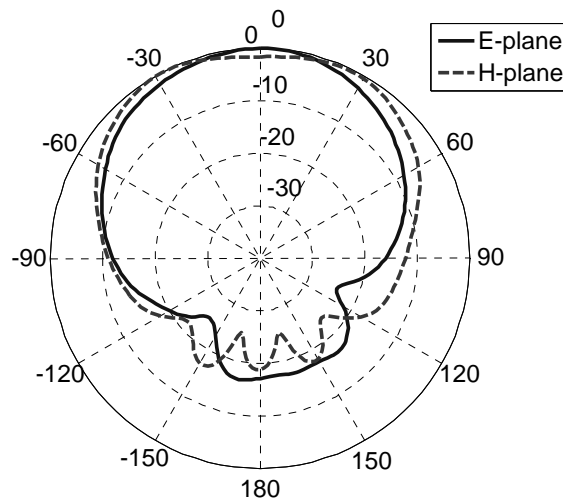


Figure 3.25 – Simulated radiation pattern at 3.5 GHz. This figure shows both E-plane (X-Z plane) and H-plane (Y-Z plane) normalized patterns at WiMAX (lower band) frequency of operation.

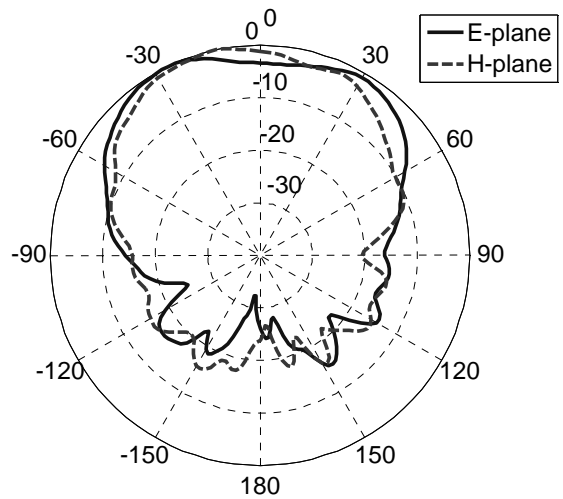


Figure 3.26 – Simulated radiation pattern at 5.5 GHz. This figure shows both E-plane (X-Z plane) and H-plane (Y-Z plane) normalized patterns at WiMAX (upper band) frequency of operation.

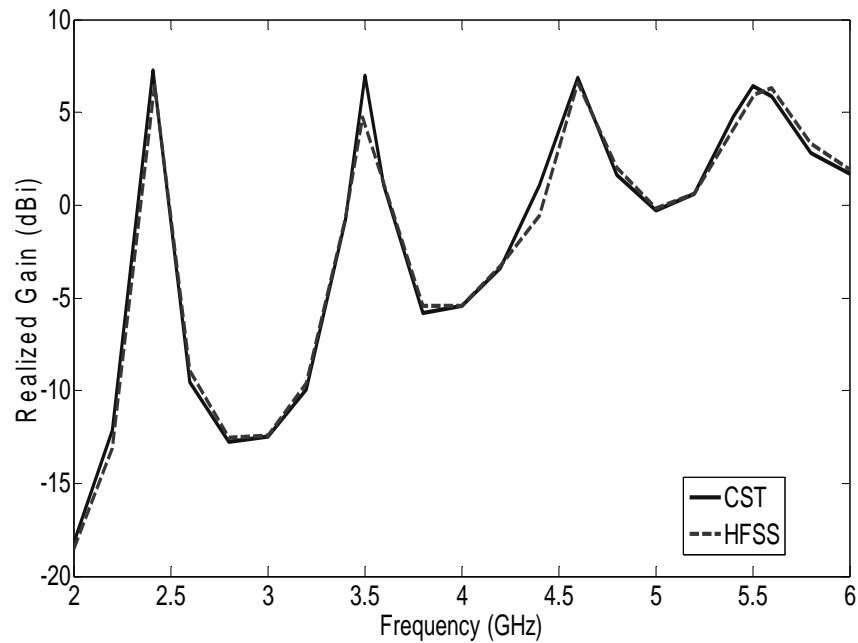


Figure 3.27 – Simulated realized gain vs. frequency for the multi-band design. This figure shows antenna gain profile as a function of frequency.

3.5 Limitations and Improvements

One of the major improvements that can be incorporated into the proposed annular ring design would be the increased bandwidth at the stated resonant frequencies. Also, in future more research could be done to implement frequency tuning technique for the proposed multi-band design. Further design miniaturization and integration of more frequency bands into the design will be the potential improvements.

3.6 Conclusion

In this chapter, a dual-band annular ring patch antenna design with independent frequency tunable characteristics has been proposed. The antenna design comprises of an annular ring patch loaded with a gap. This gap excites higher order modes of the patch, thus making the structure capable of dual band operation. The design resonates 2.45 GHz (WLAN) and 3.5 GHz (WiMAX) respectively, and possesses return loss better than 10 dB and the gain better than 5 dBi for the stated applications. The antenna design is realized on a 1.57 mm thick PTFE substrate. A novel technique to independently tune the resonant frequencies has also been introduced by cutting grooves of different lengths at the desired location. The design capability to be used as a multi-band antenna has also been explored. Prototypes for all the proposed designs have been fabricated and measured. The antenna operation has been verified using two commercially available EM solvers – CST Microwave Studio and Ansoft HFSS, and experimental results.

Chapter 4

Integrated multi-band multi-polarized microstrip antenna for wireless systems

Abstract

This chapter introduces a multi-band, multi-polarized microstrip antenna design for GPS, 3G, and WLAN applications. The proposed antenna design consists of a microstrip patch integrated with four printed monopoles that are fused with the patch. The design exhibits RHCP at 1.575 GHz for GPS applications and LPs at 2.1 GHz and 2.45 GHz for 3G and WLAN applications respectively. Two versions of the antenna designs have been proposed, namely V1 and V2. Previously, a prototype of the first version V1 was fabricated, but it was found that measurements results were not as expected. Therefore, an optimized version V2 has been proposed. Both the proposed antennas have been realized using same design methodology. The drawbacks in the V1 and the modifications brought up in the optimized version V2 have been thoroughly explained in this chapter.

4

⁴ A Version of this chapter will be submitted for publication in the Journal of IEEE Transactions on Antennas and Propagation. Current status: Manuscript under preparation.

The proposed antenna designs have been realized on a 1.58 mm thick FR4 substrate with a dielectric constant of 4.4. The optimized antenna design V2 has been validated using two commercially available EM solvers – CST Microwave studio and Ansoft HFSS designer. Good agreement has been found between the two EM solvers.

4.1 Introduction

As described, microstrip antenna configuration is a preferred choice due to low profile, low volume, low cost and refined compatibility with integrated circuits [25-32]. There are various microstrip antenna designs in the published literature exhibiting multi-frequency operation with linear polarization characteristics, such as linear polarized antennas for data transmission applications and circularly polarized antennas for GPS and SDARS applications [1-7, 18, 20, 22-24, 53, 57-58, 63, 68]. To achieve both circular and linear polarized radiation in a single microstrip antenna with a single-feed is challenging. Furthermore, as inferred to the published literature, there are only a few antenna designs that successfully realize multi-band operation with different polarizations using dual feed, dual substrate or dual patch configurations, e.g. [71-73]. Therefore, the design of a single feed, single layer microstrip antenna that can generate multi-resonance with multi-polarization characteristics is a great advantage. In this chapter, an integrated probe-fed multi-band microstrip antenna has been proposed for different polarized radiation characteristics. The antenna resonates at 1.575 GHz, 2.1 GHz and 2.45 GHz for GPS, 3G and WLAN applications respectively. The

antenna exhibits RHCP at 1.575 GHz and linear LPs at 2.1 GHz and 2.45 GHz. Two versions of the antenna design have been proposed, namely V1 and V2. A prototype of the first version V1 was fabricated and it was found that measurement results were not as desired. Therefore, another optimized version of the antenna design V2 has been designed. The drawbacks in V1 have been clearly explained in section 4.2 of the chapter. In addition, the optimized version V2 has been described in section 4.3 of this chapter. Both the design methodology and results have been described in sections 4.4 and 4.5 of this chapter respectively. The proposed optimized design V2 has been validated using two commercially available EM solvers – CST Microwave studio and Ansoft HFSS. A close agreement has been found between the EM solvers. Furthermore, in the optimized version V2, a reflector metal sheet has been added under the ground plane of the patch to achieve directive radiation characteristics. The proposed designs have been realized on a 1.58 mm thick FR4 substrate with a dielectric constant of 4.4.

4.2 Antenna design V1 and its drawbacks

In this section of the chapter, the structure of the proposed design V1 has been shown and described. Nevertheless, all the drawbacks in the design V1 have also been discussed that proposed the need to design optimized antenna V2.

4.2.1 Antenna design V1

The structure of the proposed multi-band antenna V1 comprises of a rectangular patch and a set of monopoles as shown in Fig. 4.1. Rectangular patch is fed through a single co-axial probe along the diagonal of the rectangular patch; whereas an array of monopoles is fused to the edges of the patch. The GPS patch exhibits right-hand circularly polarized radiation, while the other two resonances at 2.45 GHz and 2.1 GHz exhibit linear polarization characteristics. The rectangular patch antenna has been designed to resonate at the GPS frequency, while the monopoles resonate at the frequency of 2.45 GHz that corresponds to the 802.11 b and g variants of the popular WLAN standards. Furthermore, since the patch is fed along the diagonal, another resonant length appears between the two edges of the patch and the corresponding monopoles (c.f. Fig.4.6) that excite the third resonance at 2.1 GHz for 3G operations. The structure of the proposed antenna design V1 has been shown below in Fig. 4.1. All the dimensions are in mm and have been shown in the table in Fig. 4.1. This design is realized on a 1.58 mm thick FR4 substrate. In Fig. 4.1, the top layer metallization (red) consists of the GPS patch and WLAN monopoles; and the bottom layer (blue) represents the ground plane. The substrate (gray) supports the metal layers and the entire structure. The center conductor of the coaxial probe is fed through the substrate to the top layer patch while the ground shield is attached to the bottom layer.

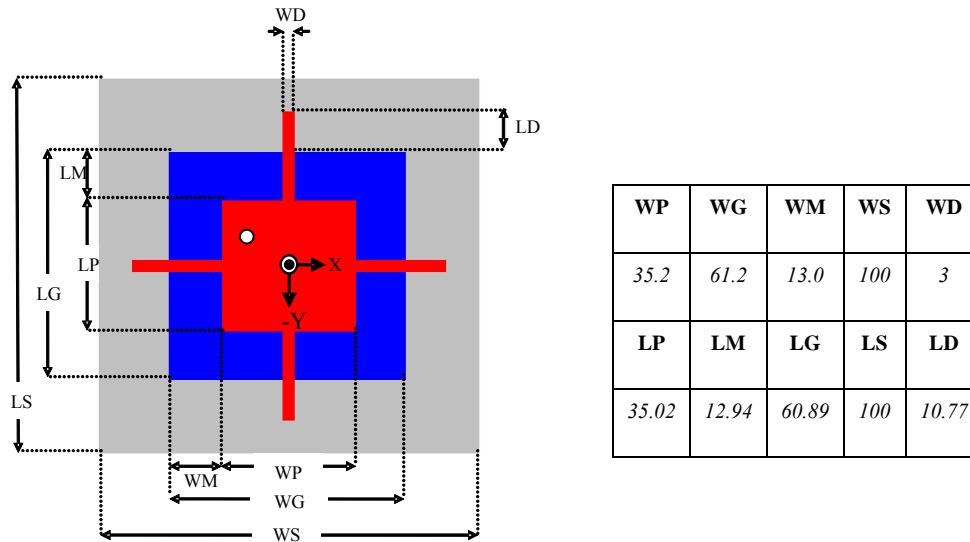


Figure 4.1 – Structure of the proposed V1 design (left). All the dimensions are in mm and have been shown in the table (right). Feed location has been shown as a white circle on the patch. The location of the feed with respect to centre is (-4.55, 4.3).

4.2.2 Drawbacks

Design V1 has been simulated using CST microwave studio and a prototype of V1 has also been fabricated as shown in Fig. 4.2. However, once the measurements were carried out, it was found that resonant frequencies were shifted and even return loss performance at 2.45 GHz was degraded. Further, investigations relating to this mismatch between the simulation and measurement results concluded that the structure definition of V1 and boundary conditions were erroneously defined in the CST microwave studio and later verified also using Ansoft HFSS designer. The measured and simulated return loss characteristics of the antenna design V1 has been shown in Fig. 4.3. This figure clearly shows the mismatch between the CST simulated results and measurements.

Furthermore, once the V1 was correctly defined in terms of structure definition and boundary conditions; it was found that the radiation peak at all the stated frequencies was tilted behind the patch due to the presence of substrate beneath the monopoles. Therefore, there was a need for an optimized antenna design V2 that achieve desired return loss performance and radiation characteristics at the stated resonant frequencies. In the optimized version V2, other than the dimensional modifications, a metal sheet has been used below the patch to tilt the radiation peak towards the zenith and to achieve directive radiation characteristics.

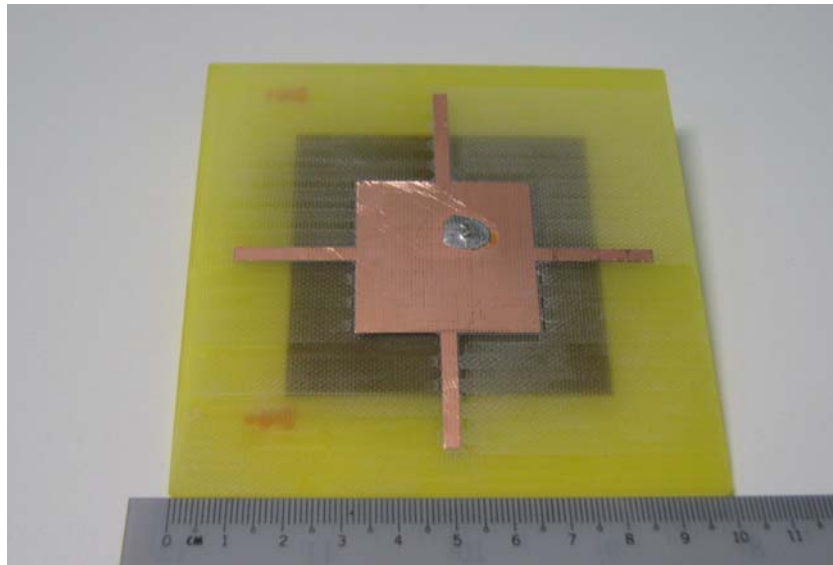


Figure 4.2 – Prototype of the proposed microstrip patch antenna. This antenna has been fabricated on a 1.58 mm thick FR4 substrate with a dielectric constant of 4.4. Fabrication process has been carried out using milling machine.

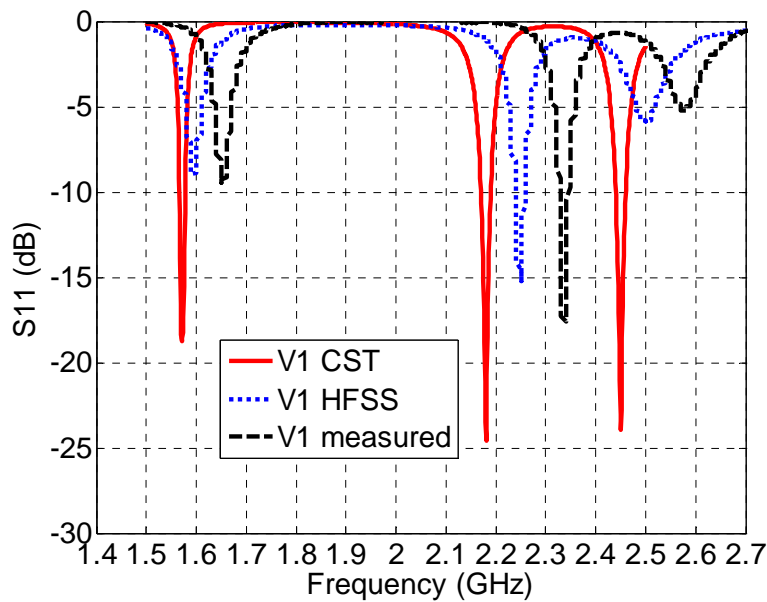


Figure 4.3 – Return loss vs. frequency. This figure shows the comparison of return loss characteristics for the proposed antenna design V1 between two EM solvers (CST microwave studio and Ansoft HFSS) and measurements.

4.3 Optimized antenna design V2 and its modifications

This section of the paper describes the structure of the optimized version of the antenna design V2. All the modifications have also been clearly described in this section.

4.3.1 Optimized antenna design V2

The structure and dimensions of the proposed V2 antenna design has been shown in Fig. 4.4. The antenna design V2 is similar to the design V1 in terms of structural outlook. The rectangular patch is fed through a single co-axial probe

along the diagonal of the patch and four printed monopoles are fused at the edges of the patch. This design also realizes RHCP at 1.575 GHz and LPs at 2.1 GHz and 2.45 GHz. The design performance of V2 has been verified using CST Microwave Studio and Ansoft HFSS. All the results have been shown in section 4.5 of the chapter and a good match has been found between the two solvers.

4.3.2 Modifications

Other than dimensional optimizations, the two major modifications brought up in the optimized design V2 are the tapered microstrip lines as feeds for printed monopoles and the introduction of metal reflector plane beneath the patch to tilt the radiation peak towards zenith. New dimensions of the optimized design V2 have been shown in Fig. 4.4.

In the optimized version V2, tapers have been used to enhance the flow of currents into the printed monopoles, thus achieving good impedance match at 2.1 GHz and 2.45 GHz. In addition, a metal sheet beneath the patch has been introduced to tilt the radiation peak. As discussed before, in V1 the radiation peak at all the three frequencies was shifted behind the patch due to the presence of dielectric substrate below the monopoles. Therefore, in order to overcome this radiation concern, a field reflection technique has been proposed. A metal sheet has been added below the actual ground plane of the patch to achieve high gain as well as desired radiation characteristics. The location of the reflector sheet has

been optimized at 5 mm below the ground plane of the patch. The design principle behind this technique is same as described in section 2.2.1.1 of the thesis i.e. to choose location of the reflector metal sheet in such a way that the reflected signal from the reflector should add in phase with the radiated signal from the patch, thus improving the gain of the proposed antenna as well as shifting the radiation bore sight towards zenith.

A parametric study on the location of the reflector plane has been carried out using EM solvers (CST Microwave Studio and Ansoft HFSS) and it has been concluded that the minimum dimension of the reflector plane is 90 X 90 mm². However, in practice, the mounting platform can be used as the reflector plane to achieve stated antenna characteristics. Antenna design V2 had been optimized with different sizes of reflector plane at different locations below the patch to find the optimum case. Using this technique, the desired antenna performance has been achieved.

4.4 Design methodology

The detailed design procedure has been explained in this section of the chapter. Sections 4.4.1, 4.4.2 and 4.4.3 explain the resonance operation at 1.575 GHz, 2.1 GHz and 2.45 GHz. Next, section 4.4.4 describes the patch integration with the monopoles, thus acting as an integrated multi-band multi-polarized design for stated applications.

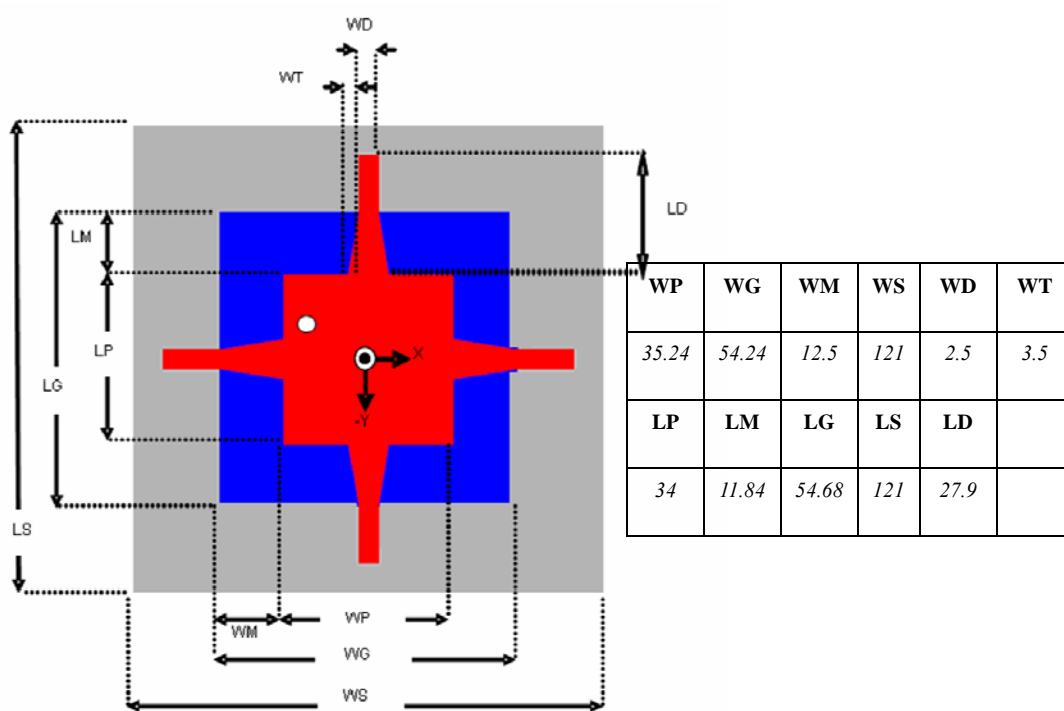


Figure 4.4 – Structure of the proposed V2 design (left). All the dimensions are in mm and have been shown in the table (right). Feed location has been shown as a white circle on the patch. The location of the feed with respect to centre is (-10.95, 6.74).

4.4.1 GPS frequency

Design methodology for the GPS patch is similar to the conventional square patch antenna. The feeding point for the probe is chosen to be on the diagonal axis of the patch to achieve circularly polarized radiation. The diagonal feeding position on the patch is also unique in the sense that it inherently phases the excitation of the vertical and horizontal edges orthogonally to produce CP radiation [99]. Appropriate selection of the diagonal axis for feeding will determine the sense of

polarization rotation [100]. Additional perturbation at the lengths of either edge pairs is necessary to optimize the axial ratio. Furthermore, an offset in the distance from the center of the antenna tunes the real and imaginary impedance so that the antenna can be matched to the feed-line characteristic impedance. For the proposed antenna design, the patch exhibits RHCP radiation at 1.575 GHz. The current distribution at 1.575 GHz has also been shown in Fig. 4.5. The figure clearly shows the presence of strong surface current on the patch.

4.4.2 3G Frequency

Resonance at 2.1 GHz has been achieved due to the current path shown in Fig. 4.6 and Fig.4.7. Both the figures show current distribution at 2.1 GHz. Fig. 4.6 has been manually drawn to illustrate the current distribution. Due to the fact that the patch has been fed on the left diagonal of the rectangular patch, the monopoles showed in Fig. 4.6 act as discontinuities for the strong patch currents. Hence, the stated current path acts as a resonant length at 2.1 GHz. Furthermore, an approximated electrical length travelled by these currents has been calculated to 76 mm, justifying the resonance at 2.1 GHz. This electrical length has been calculated based on the assumption of uniform current distribution along the current path.

4.4.3 WLAN Frequency

The WLAN monopoles are fed from the GPS patch. The monopoles are a quarter-wavelength long, including the additional electrical length due to fringing fields. Widths of the monopoles are determined by the impedance of the feeding microstrip lines. Fig 4.8 shows the current distribution on the V2 antenna structure at WLAN frequency. At resonance, current density increases around the tapers leading towards the open circuit ends of the monopole arms. The function of the tapers is to encourage the flow of currents into the arms. The tapers also act as a broadband impedance match as observed in the impedance plot (c.f. Figs. 4.10 and 4.11), in which the slope of the real and imaginary components around resonance became more gradual. Phasing of the monopoles can be determined by the patch dimensions; therefore, a trade-off is the controllability of the excitation phase. The size of the ground plane on the bottom layer affects the WLAN antenna impedance and edge lengths are tuned for optimum match.

The monopole arms on the structure can be perceived as a planar array of two elements on orthogonal planes. This produces dual-linear polarization which is suitable for a mobile user scenario in which the incident wave can be from an arbitrary angle and remains a variable. Monopoles generate a more omnidirectional radiation that can be seen in the pattern descriptions of Figs. 16 and 17 and is desired for the intended application.

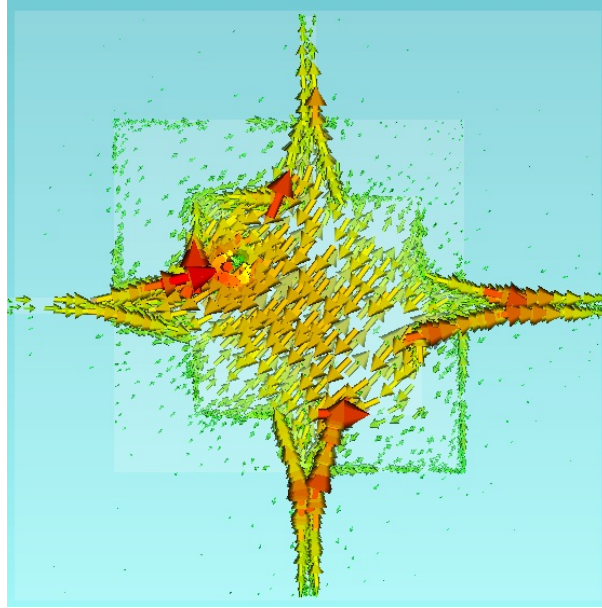


Figure 4.5 - Surface current distribution at 1.575 GHz. This figure noticeably shows that the strong surface current exists on the edges of the rectangular patch that realizes resonance at GPS frequency.

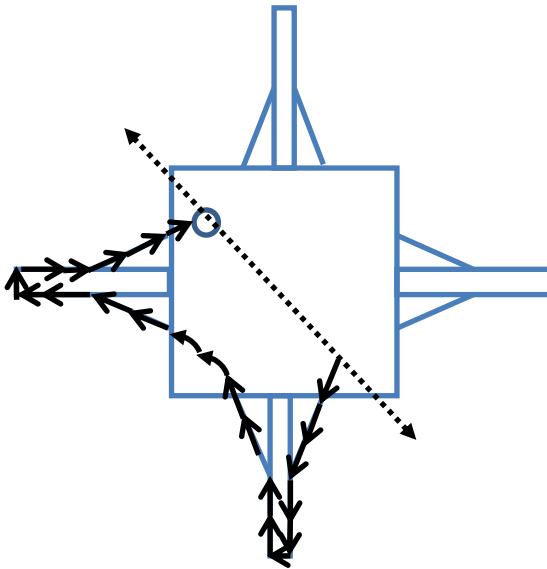


Figure 4.6 - Surface current distribution at 2.1 GHz. This figure noticeably shows that the current path exist between the two monopoles and the corresponding edges of the patch.

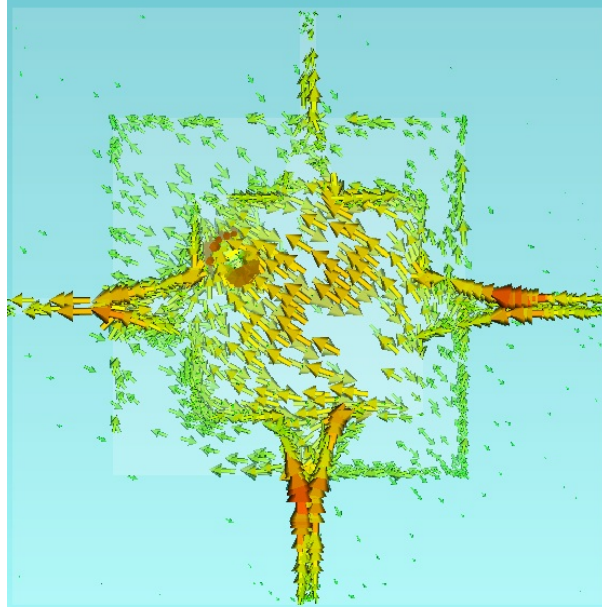


Figure 4.7 - Surface current distribution at 2.1 GHz. This figure noticeably shows that the current path exist between the two monopoles and the corresponding edges of the patch.

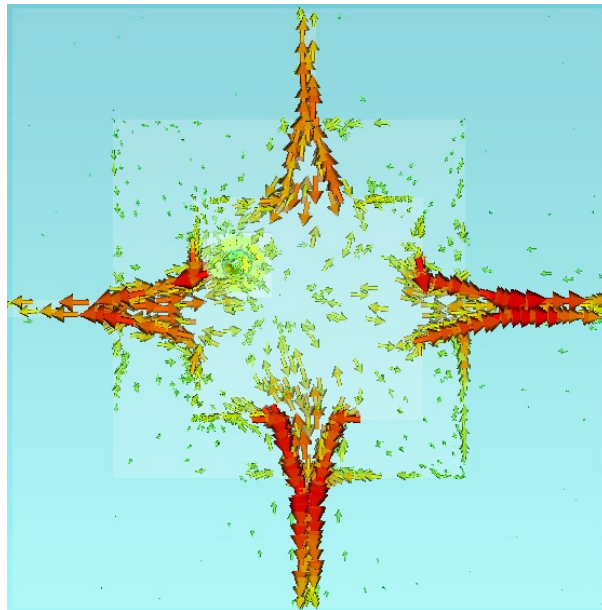


Figure 4.8 - Surface current distribution at 2.45 GHz. This figure noticeably shows that the strong current exists on the fused monopoles.

4.4.4 Design Integration

A transition from the GPS patch to the monopoles is required due to the different radiation mechanism of the individual antennas. The patch antenna radiates through fringing fields created by the potential difference between the patch edges and ground. Therefore, a ground structure is required for these fringing fields to exist. Size of the ground plane controls the impedance of the antenna at GPS frequency and the monopoles radiate because of standing wave currents developed along their lengths. Due to the requirement of the ground plane for GPS operation, part of the monopole length becomes the microstrip line structure and the remaining becomes the radiating strip. The electrical length of the monopole includes the fringing field depth. Furthermore, the size of the ground plane affects the impedance of the antenna at GPS frequency, 3G frequency as well as at WLAN frequency; therefore, the dimensions of the ground plane are optimized by considering the trade off in performance amongst all the bands.

When combined, the structure as a whole exhibits multi-band frequency response and achieve good antenna gain at all the frequencies, greater than 3 dBi (CST) and return loss better than 10 dB that makes the design suitable for mobile wireless communications integrated with location based services and localization capabilities.

4.5 Results

The design performance of the proposed V2 design has been validated using two commercially available EM solvers – CST Microwave Studio and Ansoft HFSS. The simulated and measured return loss has been shown in Fig. 4.9. The CST and HFSS simulated return loss at 1.575 GHz, 2.1 GHz and 2.45 GHz is -13.4 dB, -15.12 dB and -15.9 dB and -13.2 dB, -18.2 dB and -16.24 dB respectively. The percentage error between the two simulators with regard to shift in the resonant frequencies is around 5 %. Return loss that is better than 10 dB has been achieved at all the three stated resonant frequencies that support the design suitability for commercial applications.

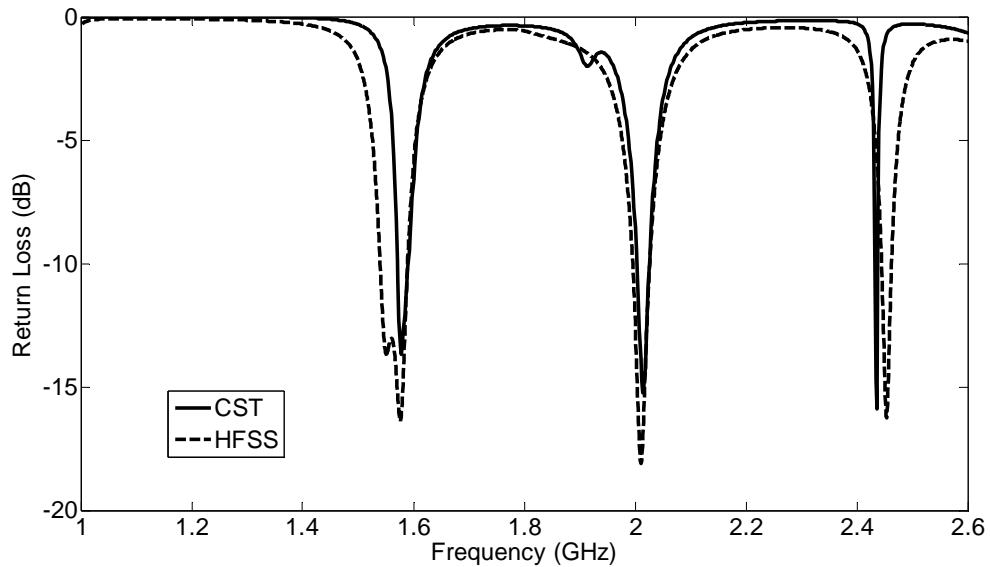


Figure 4.9 – Return loss vs. frequency. This figure shows the comparison of return loss characteristics for the proposed antenna design V2 between two EM solvers (CST microwave studio and Ansoft HFSS).

Simulated real and imaginary impedances of the antenna have been shown in Fig. 4.10 and Fig. 4.11 respectively. The CST real impedances at 1.575 GHz, 2.1 GHz and 2.45 GHz are 83.7 ohms, 44.7 ohms and 41 ohms respectively. HFSS real impedances at stated frequencies are 40 ohms, 42.3 and 43.4 ohms respectively. Furthermore, the CST imaginary impedances at the stated resonant frequencies are 7.7 ohms, 5.3 ohms and 5.4 ohms respectively and HFSS imaginary impedances are 15 ohms, 2.8 ohms and 12.8 ohms respectively. The stated impedances values justify the antenna operation for stated wireless applications.

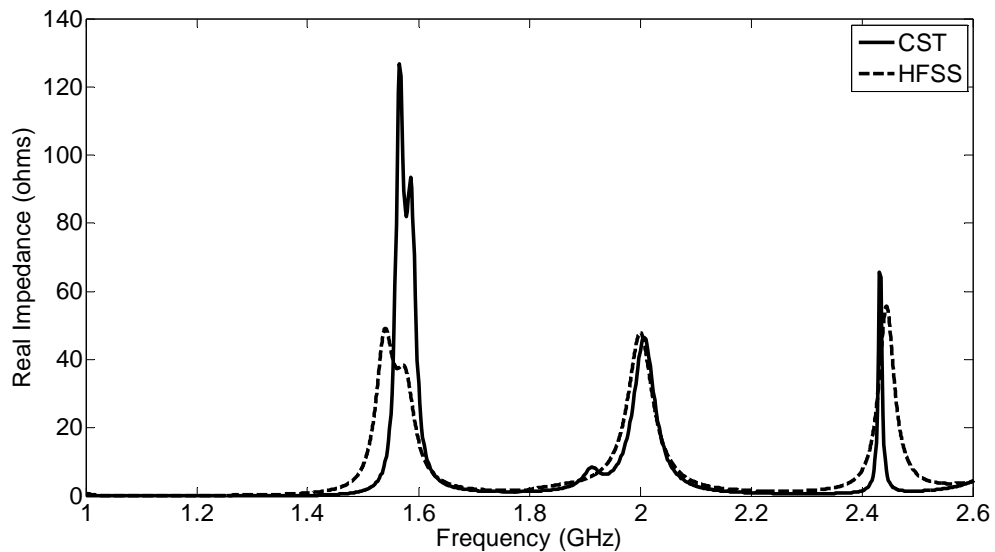


Figure 4.10 – Simulated real impedance vs. frequency. This figure represents the variation of real impedance versus frequency. It can be noticed that the real impedance is close to 50 ohms at 1.575 GHz, 2.1 GHz and 2.45 GHz as desired.

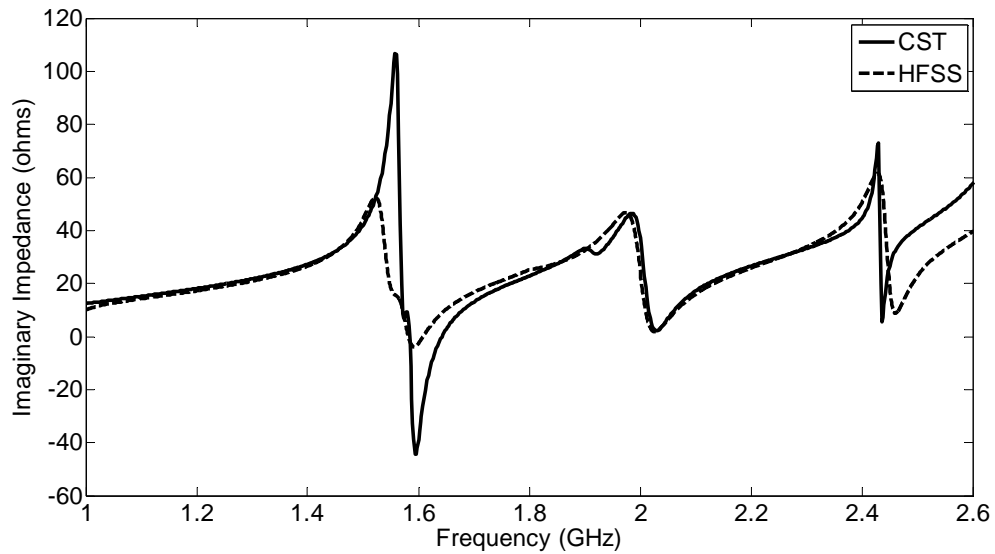


Figure 4.11 – Simulated imaginary impedance vs. frequency. This figure represents the variation of imaginary impedance versus frequency. It can be noticed that the imaginary impedance is close to 0 ohms at 1.575 GHz, 2.1 GHz and 2.45 GHz as desired.

Simulated E-plane (X-Z plane) radiation patterns of the antenna at GPS, 3G and WLAN frequencies have also been shown in Fig. 4.12, Fig. 4.14 and Fig. 4.16. However, simulated H-plane (Y-Z plane) patterns at stated frequencies have been shown in Fig. 4.13, Fig. 4.15 and Fig. 4.17 respectively. The CST simulated radiation patterns are similar to the HFSS simulated patterns. All the patterns shown below are the normalized patterns. The simulated beamwidths in E-plane and H-plane at the specified resonant frequencies are around 60° and 70.1° respectively.

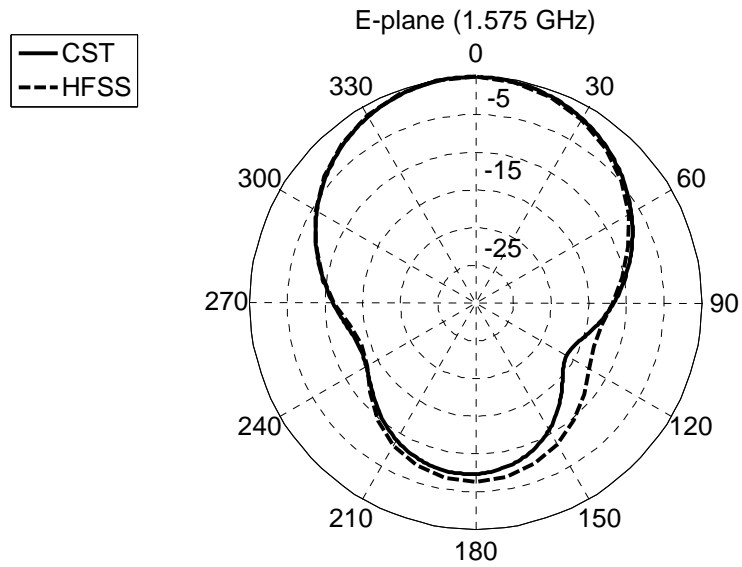


Figure 4.12– CST (solid line) and HFSS (dash line) E-plane radiation patterns at 1.575 GHz. This figure clearly shows that the radiation peak is towards zenith as desired for satellite based applications such as GPS for better signal reception.

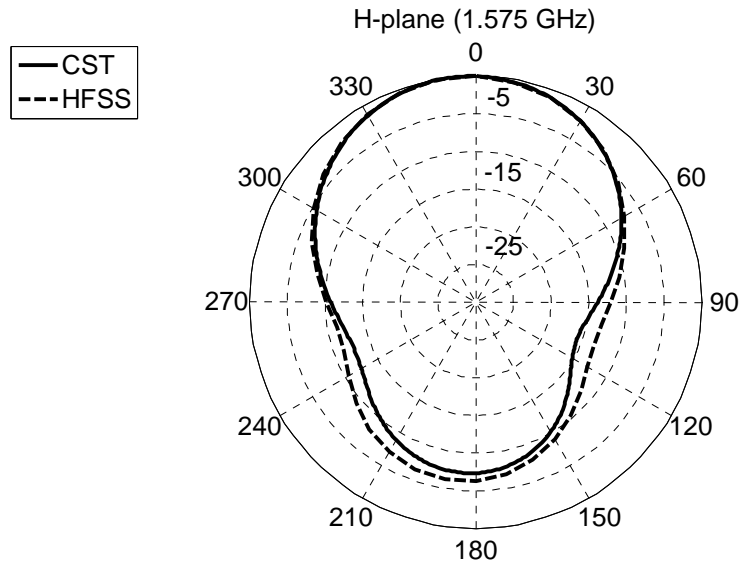


Figure 4.13– CST (solid line) and HFSS (dash line) H-plane radiation patterns at 1.575 GHz. This figure clearly shows that the radiation peak is towards zenith as desired for satellite based applications such as GPS for better signal reception

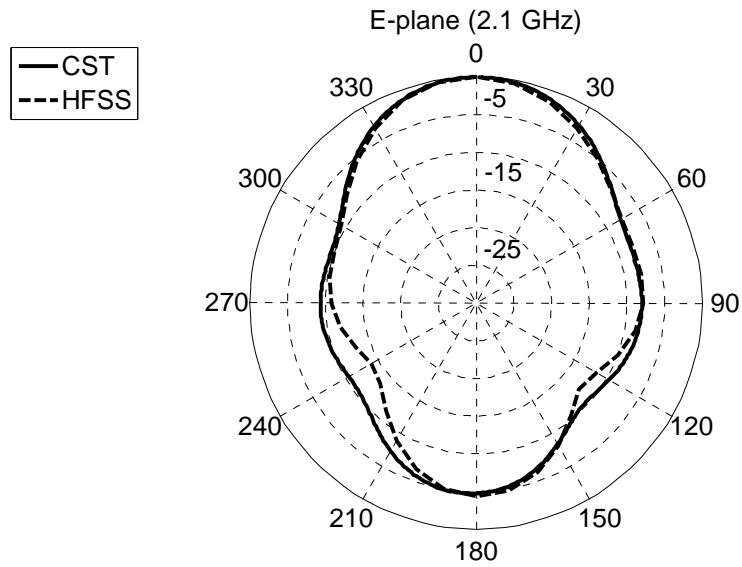


Figure 4.14 – CST (solid line) and HFSS (dash line) E-plane radiation patterns at 2.1 GHz. This figure shows radiation characteristics for 3G applications.

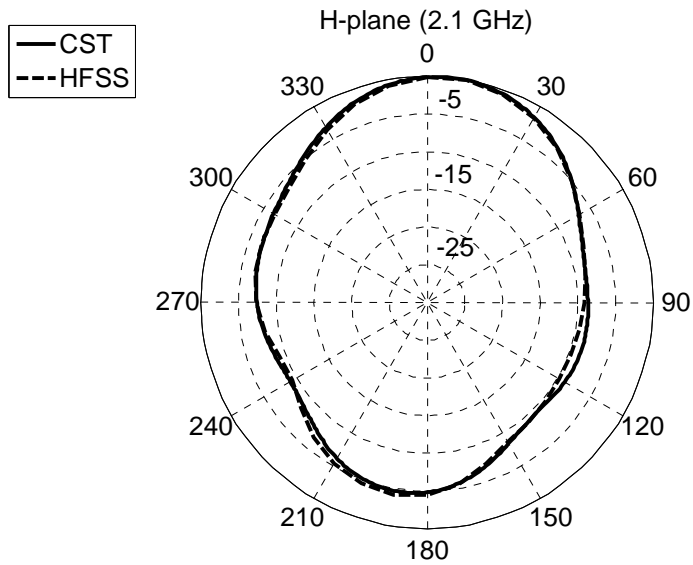


Figure 4.15 – CST (solid line) and HFSS (dash line) H-plane radiation patterns at 2.1 GHz. This figure shows radiation characteristics for 3G applications. The simulated patterns are quite close to the desired patterns such a way that connectivity to the base station is ubiquitously maintained.

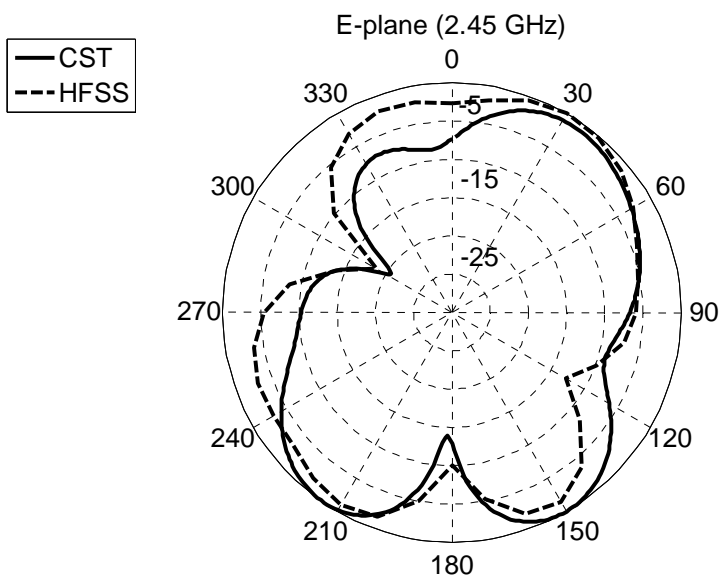


Figure 4.16 – CST (solid line) and HFSS (dash line) E-plane radiation patterns at 2.45 GHz. This figure shows the radiation characteristics for WLAN operation. The simulated patterns are similar to the desired patterns i.e. sideways for better signal connectivity.

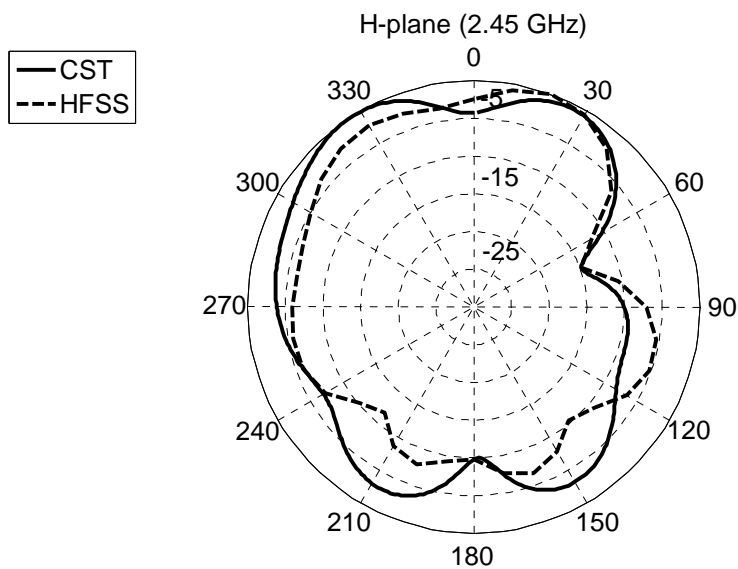


Figure 4.17 – CST (solid line) and HFSS (dash line) H-plane radiation patterns at 2.45 GHz. This figure shows the radiation characteristics for WLAN operation. The simulated patterns are similar to the desired patterns i.e. sideways for better signal connectivity

The simulated realizable gain has been shown in Fig. 4.18. The simulated (CST) realizable gain at all the resonant frequencies is better than 3 dBi that explains the function of reflector ground plane to achieve directive radiation characteristics. The CST simulated realizable gain at 1.575 GHz, 2.1 GHz and 2.45 GHz is 6.83 dBi, 6.82 dBi and 3.9 dBi respectively. HFSS simulated gain is 3.4 dBi, 5.2 dBi and 0.79 dBi respectively. The simulated axial ratio characteristics have also been discussed in this section of the chapter. The simulated E-plane and H plane axial ratio at 1.575 GHz is shown in Fig. 4.19 and Fig. 4.20 respectively. The CST and HFSS simulated boresight axial ratios at GPS frequency are 2.43 dB and 0.8 dB respectively. The stated axial ratio values at 1.575 GHz supports the usability of design for GPS applications exhibiting good right hand circularly polarized radiation. Furthermore, the simulated boresight axial ratio vs. frequency characteristics has been shown in Fig. 4.21.

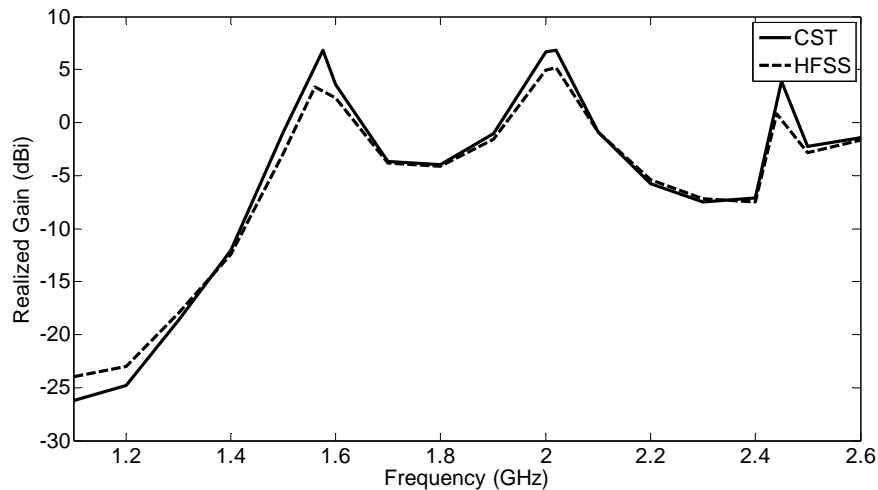


Figure 4.18 – CST (solid line) and HFSS (dash line) realized gain vs. frequency. This figure shows antenna gain profile as a function of frequency.

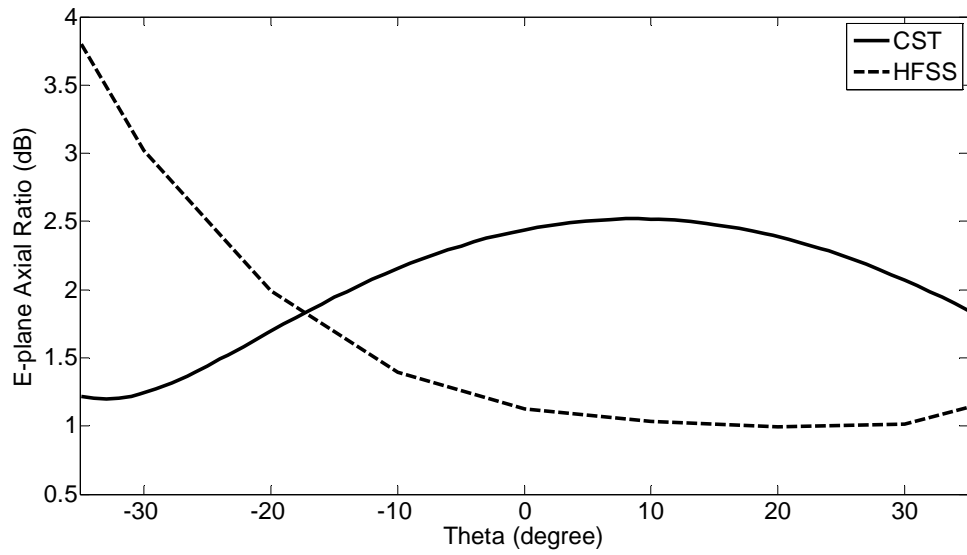


Figure 4.19 – CST (solid line) and HFSS (dash line) E-plane axial ratio vs. theta. This figure justifies the antenna applicability at GPS frequency exhibiting right hand circular polarization.

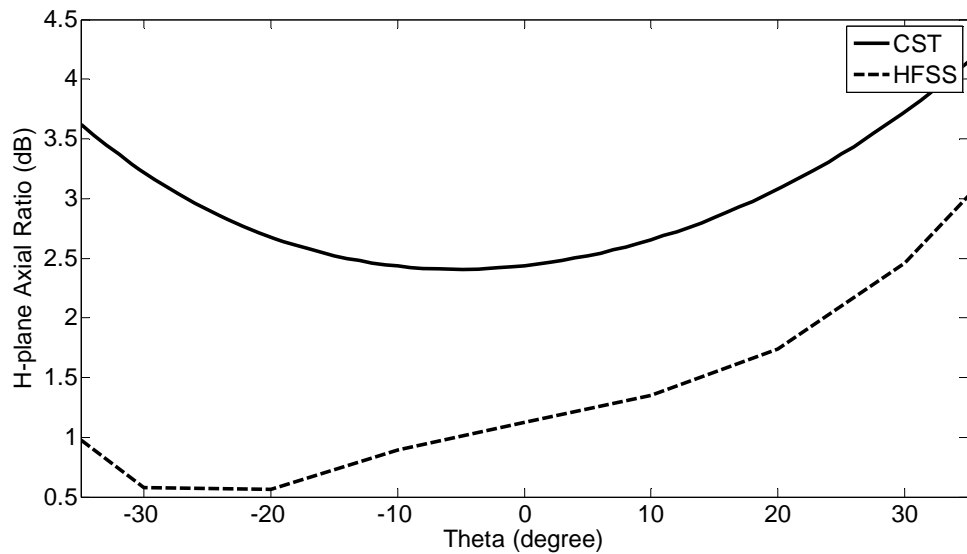


Figure 4.20 – CST (solid line) and HFSS (dash line) H-plane axial ratio vs. theta. This figure justifies the antenna applicability at GPS frequency exhibiting right hand circular polarization.

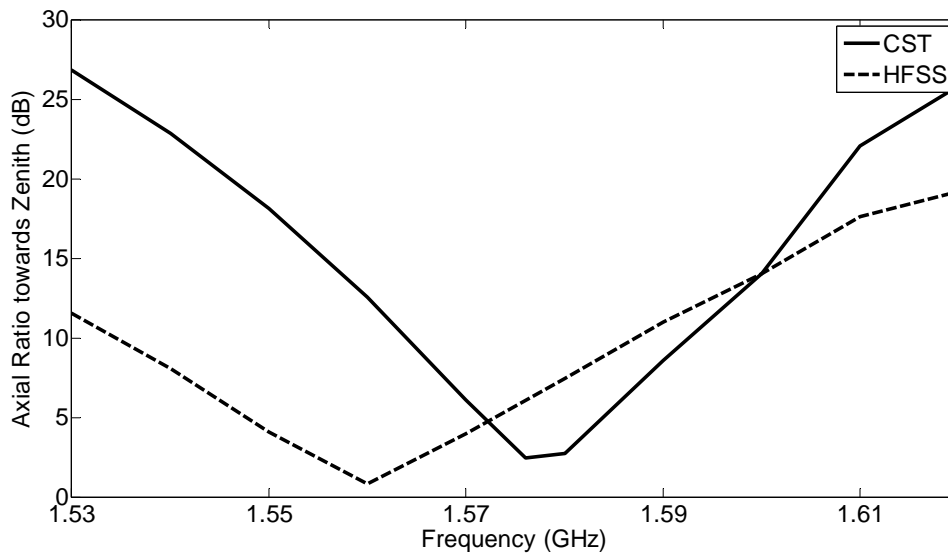


Figure 4.21 – CST (solid line) and HFSS (dash line) boresight axial ratio vs. frequency. This figure justifies the antenna applicability at GPS frequency exhibiting right hand circular polarization.

4.6 Limitations and Improvements

One of the major drawbacks of the design is the limited bandwidth. Some of the ideas that can be implemented for the proposed designs to improve the bandwidth are: by using broadband configurations of monopoles [87-88], using modified ground planes [89] or by changing the substrate properties like thickness and dielectric constants [26]. Furthermore, broad-banding can be achieved through slight adjustments to each monopole length to generate multiple overlapping resonances. The same concept can also be applied to realize multiple (up to quad-) bands with linear polarization for each individual resonance. Miniaturization can also be realized through folding of the monopole arms.

4.7 Conclusion

An integrated multi-band microstrip patch antenna has been proposed for GPS, 3G and WLAN applications. Two versions of the antenna design have been proposed. A prototype of the first version, V1, was fabricated and measurements were carried out. It was found that measurement results were not similar to simulated results due to the inaccuracies in the structure definition in the EM solvers. Therefore, an optimized version, V2, has been proposed. Both the versions have been designed using same design principle. In addition, optimizations in the V2 have been explained in the section 4.3 of the chapter. The design performance has been verified using CST Microwave Studio and Ansoft HFSS. A workable agreement has been found between two solvers. The proposed designs are realized on a 1.58 mm thick FR4 substrate. A field reflection technique has also been proposed to achieve directive radiation characteristics.

Chapter 5

Multi-band antenna designs for future research

Abstract

Design methodologies to achieve single probe-fed multi-band antennas with different polarization requirements incorporating independent frequency tunability have been proposed. Three prospected antenna designs have been described in this chapter of the thesis. The first design can be used to generate two circular polarizations and one linear polarization; the second design can be realized to generate three circular polarizations and the third design can be made capable to generate seven different resonances with different polarization requirements. The stated design methodologies have been proposed as future research problems and further research needs to be carried out to validate the antenna designs.

5.1 Introduction

As described in the previous chapters of the thesis, integrated multi-band patch antennas have been designed for various wireless applications such as WLAN, WiMAX, GPS, SDARS, PCS and 3G. All of these antenna designs are based on single substrate layer and single probe feed configuration and achieve desired radiation characteristics for the stated applications. Radiation pattern requirements are different for each application. For example, GPS and satellite radio applications such as SDARS need its pattern to be focussed towards zenith; whereas cellular and data transmission applications need omni-directional pattern in azimuth plane. In chapter 2 and chapter 3 of the thesis, three independently tunable antenna designs have been realized for WLAN, WiMAX and PCS operations with multi linear polarization characteristics. Similarly, in chapter 4, a circularly and linearly polarized antenna has been proposed for GPS, 3G and WLAN applications. This antenna design realizes right hand circular polarization at GPS frequency and two linear polarizations at 3G and WLAN frequencies respectively.

Therefore, in order to achieve multi-CP and multi-LP characteristics with independent frequency tunability, a few prospected antenna designs have been proposed in this chapter. However, further research needs to be carried out to realize actual performance of the proposed antenna designs in future. In this chapter, three independently tunable antenna designs have been proposed which

are capable of achieving multi-resonance with different polarization characteristics.

5.2 Design 1

Triple-band Applications; Polarization requirements: circular, circular and linear

The design of triple-band systems for GPS-SDARS-WLAN or GSM-GPS-SDARS is more complex than the design for GSM-GPS-WLAN due to the different polarization requirements. The design of a single antenna for applications that require RHCP, LHCP and LP is very challenging. In this research, a frequency tunable antenna design is proposed that can achieve three resonant frequencies and three different polarizations i.e. RHCP, LHCP and LP respectively. The proposed design is based on single probe feed configuration and is a subset of the antenna design realized in chapter 4 of the thesis. As described before, the design proposed in chapter 4 consists of a patch fused with printed monopoles along the edges of the patch. The patch is responsible for RHCP at 1.575 GHz for GPS applications and the monopoles are resonating at 2.1 GHz and 2.45 GHz for 3G and WLAN applications. Similarly, for the proposed future design, another patch can be cut on the existing patch by introducing slots to achieve LHCP at different level of frequency [65]. This planar design can be achieved by coupling the signal between the outer and inner patch through the slots that separate the two patches. The first two resonant frequencies can be

controlled by the dimensions of the outer patch and inner patch respectively that can provide two circular polarizations. The third resonant frequency can be realized by tuning the length of the monopoles requiring linear polarization. The sense of polarization of the patch can also be controlled by perturbing the patch with respect to the feed point. Other combination of polarizations can also be achieved using the similar antenna structure with appropriate inner and outer patch antenna designs. Since, the proposed design offers the capability to realize independent frequency tunability, the polarization control in the design with desired radiation characteristics is achievable.

5.3 Design 2

Triple-band Applications; Polarization requirements: circular, circular and circular

Achieving three resonances with two RHCP and one LHCP, or two LHCP and one RHCP with a single feed and single layer antenna will be considered as a bench mark design. This challenging task can be realized by using the above proposed design methodology and sequential rotation technique (SRT) [73]. The sequential rotation technique can be used to generate third circular polarization.

As discussed before, inner and outer patches of the antenna can be used to generate the first two circular polarizations and third circular polarization can be achieved with SRT by shifting the location of monopoles for 90 degree

progressive shift, on the periphery of the outer patch. Locations of the monopoles and their width can also be used to adjust the progressive shift of the monopoles to achieve third circular polarization. Using this design methodology, frequency tunable multi circularly polarized antenna can be designed with desired radiation characteristics.

5.4 Design 3

Multi-band Applications; Polarization requirements: multi-CP and multi-LP

The proposed design methodology in this section is capable of generating seven different resonant frequencies, and these can be two circular polarizations and five linear polarizations or all linear polarizations. First two resonances can be achieved through outer and inner patches, next four resonances can be achieved by changing the length of the printed monopoles i.e. each monopole will be responsible for the different frequency operation. Furthermore, the seventh resonance can be generated by cutting a slot on the patch where the slot length can be adjusted for a desired resonant frequency.

5.5 Conclusion

In this chapter, antenna design methodologies have been proposed to realize frequency tunable multi-band antennas for wireless applications with different polarization requirements such as two CP and one LP, three CP or multiple CP

and multiple LP in a single antenna design. These methodologies have been proposed on the basis of knowledge of antenna theory and experience gained while designing other antennas as described in chapter 2, chapter 3 and chapter 4 of the thesis. However, further research and analysis needs to be carried out to validate the performance of the proposed antenna designs.

Bibliography

- [1] Sheng-Bing Chen, Yong-Chang Jiao, Wei Wang, and Fu-Shun Zhang, "Modified T-shaped planar monopole antennas for multiband operation," *IEEE Trans. Microwave Theory and Techniques*, vol.54, no.8, pp.3267-3270, Aug. 2006.
- [2] M. Martinez-Vazquez, O. Litschke, M. Geissler, D. Heberling, A.M. Martinez-Gonzalez, and D.Sanchez-Hernandez, "Integrated planar multiband antennas for personal communication handsets," *IEEE Trans. Antennas and Propagation*, vol.54, no.2, pp.384-391, Feb. 2006.
- [3] R.K. Raj, M. Joseph, B. Paul, and P. Mohanan, "Compact planar multiband antenna for GPS, DCS, 2.4/5.8 GHz WLAN applications," *Electronics Letters*, vol.41, no.6, pp. 290-291, 17 March 2005.
- [4] Pui Yi Lau, E.K.N. Yung, and K.K.O. Yung, "Compact dual-band patch antenna for wireless communication applications," *IEEE Antennas Propag. Int. Symp.*, pp.633-636, June 2007.
- [5] H. Seok Choi, K. Jong Park, K. Sun Kim, and S. Hak Kim, "Design of dual-band antenna for the ISM band using a backed microstrip line," *Microwave and Optical Technology Letters*, vol.41, no.6, pp. 457-460, 23 April 2004.

- [6] M. Ben Ahmed, M. Bouhorma, F.Elouaai, and A.Mamouni, "Design of New Multi Standard Patch Antenna GSM/PCS/UMTS/HIPERLAN for Mobile Cellular Phones," *European Journal of Scientific Research*, vol.32.no.2, pp.151-157, 2009.
- [7] Shun-Yun Lin; Kuang-Chih Huang; , "A compact microstrip antenna for GPS and DCS application," *Antennas and Propagation, IEEE Transactions on* , vol.53, no.3, pp. 1227- 1229, March 2005.
- [8] Hua-Ming Chen; Yi-Fang Lin; Chin-Chun Kuo; Kuang-Chih Huang; , "A compact dual- band microstrip-fed monopole antenna," *Antennas and Propagation Society International Symposium, 2001. IEEE* , vol.2, no., pp.124-127 vol.2, 2001.
- [9] WiMAX Forum Spectrum and Regulatory Database. [Online]. Available: <http://www.wimaxforum.org/>.
- [10] Lopes, L.; Viller, E.; Ludden, B.; , "GSM standards activity on location," *Novel Methods of Location and Tracking of Cellular Mobiles and Their System Applications (Ref. No. 1999/046), IEE Colloquium on* , vol., no., pp.7/1-7/7, 1999.
- [11] Honkasalo, H.; Pehkonen, K.; Niemi, M.T.; Leino, A.T.; , "WCDMA and WLAN for 3G and beyond," *Wireless Communications, IEEE* , vol.9, no.2, pp. 14- 18, April 2002.

- [12] Stuart Kerry (2003, June). Popular wireless local area networks gain large boost in speed. Piscataway, N.J, USA. [Online]. Available: <http://standards.ieee.org/announcements/80211gfinal.html>.
- [13] IEEE Std 802.11-2007, "IEEE standard for information technology- Telecommunications and information exchange between systems - Local and metropolitan area networks-specific requirements - Part 11: Wireless LAN medium access control (MAC) and physical layer (PHY) specifications," LAN/MAN Standards Committee, New York, NY, USA, pp. C1-1184, June 2007.
- [14] Samukic, A., "UMTS Universal Mobile Telecommunications System development of standards for the third generation," *Personal, Indoor and Mobile Radio Communications, 1998. The Ninth IEEE International Symposium on*, vol.2, no., pp.978-984 vol.2, 8-11 Sep 1998.
- [15] Hossain, E., "IEEE802.16/WiMAX-Based Broadband Wireless Networks: Protocol Engineering, Applications, and Services," *Communication Networks and Services Research, 2007. CNSR '07. Fifth Annual Conference on*, vol., no., pp.3-4, 14-17 May 2007.

- [16] Koon Hoo Teo; Zhifeng Tao; Jinyun Zhang, "The Mobile Broadband WiMAX Standard [Standards in a Nutshell]," *Signal Processing Magazine, IEEE*, vol.24, no.5, pp.144-148, Sept. 2007.
- [17] BroadbandPCS[Online]. Available: http://wireless.fcc.gov/services/index.htm?job=service_bandplan&id=broadband_pcs.
- [18] Mariottini, F.; Albani, M.; Toniolo, E.; Amatori, D.; Maci, S.; , "Design of a Compact GPS and SDARS Integrated Antenna for Automotive Applications," *Antennas and Wireless Propagation Letters, IEEE*, vol.9, no., pp.405-408, 2010.
- [19] Young-Pyo Hong and al: "S-Band Dual-Path Dual-Polarized Antenna System for satellite Digital AudioRadio Service (SDARS) Application", *IEEE transactions on microwave theory and techniques*, Vol. 54, N^o. 4, April 2006.
- [20] Koch, N.;, "Triple-service GPS-DAB/DMB-WiMAX patch antenna for automotive applications," *Antennas & Propagation Conference, 2009. LAPC 2009. Loughborough*, vol., no., pp.605-608, 16-17 Nov. 2009.
- [21] Vittorini, L.D.; Robinson, B.;, "Application of low cost frequency standards for commercial and military GPS," *Frequency Control Symposium, 1993. 47th., Proceedings of the 1993 IEEE International* , vol., no., pp.821-834, 2-4 Jun 1993.

- [22] Yuan-chih Lin; Shun-Yun Lin; Hong-Wen Wu; Wen-shyng Cheng; , "A $\lambda/2$ loop antenna for GPS application in mini-laptop," *Microwave Conference, 2009. APMC 2009. Asia Pacific* , vol., no., pp.1852-1855, 7-10 Dec. 2009.
- [23] G. Beddeleem, J.M. Ribero, G. Kossiavas, R. Staraj, and E. Fond, "Combined multi-band antenna for GPS and WLAN applications," in *Proc. 3rd European Antennas and Propagation Conf.*, Mar. 2009, pp. 366-369.
- [24] A.T.M. Sayem, and M. Ali, "A Dual-Band Hilbert Slot Antenna for GPS and Bluetooth Application," *IEEE Antennas Propag. Int. Symp.4*, pp.44-47, July 2005.
- [25] J.R. James, and P.S. Hall, *Handbook of microstrip patch antennas*. London: Peter Perigrinus, 1989.
- [26] C.A. Balanis, *Antenna Theory Analysis and Design*. New Jersey: John Wiley & Sons, 2005.
- [27] B. Smith, K.L.Wong, "An approach to graphs of Compact and Broadband Microstrip antennas, NewYork: Wiley, 2002.

- [28] Ramesh Garg, Prakash Bhartia, et al, *microstrip antenna design handbook*, Boston: Artech House Inc., 2001.
- [29] S.Maci and GBiffi Gentili, Dual-frequency patch antennas, *IEEE Antennas and Propagation Magazine*, 1997, Vol.39, No.6, p.13-19.
- [30] Deepuku mar M, George'J, et al, Broadband dual frequency microstrip antenna, *Electron Lett*, 1996,32(17), p.1531-1532.
- [31] Jan.J.Y and Wong. K.L, Single-feed dual-frequency circular microstrip antenna with an open-ring slot, *Microw. Opt. Technol. Lett*, 1999, 22, p.157-160.
- [32] G.B. Hsieh, M.H. Chen, and K.L. Wong, "Single-feed dual-band circularly polarised microstrip antenna", *Electronics Letters*, vol. 34, no.12, pp. 238- 240, June 1998.
- [33] S. T. Fang, and K.L Wong, "A dual frequency equilateral-triangular microstrip antenna with a pair of narrow slots" *Microwave Optical Technol. Lett.*, vol. 23, pp.82-84, Oct. 1999.
- [34] Vijay Sharma , S. Shekhawat , V. K. Saxena , J. S. Saini , K. B. Sharma , B. Soni , and D. Bhatnagar, "Right Isosceles triangular microstrip

antenna with narrow l-shaped slot” *Microwave Optical Technol. Lett.*, Vol. 51, no. 12, Dec. 2009.

- [35] Y. X. Guo, K. M. Luk, K. F. Lee “Small broadband semicircular patch antenna with an L Probe feeding” *Microwave and Optical Technology Letters*, vol. 29, no. 5, pg. 289-290, 2001.
- [36] Y. X. Guo, K. M. Luk, K. F. Lee “Regular circular and compact semicircular patch antennas with a T-probe feeding” *Microwave and optical Technology Letters*, vol. 31, no. 1, pg. 68-71, 2001.
- [37] J. C. Batchelor and R. J. Langley, “Microstrip annular ring slot antennas for mobile applications,” *Electron. Lett.*, vol. 32, pp. 1635–1636, 1996.
- [38] S. Y. Lin and K. L. Wong, “Enhanced performances of a compact conical-pattern annular-ring patch antenna using a slotted ground plane,” *in Proc. 2001 Asia-Pacific Microwave Conf.*, pp. 1036–1039.
- [39] Qihong Zhong; Yuanxin Li; Hongyan Jiang; Yunliang Long; , "Design of a novel dual-frequency microstrip patch antenna for WLAN applications," *Antennas and Propagation Society International Symposium, 2004. IEEE* , vol.1, no., pp. 277- 280 Vol.1, 20-25 June 2004.

- [40] Han-Cheol Ryu; Hee-Ran Ahn; Sang-Hwa Lee; Wee Sang Park; , "Triple-stacked microstrip patch antenna for multiband system," *Electronics Letters* , vol.38, no.24, pp. 1496- 1497, 21 Nov 2002.
- [41] Viet-Anh Nguyen; Bhatti, R.-A.; Seong-Ook Park; , "A Simple PIFA-Based Tunable Internal Antenna for Personal Communication Handsets," *Antennas and Wireless Propagation Letters, IEEE* , vol.7, no., pp.130-133, 2008.
- [42] Pazin, L.; Telzhensky, N.; Leviatan, Y.; , "Multiband Flat-Plate Inverted-F Antenna for Wi-Fi/WiMAX Operation," *Antennas and Wireless Propagation Letters, IEEE*, vol.7, no., pp.197-200, 2008.
- [43] Yong-Xin Guo; Chia, M.Y.W.; Chen, Z.N.; , "Miniature built-in quad-band antennas for mobile handsets," *Antennas and Propagation Society International Symposium, 2003. IEEE* , vol.3, no., pp. 91- 94 vol.3, 22-27 June 2003.
- [44] Nepa, P.; Manara, G.; Serra, A.A.; Nenna, G.; , "Multiband PIFA for WLAN mobile terminals," *Antennas and Wireless Propagation Letters, IEEE* , vol.4, no., pp. 349- 350, 2005.

- [45] Zuazola, I.J.G.; Batchelor, J.C.; , "Compact multiband PIFA type antenna," *Electronics Letters* , vol.45, no.15, pp.768-769, July 16 2009.
- [46] Wen-Shan Chen; Yu-Chen Chang; Hong-Twu Chen; Fa-Shian Chang; Hsin-Cheng Su; "Novel design of printed monopole antenna for WLAN/WiMAX applications," *Antennas and Propagation Society International Symposium, 2007 IEEE*, pp.3281-3284, 9-15 June 2007.
- [47] Yuehe Ge; Esselle, K.P.; Bird, T.S.; , "A Spiral-Shaped Printed Monopole Antenna for Mobile Communications," *Antennas and Propagation Society International Symposium 2006, IEEE* , vol., no., pp.3681-3684, 9-14 July 2006.
- [48] Manz, M.; Nevermann, P.; , "Compact hexa-band folded dipole antenna," *Antennas and Propagation Society International Symposium, 2008. AP-S 2008. IEEE* , vol., no., pp.1-4, 5-11 July 2008.
- [49] F. Tefiku and E. Yamashita, "Double-Sided Printed Strip Antenna for Dual Frequency Operation," presented at IEEE *Antennas and Propagation Society International Symposium*, Baltimore, 1996.
- [50] Kimouchee, H.; Bitchikh, M.; Atrouz, B.;, "Novel Design of a Fractal Monopole Antenna for Wireless Communications," *Microwave*

Techniques, 2008. COMITE 2008. 14th Conference on , vol., no., pp.1-5, 23-24 April 2008.

- [51] Sanchez, J.L.; de Haro, L.; , "Experiences on multiband fractal antennas," *Antennas and Propagation Society International Symposium, 2001. IEEE*, vol.4, pp.58-61 vol.4, 2001.

- [52] Kiyun Han; Harackiewicz, F.J.; , "Stacked multiband fractal patch antennas," *Antennas and Propagation Society International Symposium, 2003. IEEE* , vol.4, no., pp. 234- 237 vol.4, 22-27 June 2003.

- [53] Jun-Hwa Oh; Young-Pyo Hong; Jong-Gwan Yook; , "Dual circularly-polarized stacked patch antenna for GPS/SDMB," *Antennas and Propagation Society International Symposium, 2008. AP-S 2008. IEEE* , vol., no., pp.1-4, 5-11 July 2008.

- [54] J.A. Pros and C.P. Ballarda, "Multifrequency Microstrip patch antenna with parasitic coupled elements," *US Patent-7202818*, April 2007.

- [55] Pigaglio, O.; Raveu, N.; Pascal, O.; , "Design of multi-frequency band Circularly Polarized Stacked Microstrip patch Antenna," *Antennas and Propagation Society International Symposium, 2008. AP-S 2008. IEEE* , vol., no., pp.1-4, 5-11 July 2008.

- [56] Mythili, P.; Cherian, P.; Mridula, S.; Paul, B.; , "Design of a Compact Multiband Microstrip Antenna," *India Conference (INDICON), 2009 Annual IEEE* , vol., no., pp.1-4, 18-20 Dec. 2009.
- [57] Zhou, Y.; Chen, C.-C.; Volakis, J. L.; , "Dual Band Proximity-Fed Stacked Patch Antenna for Tri-Band GPS Applications," *Antennas and Propagation, IEEE Transactions on* , vol.55, no.1, pp.220-223, Jan. 2007.
- [58] Sun, X.; Zhang, Z.; Feng, Z.; , "Dual-Band Circularly Polarized Stacked Annular-Ring Patch Antenna for GPS Application," *Antennas and Wireless Propagation Letters, IEEE* , vol.10, no., pp.49-52, 2011.
- [59] F. Croq and D. M. Pozar, "Multifrequency Operation of Microstrip Antennas Using Aperture Coupled Parallel resonators," *IEEE Trans. Antennas Propagat.*, vol. 40, no. 11, pp. 1397-1374, 1992.
- [60] S. Maci, G. B. Gentili, P. Piazzesi, and C. Salvador, "Dual band slot loaded patch antenna," *IEE Proceedings - Microwaves Antennas and Propagation*, vol. 142, No.3, pp. 225-232, 1995.
- [61] Huang, C.-Y.; Ling, C.-W.; Kuo, J.-S.; , "Dual-band microstrip antenna using capacitive loading," *Microwaves, Antennas and Propagation, IEE Proceedings -* , vol.150, no.6, pp. 401- 404, Dec 2003.

- [62] Liang, M.C.; Lai, W.C.; Yen, Y.M.; Kuo, Y.L.; , "A capacitor-loaded broadband circular patch antenna," *Antennas and Propagation Society International Symposium, 2001. IEEE* , vol.3, no., pp.302-304 vol.3, 2001.
- [63] L. Boccia, G. Amendola, and G. Di Massa, "A dual frequency microstrip patch antenna for high-precision GPS applications," *IEEE Antennas and Wireless Propag. Letters*, vol. 3, pp. 157-160, 2004.
- [64] Schez-Hernandez and I. Robertson, "Analysis and design of a dual-band circularly polarized microstrip patch antenna," *IEEE Trans. Antennas and Propagation*, vol. 43, pp. 201-205, Feb. 1995.
- [65] G. Beddeleem, J.M. Ribero, G. Kossiavas, R. Staraj, and E. Fond, "Dual frequency circularly polarised antenna", *Microwave and Optical Technology Letters*, vol. 50, no. 1, pp. 177-180, Jan. 2008.
- [66] S.H. Choi, J.H. Yoon, H.C. Lee, and K.S. Kwak, "Design of a weathercock-shaped microstrip patch antenna with a T-slot for the hiperlan band", *Microwave and Optical Technology Letters*, vol. 48, no. 5, pp. 911-913, May 2006.

- [67] J. S. Roy, N. Chattoraj, and N. Swain, "Short-circuited microstrip antennas for multiband wireless communications," *Microwave and Optical Technology Letters*, vol. 48, no. 12, pp.2372-2375, Sep 2006.
- [68] Zhang Peng; Miura, Y.; Shiokawa, T.; , "Dual-band GPS antennas with single-feed and low-profile configurations," *Antennas and Propagation Society International Symposium, 2008. AP-S 2008. IEEE* , vol., no., pp.1-4, 5-11 July 2008.
- [69] Liu, Z.D.; Hall, P.S.; Wake, D.; , "Dual frequency planar circularly polarized antenna at S and L bands ," *Antennas and Propagation, Tenth International Conference on (Conf. Publ. No. 436)* , vol.1, no., pp.378-380 vol.1, 14-17 Apr 1997.
- [70] Yim, H.-Y.A.; Kong, C.-P.; Cheng, K.-K.M.;, "Compact circularly polarised microstrip antenna design for dual-band applications," *Electronics Letters* , vol.42, no.7, pp. 380- 381, 30 March 2006.
- [71] Jui-Han Lu and Kai-Ping Yang,, "A Simple Design for Single-feed Circularly-Polarized Microstrip Antennas" in *Proc. National Science Council R.O.C (A)*, vol. 24, no.2,pp. 131-133, 2000.
- [72] Chin-Long Tsai, Sheng-Ming Deng, Ching-Hung Tseng, and Sheau-Shong Bor, "A shorted square-ring slot antenna with a branched slot for

the 1575 MHz and 2.4 GHz Dual-band operations,” *Microwave and Optical Technology Letters*, vol. 51, no. 2, pp. 402-405, Dec. 2008.

- [73] P.S. Hall, J.S. Dahele, and J.R. James, “Design principles of sequentially fed, wide bandwidth, circularly polarised microstrip antennas,” *Microwaves, Antennas and Propagation, IEE Proceedings H*, vol.136, no.5, pp. 381-389, Oct 1989.
- [74] H.R. Hassani, D. Mirshekar-Syahkal, "Analysis of triangular patch antennas including radome effects," *Microwaves, Antennas and Propagation, IEE Proceedings H*, vol.139, no.3, pp.251-256, Jun 1992.
- [75] K.L Wong, M.C. Pan, and W.H. Hsu, “Single feed dual frequency triangular microstrip antenna with a V shaped slot” *Microwave Optical Technol. Lett.*, vol. 20, pp. 133-134, Jan. 1999.
- [76] Sharma, L.N.; Das, S.; Gogoi, A.K.; , "ISM Band Triangular Patch Antenna on FR4 Substrate with 'U' Pattern Slots," *INDICON, 2005 Annual IEEE* , vol., no., pp. 184- 187, 11-13 Dec. 2005.
- [77] Tilanthe, P.; Sharma, P.C.; , "An equilateral triangular patch antenna with T - shaped notch for enhanced gain," *Wireless Communication and Sensor Networks, 2008. WCSN 2008. Fourth International Conference on* , vol., no., pp.179-180, 27-29 Dec. 2008.

- [78] Singh, N.; Yadav, D.P.; Singh, S.; Sarin, R.K.; , "Compact corner truncated triangular patch antenna for WiMax application," *Microwave Symposium (MMS), 2010 Mediterranean* , vol., no., pp.163-165, 25-27 Aug. 2010.
- [79] Chaturvedi, A.; Bhomia, Y.; Yadav, D.; , "Truncated tip triangular microstrip patch antenna," *Antennas Propagation and EM Theory (ISAPE), 2010 9th International Symposium on* , vol., no., pp.212-214, Nov. 29 2010-Dec. 2 2010.
- [80] Keon-Myung Lee; Young-Je Sung; Jung-Woo Baik; Young-Sik Kim, "A triangular microstrip patch antenna for multi-band applications," *Microwave Conference, 2008. APMC 2008. Asia-Pacific*, pp.1-4, 16-20, Dec. 2008.
- [81] Yuan Li; Chair, R.; Luk, K.M.; Lee, K.F.; , "Broadband triangular patch antenna with a folded shorting wall," *Antennas and Wireless Propagation Letters, IEEE* , vol.3, no.1, pp.189-192, Dec. 2004.
- [82] S. C Pan and K.L. Wong, "Dual frequency triangular microstrip antenna with a shorting pin" *IEEE Trans. Antennas and Propagation*, vol. 45, pp. 1889– 1891, Dec. 1997.

- [83] Chow Yen Desmond Sim; Tuan-Yung Han; Row, J.-S.; , "Dual-frequency shorted triangular patch antenna," *Microwave Conference Proceedings, 2005. APMC 2005. Asia-Pacific Conference Proceedings*, vol.4, no., pp. 4 pp., 4-7 Dec. 2005.
- [84] Vijay Sharma , S. Shekhawat , V. K. Saxena , J. S. Saini , K. B. Sharma , B. Soni , and D. Bhatnagar, "Right Isosceles triangular microstrip antenna with narrow l-shaped slot" *Microwave Optical Technol. Lett.*, Vol. 51, no. 12, Dec. 2009.
- [85] Wenjun Chen, Binhong Li, and Xie Tao, "Compact dual-frequency semi-circular microstrip antenna" *Microwave and Optical Technology Letters*, vol. 4, no. 5, pg. 430-43, 2004.
- [86] Wideband Coplanar Microstrip Patch antenna, *Progress in Electromagnetic research Letters*, 2008.
- [87] J.M. Johnson and Y. Rahmat-Samii, "The tab monopole" *IEEE Trans. Antennas and Propagation*, vol.45, no.1, pp.187-188, Jan1997.
- [88] Xiao-Rong Yan, Shun-Shi Zhong, and Xue-Xia Yang , "Compact Printed Monopole Antenna with Super-wideband" *Microwave, Antenna, Propagation and EMC Technologies for Wireless Communications*, 2007 International Symposium, pp.605-607, 16-17 Aug. 2007.

- [89] Liu, L.; Zhu, S.; Langley, R.;, "Dual-band triangular patch antenna with modified ground plane," *Electronics Letters* , vol.43, no.3, pp.140-141, Feb. 1 2007.
- [90] I. J. Bahl, S. S. Stuchly, and M. A. Stuchly, "A new microstrip radiator for medical application," *IEEE Trans. Microw. Theory Tech.*, vol. MTT-28, pp. 1464–1468, Dec. 1980.
- [91] P. M. Bafrooei and L. Shafai, "Characteristics of single- and double layer microstrip square ring antennas," *IEEE Trans. Antennas Propag.*, vol. 47, pp. 1633–1639, Oct. 1999.
- [92] I. Saha and S. K. Chowdhury, "Experiments on impedance and radiation properties of concentric microstrip ring resonators," *Electronic Lett.*, vol. 31, pp. 421–422, Mar. 1995.
- [93] Mahajan, M.; Chakravarty, T.; Khah, S.K.;, "Study of bandwidth and radiation properties of loaded annular ring antenna," *Recent Advances in Microwave Theory and Applications, 2008. MICROWAVE 2008. International Conference on*, vol., no., pp.892-893, 21-24 Nov. 2008.

- [94] M. A. Sultan, "The mode features of an ideal-gap open-ring microstrip antenna," *IEEE Trans. Antennas Propag.*, vol. 37, no. 2, pp. 137–142, Feb. 1989.
- [95] Latif, S.I.; Shafai, L., "Polarization Characteristics of Multiband Loaded Microstrip Annular Ring Antennas," *Antennas and Propagation, IEEE Transactions on*, vol.57, no.9, pp.2788-2793, Sept. 2009.
- [96] R. Garg and V. S. Reddy, "Edge feeding of microstrip ring antennas", *IEEE Trans. Antennas Propagat.*, vol. 51, 2003, 1941-1946.
- [97] A. K. Bhattacharyya and L. Shafai, "A wider band microstrip antenna for circular polarization," *IEEE Trans. Antennas Propag.*, vol. 36, no. 2, pp. 157–163, Feb. 1988.
- [98] S.-S. Oh and L. Shafai, "Investigation into the cross-polarization of loaded microstrip ring antennas," in *Proc. IEEE AP-S Intl. Symp., USNC/URSI Meeting*, Washington, DC, Jul. 3–8, 2005, pp. 243–246, 1A.
- [99] K. Rambabu, M.Z. Alam, and J. Bornemann, "Design of Compact Dual-Polarized Printed-Circuit Antenna for Ultra-Wideband applications," in *Proc. 36th European Microwave Conf.*, Sept. 2006, pp.626-629.

[100] R. Bancroft, *Microstrip and Printed Antenna Design*. Atlanta: Noble Publishing, 2004.